MECHANISTIC INVESTIGATION OF HUMAN CYTOCHROMES P450 INVOLVED IN HORMONE BIOSYNTHESIS

BY

RUCHIA DUGGAL

DISSERTATION

Submitted in partial fulfillment of the requirements
for the degree of Doctor of Philosophy in Biochemistry
in the Graduate College of the
University of Illinois at Urbana-Champaign, 2017

Urbana, Illinois

Doctoral Committee:

Professor Stephen G. Sligar, Chair
Professor Mary A. Schuler
Professor Emad Tajkhorshid
Professor Robert B. Gennis

Abstract

CYP17A1 and CYP19A1 are the key cytochromes P450 involved in steroidogenesis. Mutations causing hypo- or hyper-activation of both these enzymes results in diseased states, including cancers. In addition to carrying out mono-oxygenation reactions, both CYP17A1 and CYP19A1 also catalyze carbon-carbon lyase reactions. There is significant interest in developing therapeutics capable of specifically targeting the CYP17A1 lyase reaction to target androgen synthesis without impacting glucocorticoid production, and understanding of CYP19A1 reaction mechanism could similarly help guide design of mechanism based inhibitors for certain breast cancers. To interrogate mechanistic aspects of both these enzymes, I used Nanodisc technology for reconstituting active forms of these proteins in functional complexes with their effector proteins in a native-like membrane environment.

Cytochrome P450 17A1 (CYP17A1) is a multi-functional enzyme, catalyzing synthesis of glucocorticoid precursors by hydroxylation of pregnene nucleus, and androgen biosynthesis by a second C-C lyase step, at the expense of glucocorticoid production. It has been recently confirmed in our lab that when 17-hydroxy-pregnenolone is a substrate, CYP17A1 lyase reaction proceeds through a non-conventional hemiketal intermediate. However, it remains unknown if the alternate substrate, 17-hydroxy-progesterone (OH-PROG) is transformed to androstenedione via this novel mechanism, by the traditional compound I (Cpd I) mechanism, or by a combination of the two. To this end, I investigated kinetic solvent isotope effects on steady state turnover for lyase reaction on OH-PROG. Further, cryo-trapped peroxo-anion intermediate was spectroscopically followed as the samples were thermally annealed. Resonance Raman spectroscopy (rR) on the trapped intermediate was also performed. Our results strongly indicate that the CYP17A1 mediated OH-PROG lyase proceeds through a hemiketal intermediate.

Cytochrome b_5 (cyt b_5) is a small heme-protein, known to enhance the rate of the CYP17A1 lyase reaction by ~5 fold, while having little effect on hydroxylation. Investigation with a redox inactive form of cyt b_5 indicated that for lyase enhancement, cyt b_5 critically requires a redox effector role. In order to investigate the electron transfer by cyt b_5 to CYP17A1, I employed stopped flow spectroscopy and compared the CYP17A1 reduction rates by cyt b_5 that by cytochrome P450 reductase (CPR). rR was also performed on CYP17A1—cyt b_5 complex investigate any conformational perturbations. Taken together, our results suggest that cyt b_5 critically requires a redox transfer role is essential to enhance lyase reaction, and it reduces CYP17A1 oxy-complex ~10fold faster than CPR. rR on oxyferrous CYP17A1—cyt b_5 complex indicated subtle conformational changes in the active site, which were heavily dependent on the identity of the substrate.

CYP19A1 produces estrogens in a three-step reaction, the first two being hydroxylation steps, while the third step comprises a lyase step. The hydroxylation reactions are expected to proceed through the conventional Cpd I intermediate, but the active intermediate for the lyase step is not known. We investigated kinetic solvent isotope effects on the steady state turnover for the three-step reaction, and our results suggest that CYP19A1 lyase chemistry, unlike CYP17A1, proceeds through the Cpd I intermediate.

My thesis is a mechanistic study of the androgenic CYP17A1 and the estrogenic CYP19A1. I investigated the active intermediates in the final lyase step by employing various biochemical and biophysical techniques to Nanodisc reconstituted enzymes. While CYP19A1 lyase step is suggested to proceed through the Cpd I intermediate, in the case of CYP17A1 lyase reaction, a hemiketal intermediate is implicated. Furthermore, the biological regulator of androgen synthesis, cyt b_5, acts as a faster redox donor than CPR in the lyase reaction cycle, and also exerts subtle conformational changes dependent on the identity of the substrate in the active site.

Acknowledgements

The debts I have incurred in my graduate career are many and large. Foremost, I owe my deepest gratitude to Prof. Stephen Sligar for being an exceptional mentor. With his deft hand, he gave me a little push whenever I needed and knew when to let me learn from my mistakes. Without his motivation to constantly improve and inspiration to excel, this thesis wouldn't have been possible. I remember the time I was working on a Sunday and he made me a cup of coffee and brought me cookies from the vending machine, since I had skipped lunch that day. I am thankful that he cares so much about his students and their professional growth. I am extremely thankful to Dr. Ilia Denisov, who took time out to answer all of my many questions through the years. I am grateful that I got to learn so much from him, his profound wisdom and advice have helped me grow into a better scientist. I will always look up to him as a brilliant thinker, a great teacher, a very interesting conversationalist and will always marvel at his impeccable memory. I will always remember fondly the many discussions that I shared with Ilia and Lena over lunch about all things under the sun. Dr. Mark McLean is one of the nicest people I have ever known. I will cherish all the fun conversations and internet videos we shared. Dr. Michael Gregory is a great source of expertise in many diverse fields. I can't thank him enough for bringing me on the CYP17 project, helping me all along the way and teaching me so much. I am also grateful to Dr. Yogan Khatri and Dr. Abhinav Luthra who helped me get started in the lab with CYP19 project, and to our collaborators for the CYP17 resonance Raman experiments at Marquette University; Dr. Yilin Liu, Dr. Piotr Mak and Prof. James Kincaid are exceptional people to work with. I am grateful to Prof. Robert Gennis and Ziqiao Ding for help with stopped flow spectroscopy experiments. I would be remiss if I didn't thank former lab members and my friends Aretta, Xin and Ivan, and the many lunches and happy hours that we all shared.

My sister, my rock, my closest friend, who I cannot even bear to be without for one moment, has been my source of encouragement and positivity throughout my life. I am thankful to her for inspiring me to apply to grad schools in the US and not settling for just anything, for believing in me even in the moments when I did not, and for the countless little things I may have forgotten but am thankful for all the same. My lovely mother, who while raising us in a tiny town in India, always pushed us to dream big, deserves buckets of gratitude. My father taught me in his own way, how important hard work and self-dependence are. My parents were groundbreakers in our little town in teaching their two little daughters to be ambitious and to never think of themselves less than men, and I am grateful that they didn't let the stares they got stop them from encouraging us to aim higher. My little nephew Avyaan's dimpled smile lifts me up whenever I am down. I will remember to tell him as soon as he is old enough, that videos of him playing were the best thing to cheer myself up whenever I had challenging days in grad school. Umair has been the best friend I could ask for and a constant source of encouragement on an almost daily basis, even after moving 200 miles away. I will be the first PhD graduate in my entire family, and I could not have come so far without all of you. Gratitude also goes to the few not-so-helpful people in my life, they motivated me to rise and do better, without realizing they were doing me a huge favor.

Again, thank you Sligar lab, I will miss you, and will be craving cookies every Monday afternoon for the rest of my life.

To my Mom

Table of Contents

List of Abbreviations

3β-HSD	3β-Hydroxysteroid dehydrogenase
Δ-ALA	Δ-Aminolevulinic acid
ACTH	Adrenocorticotrophic hormone
AD	Androstenedione
AFM	Atomic force microscopy
AMP	Adenosine monophosphate
ApoA-I	Apolipoprotein A-I
AR	Androgen receptor
ATP	Adenosine triphosphate
β-ME	β-mercaptoethanol
Cpd 0	Compound 0
Cpd I	Compound I
CPR	Cytochrome P450 reductase
CRPC	Castration resistant prostate cancer
CYP	Cytochrome P450
CYP17A1:ND	CYP17A1 incorporated into nanodiscs
Cyt b_5	Cytochrome b_5
DEAE-sepharose	Diethylaminoethyl sepharose
DHEA	Dehydroepiandrosterone
DTT	Dithiothreitol
E. coli	*Escherichia coli*
EM	Electron microscopy
ENDOR	Electron nuclear double resonance
EPR	Electron paramagnetic resonance
ER	Estrogen receptor

FAD	Flavin adenine dinucleotide
FMN	Flavin mononucleotide
GPCR	G-protein coupled receptor
IPTG	Isopropyl β-D-1-thiogalactopyranoside
KPi	Potassium phosphate
KSIE	Kinetic solvent isotope effect
LB	Lysogeny broth
Mn b5	Manganese substituted cytochrome b_5
MSP	Membrane scaffold protein
MWCO	Molecular weight cutoff
NADPH	Nicotinamide adenine dinucleotide phosphate-reduced
Ni-NTA	Nickel-nitrilotriacetic acid
NMR	Nuclear magnetic resonance
OD	Optical density
OH-PREG	17α-hydroxy-pregnenolone
OH-PROG	17α-hydroxy-progesterone
PCOS	Polycystic ovarian syndrome
PMSF	Phenylmethylsulfonyl fluoride
POPC	1-palmitoyl-2-oleoyl-sn-glycero-3-phosphocholine
PREG	Pregnenolone
PROG	Progesterone
rR	Resonance Raman
Rz ratio	Reinheitszahl ratio (Soret absorbance/protein absorbance)
SAXS	Small angle X-ray scattering
SPR	Surface plasmon resonance
TB	Terrific broth

Chapter 1

Introduction

1.1 Overview

Hormone biosynthesis in humans is a complicated process involving a series of steps catalyzed by multiple enzymes, with the final hormone levels being a result of a delicate balance between androgens and estrogens. The hormone biosynthetic pathway involves multiple steps catalyzed by various enzymes, most important of them being the cytochrome P450 (CYP) enzymes. These are oxygenases which can efficiently catalyze a variety of difficult biotransformation reactions (Guengerich, 2001). The first P450 crystal structure was solved in 1987, of the bacterial CYP101, and the growing structural information of many P450s over the past ~30 years (DeVore and Scott, 2012; Ghosh et al., 2010; De Montellano, 2015; Poulos et al., 1987) has helped immensely in furthering the understanding of the catalytic active site, the orientation of substrates and in providing reasonable hypotheses regarding the orientation of these proteins in the membranes. Mechanism of the complex catalysis by these heme-proteins have been long studied, on P450s ranging from the soluble bacterial CYP101 to the complex membrane bound mammalian P450s. Understanding of the mechanistic intermediates formed during androgen biosynthesis is essential to inform specific mechanism based

Reproduced in part with permission from

Duggal, R., Liu, Y., Gregory, M.C., Denisov, I.G., Kincaid, J.R., and Sligar, S.G. Evidence that cytochrome b5 acts as a redox donor in CYP17A1 mediated androgen synthesis. Biochemical and Biophysical Research Communications (2016) 477, 202–208. Copyright 2016 Elsevier. The published version may be found online at https://dx.doi.org/10.1016/j.bbrc.2016.06.043.

Khatri, Y., Luthra, A., Duggal, R., and Sligar, S.G. Kinetic solvent isotope effect in steady-state turnover by CYP19A1 suggests involvement of Compound 1 for both hydroxylation and aromatization steps. FEBS Letters (2014) 588, 3117–3122. Copyright 2014 John Wiley and Sons. The published version may be found online at https://dx.doi.org/10.1016/j.febslet.2014.06.050.

inhibitors for targeting hyper-production of androgens in pathogenic states like castration resistant prostate cancer and polycystic ovarian syndrome (PCOS). A better understanding of the mechanism of estrogen synthesis is expected to guide development of mechanism based inhibitors for targeting excessive hormone synthesis in estrogen dependent breast cancer patients. Some P450s are also known to be modulated by the association of specific effector proteins, with the androgenic reaction by CYP17A1 being affected by association with a small heme-protein cytochrome b_5 (cyt b_5). Information about this interaction is expected to guide development of specific therapeutics targeting androgen production with minimal off-target effects.

This study is a compilation of investigation of the mechanism of androgenic product androstenedione synthesis by CYP17A1 and of cyt b_5 mediated modulation of CYP17A1 catalyzed androgen synthesis. It has been shown previously that the presence of a stable membrane anchor is crucial in the study of these membrane associated enzyme complexes (Holmans et al., 1994; Sergeev et al., 2014). Therefore, throughout the course of this study, Nanodisc technology was employed to generate functional complexes of these enzymes associated with a native-like lipid bilayer. A short study on the nature of the mechanistic intermediate in CYP19A1 catalyzed estrogen synthesis was also performed, which provides a beautiful contrast between the two enzymes and makes one marvel at the marked diversity in the mechanistic aspects of two closely related enzymes, that have evolved to perform such different chemistries. In addition to providing insight towards design of specific mechanism based inhibitors, this study also hopes to guide development of therapeutic inhibitors of cyt b_5–CYP17A1 interaction, for improving prognosis in castration resistant prostate cancer patients as well as in females suffering from polycystic ovarian syndrome.

1.2 Cytochromes P450

1.2.1. Introduction:

Cytochromes P450 (CYPs, P450s) are ubiquitous heme-protein enzymes, found in organisms ranging from archaea and viruses to higher eukaryotes. They have been the subject of tremendous interest over many decades owing to their efficient catalysis of unusually difficult reactions including alkane hydroxylation, heteroatom oxidation, epoxidation, N-dealkylation etc. (Guengerich, 2001). P450s belong to a superfamily of >300,000 sequenced members (Nelson, 2017), amd despite having less than 20% sequence homology across the gene superfamily, these proteins have a common overall fold. In addition to their role in xenobiotic detoxification, their involvement in steroidogenic pathways has been the center of great attention. P450s contain one heme, an iron (III) protoporphyrin IX center coordinated to an axial cysteine thiolate. They are known to catalyze hydroxylations of alkane carbons and epoxidation of alkenes, by efficiently providing an “active oxygen” (De Montellano, 2015). In terms of drug metabolism, this increase in polarity of the substrates contributes to the first step in the clearance from the body. In addition to the conventional hydroxylation reactions, the steroidogenic P450s like CYP51, CYP11A1, CYP17A1 and CYP19A1 also catalyze acyl-carbon bond cleavage reactions in the same active site.

In contrast to the soluble P450s in bacteria, mammalian P450s are membrane associated, mostly with endoplasmic reticulum, although some P450s involved in steroid, sterol and bile acid synthesis are located in the inner membrane of mitochondria. The enzyme has a 30-50 amino acid long N terminal polypeptide chain involved in membrane interaction, followed by a catalytic domain. The active site is created by three parallel D, L and I helices and an antiparallel E helix. As compared to bacterial P450s, eukaryotic CYP enzymes have a longer region between F and G helices, that makes F’ and G’ helices. This region, together with the proline rich N-terminal region and A helix forms a hydrophobic surface near the membrane (Williams et al., 2000). The interaction of F and G helices with the membrane possibly promotes the transfer of hydrophobic substrates from the membrane to the P450. The P450 heme iron is connected via a thiolate linkage to a highly-conserved cysteine residue which is housed

in a β-bulge preceding the L-helix. This rigid architecture helps protect the Cys and hold it in place to accept hydrogen bonds from peptide NH- group. Studies with model porphyrins have shown that this axial ligand is the origin of the characteristic 450 nm Soret absorption of carbon monoxide adducts of P450s (Collman and Sorrell, 1975). In resting state, the sixth axial ligand position for heme iron is occupied by a water molecule which is responsible for its low spin state (S=1/2).

In one productive reaction cycle, a P450 molecule consumes two reducing equivalents in the form of NAD(P)H, which are provided by the associated redox partners. Bacterial and eukaryotic mitochondrial P450s associate with a short electron transfer chain of two proteins, an FAD-containing NADH-putidaredoxin reductase/adrenodoxin reductase and an iron sulfur ferredoxin, called putidaredoxin/adrenodoxin. The reductase receives two electrons as hydride from NAD(P)H and delivers these as single reducing equivalents to two molecules of the ferredoxin, which is responsible for reduction of the associated P450 enzyme. Microsomal P450s, on the other hand, interact with a single enzyme called cytochrome P450 reductase (CPR), which is a membrane bound diflavin protein. CPR has a hydrophobic N terminal domain which is associated with the membrane, and the two flavin containing domains linked together via a linker region. CPR catalyzes the transfer of two electrons sequentially from NADPH via its flavin cofactors to P450s and other acceptor proteins as:

$$\text{NAD(P)H} \longrightarrow \text{FAD} \longrightarrow \text{FMN} \longrightarrow \text{P450}$$

In addition to CPR, some P450s are known to interact with other effector proteins that can affect catalysis. One of such proteins is a small heme-protein, Cytochrome b_5 (cyt b_5). It is a ~17kD membrane associated protein which is known to interact with many P450s, including the drug metabolizing CYP2B4, 2B6, 2C9, 2C19, 2E1, 3A4, and the steroidogenic CYP17A1. Cyt b_5 may stimulate or inhibit the P450 mediated catalysis depending on the P450 isozyme, experimental conditions and the substrate. For instance, CYP2B4 catalyzed metabolism of the anesthetic methoxyflurane is highly enhanced by the presence of cyt b_5, whereas the reaction with

benzphetamine is not affected at all (Canova-davis and Waskell, 1984). Cyt b_5 null mice have been shown to have significant changes in metabolism of various substrates, while hepatic deletion of cyt b_5 showed decreased activity of CYP3A and 2C families (Finn et al., 2008; McLaughlin et al., 2010).

Another highly conserved region in P450s structure is a portion of I helix near the heme iron. Thr 252 in CYP101A1 is involved in a local distortion in the I helix in a manner such that its side chain hydroxyl group forms a hydrogen bond with a peptide carbonyl oxygen that would normally form a hydrogen bond with the backbone NH- group. This distortion has been seen to be significant for proton delivery to the heme Fe–OO adduct, causing scission of O–O linkage resulting in the formation of the reactive Fe–O intermediate. The acid-alcohol pair in I-helix has been identified to be composed of Asp251 and Thr252 in CYP101A1. Mutagenesis studies of this acid-alcohol pair have verified their role in proton delivery to the heme. T252A mutant was shown to have completely uncoupled pyridine nucleotide reduction, whereas D251N mutant had a 20-fold slower turnover with the second proton transfer becoming the rate determining step (Gerber and Sligar, 1994; Makris et al., 2002). It has been suggested that the ordered solvent at the active site serves as the direct proton donor to the iron-oxy adduct (Benson et al., 1997; Vidakovic et al., 1998).

1.2.2. Reactive intermediates in P450 catalysis:

Seminal studies with oxygen isotopes in the 1950s demonstrated that the oxygen incorporated by P450s comes from atmospheric O_2 and not water (Hayaishi et al., 1955; Hayano et al., 1955). P450s function by activating molecular oxygen and incorporating one of the oxygen atoms into a wide variety of substrates, while the other oxygen atom is converted to water. Information about the reaction intermediates has been the fruit of major efforts with various spectroscopic techniques, judiciously labelled diagnostic substrates and by studies with synthetic metalloporphyrins (Denisov et al., 2005a; Mak and Denisov, 2017; De Montellano, 2015).

The canonical P450 reaction cycle is depicted in **Figure 1.1** and it starts with the resting state of the enzyme, the ferric low spin state (S=1/2), which is a result of the aquo- entity as the sixth ligand to the heme iron.

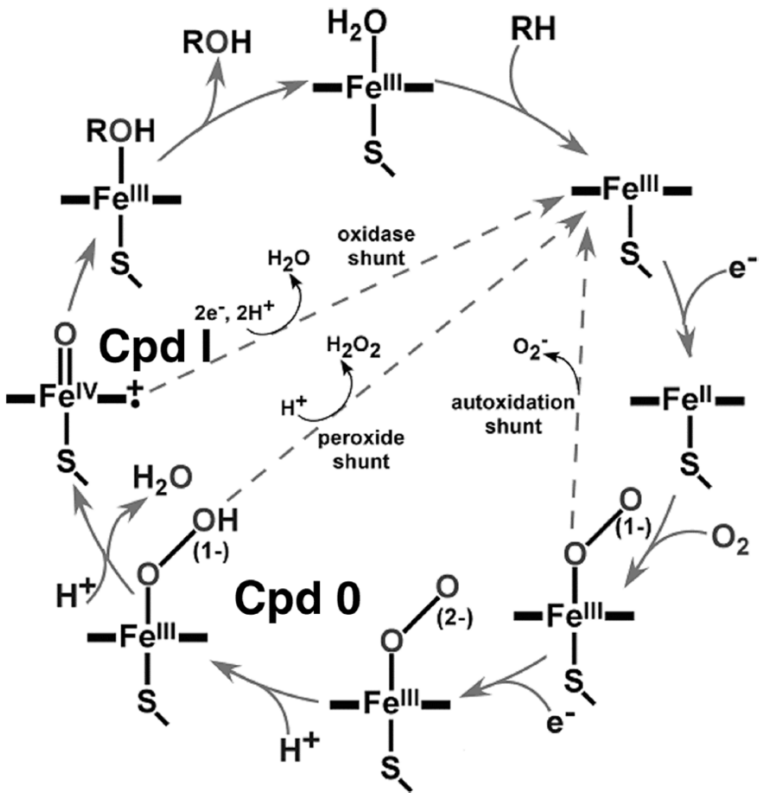

Figure 1.1: P450 catalytic cycle

(Denisov et al., 2005a)

Upon substrate binding, the water molecule gets partially or completely displaced, resulting in the formation of a ferric high spin heme iron (S=5/2). Substrate binding also makes the redox potential of the heme iron more positive (by 100-130mV), which then gets reduced by an associated redox partner, cytochrome P450 reductase (CPR) for microsomal P450s, and results in the formation of a ferrous complex. The ferrous complex immediately takes a molecule of oxygen and forms a ferrous-oxy state

(oxy-complex), which has a redox potential of ~0-20mV (Pompon and Coon, 1984). This intermediate is the last intermediate in the reaction pathway that can be easily observed and constitutes the first of three branch points in the P450 catalytic cycle. It can either unproductively decay to release a superoxide ion and form ferric form again, or consume another electron to pursue the productive path. Upon this second reduction, the oxy-complex forms a peroxo- anion species, which readily accepts a proton through the proton delivery pathway usually formed by an acid-alcohol pair of amino acids in the I-helix. This gives rise to hydroperoxo- form. The peroxo- and hydroperoxo- species are collectively termed compound 0 (Cpd 0). The hydroperoxo- species constitutes the second branch point between the productive and unproductive routes. It can either get protonated at the proximal oxygen and unproductively release a molecule of hydrogen peroxide returning to the ferric state, or it can get protonated at the distal oxygen to release a molecule of water and form a higher valent ferryl-oxo species, also called Compound I (Cpd I). Cpd I is a highly reactive species and is the third branch point in the cycle. Cpd I either takes up two electrons and two protons to produce a molecule of water and unproductively return to initial ferric state, or abstract a hydrogen molecule from the substrate and through an oxygen rebound mechanism (Groves and McClusky, 1976) insert an oxygen atom, forming the hydroxylated product before returning to the ferric low spin state.

The autoxidation and peroxide shunts result in the formation of superoxide ions and hydrogen peroxide, which are potentially harmful species and collectively are called reactive oxygen species (ROS). The unproductive pathways are collectively termed uncoupling pathways, and the rates at which uncoupling pathways occur determine the overall efficiency of the enzyme (Denisov et al., 2005a; De Montellano, 2015). Coupling efficiency varies in different P450 isozymes, and coupling depends on many factors, including substrate structure and orientation, efficiency and rate of proton delivery to the peroxo-anion species, and on the efficiency of electron transfer from associated redox partners.

1.3 P450s in hormone biosynthesis

Hormone biosynthesis in humans is a result of the steroidogenic pathway **(Figure 1.2)** that begins with the side chain cleavage of cholesterol to form pregnenolone (PREG) catalyzed by CYP11A1 in the mitochondrial inner membrane of adrenal cortical cells. PREG is transported out of the mitochondria to the endoplasmic reticulum where it can be converted to progesterone by a non-P450 3β-hydroxysteroid dehydrogenase (3β-HSD) enzyme. Both PREG and PROG are substrates for the androgenic CYP17A1, producing 17α-hydroxy products (OH-PREG and OH-PROG). These can be converted by CYP17A1 to androgens. PROG and OH-PROG can be shunted towards corticosteroid production, following hydroxylation at carbon-21 by CYP21A2, with PROG forming deoxy-corticosterone and OH-PROG giving rise to 11-deoxycortisol. These are then oxygenated by CYP11B1 to form corticosterone and the glucocorticoid cortisol, and the former is further acted upon by another P450, CYP11B2 to form the mineralocorticoid aldosterone. These enzymes are localized to the zona glomerulosa of the adrenal cortex. Mineralocorticoids are essential for maintenance of salt and water balance thereby ensuring blood pressure homeostasis.

It has been known since 1939 that estrogens are a product of androgen precursors (Nathanson et al., 1939). The androgens androstenedione and testosterone act as substrates for CYP19A1 which catalyzes a three-step reaction resulting in the formation of estrogens. The reactions catalyzed by CYP17A1 and CYP19A1 in the steroidogenic scheme from PREG and PROG onwards are discussed in the following sections.

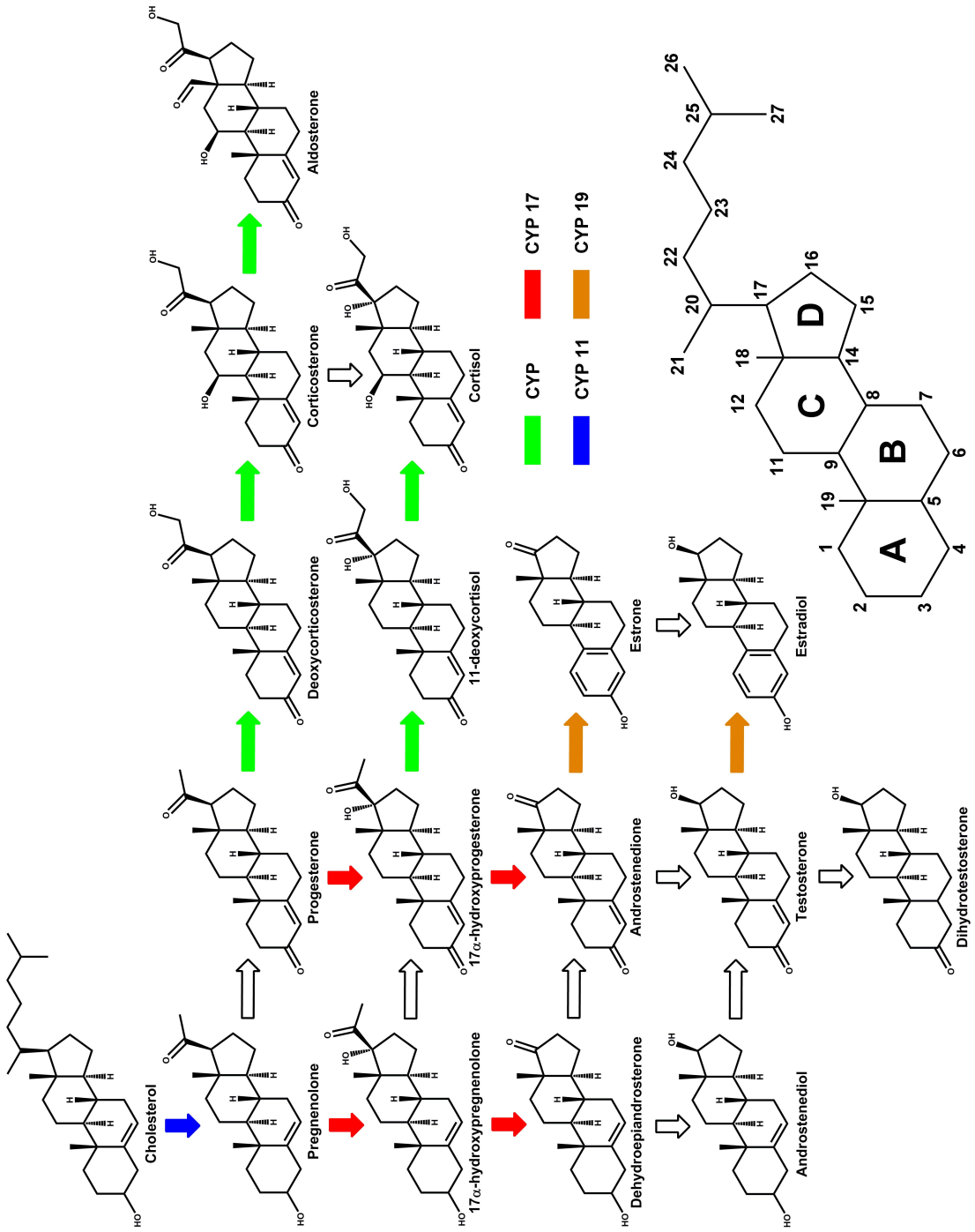

Figure 1.2: Steroidogenic pathway (red arrows depict CYP17A1 catalyzed steps, brown arrows represent CYP19A1 mediated reactions; green arrows represent reactions catalyzed by P450; open arrows represent reactions catalyzed by non-P450 enzymes).

(Gregory, 2016)

1.3.1. CYP17A1 mediated androgen synthesis:

CYP17A1 is a bifunctional enzyme sitting at the crossroads of corticoisteroid and androgen synthesis. It is expressed primarily in zona fasciculata and zona reticularis of adrenal cortex, Leydig cells of the testis and in small quantities in the brain, placenta and kidneys. CYP17A1 acts on PREG and PROG substrates and catalyzes the formation of OH-PREG and OH-PROG. Both these products and their substrates can be converted to corticosteroids, resulting in the formation of aldosterone, corticosterone and cortisol. OH-PREG and OH-PROG are also substrates for a subsequent reaction catalyzed by CYP17A1, in which the C17–C20 bond is cleaved to form androgenic products dehydroepiandrosterone (DHEA) and androstenedione (AD) respectively. These products can be converted to the active androgens- androstenediol and testosterone by 3β-HSD, or to estrogens by CYP19A1 according to the requirement in the body.

Prostate cancer affects millions in the United States each year, and more than 80% of the cases are driven by the action of androgens. Targeting disease progression in PC patients is accomplished by prevention of androgen synthesis by surgical castration or by blocking the hypothalamic-pituitary-gonadal (HPG) axis (chemical castration). This is called Androgen Deprivation Therapy (ADT) and is achieved by targeting the gonadotropin-releasing hormone (GnRH) receptor which ultimately inhibits androgen production in the testes. However, androgen production from adrenals still goes unhindered, which requires co-administration of androgen receptor (AR) antagonists. This treatment strategy is rarely curative since most patients relapse and advance to castration resistant prostate cancer (CRPC). If untreated, CRPC patients die in less than a year. Reports suggesting that CRPC remains dependent on AR signaling led to interest in therapeutics targeting the latter, invariably by strategies inhibiting CYP17A1 mediated androgen synthesis itself. In December 2012, the FDA approved abiraterone acetate (Zytiga® tablets, made by Janssen Biotech, Inc.), which is a type II binding inhibitor of CYP17A1 for use in CRPC patients. Abiraterone binds to the heme iron in CYP17A1 active site and as such prevents any activity of the enzyme. However, this treatment strategy is far from

perfect. In addition to inhibiting lyase reactions, this also results in inhibition of the 17α-hydroxylation activity, which is required for glucocorticoid synthesis and ablation of hydroxylation activity results in increased production of mineralocorticoids. This causes elevated levels of adrenocorticotrophic hormone (ACTH) and manifests as hypertension, hypokalemia and peripheral edema (Auchus, 2001). For this reason, treatment with abiraterone requires co-administration of a synthetic corticosteroid, prednisone (Stein et al., 2012).

Current efforts towards better therapeutics for CRPC patients focus on specific targeting of CYP17A1 lyase activity, without causing any effect on the essential hydroxylation reactions. Considering the stark differences between the two activities, a better mechanistic understanding provides hope for better therapeutics for CRPC. There is also a need for better anti-androgens for treating androgen excess in females suffering from polycystic ovarian syndrome (PCOS). PCOS is one of the most common metabolic disorders affecting women of reproductive age and is characterized by hyperandrogenism and ovulatory dysfunction, and is associated with metabolic syndrome, type 2 diabetes, insulin resistance and increased risk for cardiac disease. Current treatment options include anti androgen therapy with steroidal AR antagonist Cyproterone acetate combined with progestogens. However, this regimen is marred by serious adverse effects of thromboembolism and hepatotoxicity, as well as depression. Clearly, a better understanding of androgen synthesis would fulfill the need for improved therapeutics for PCOS patients suffering from androgen excess.

1.3.2. Mechanistic questions in CYP17A1 mediated androgen synthesis:

As mentioned in section 1.2.2 above, all P450 mediated hydroxylation proceeds through a ferryl-oxo intermediate called compound I, which abstracts a hydroen before inserting the active oxygen, resulting in the formation of a hydroxylated product. On the other hand, the mechanism of the CYP17A1 mediated scission of the carbon-carbon linkage has been a subject of intense research but

controversial. Akhtar and coworkers have suggested that while the hydroxylation and lyase reactions both occur in the same active site of the protein, they involve different iron-oxygen species. While hydroxylation proceeds through a ferryl-oxo (Cpd I) intermediate, lyase reaction involves a direct involvement of peroxo-anion species (Akhtar et al., 1994). This proposal has received some support over the years, but definitive proof had been wanting until 2015, when Gregory and Mak succeeded in spectroscopic isolation of an intermediate which was characterized to be the hemiketal intermediate formed as a result of peroxo-anion mediated nucleophilic attack on carbonyl-20 of OH-PREG (Mak et al., 2015). This was a seminal finding, a result of years of research probing the catalysis of DHEA formation from OH-PREG.

Initial indication of peroxo-anion mediated scheme being the major mechanistic route for this reaction came from the observation of inverse kinetic solvent isotope effect (KSIE) in this reaction (Gregory et al., 2013b). KSIE is the ratio of product turnover rates in protiated versus deuterated solvents. For most P450 catalyzed reactions observed KSIE is in the range 1.5 – 2.5, indicating rate-limiting protonation steps on the path to Cpd I formation. The unusual inverse KSIE in OH-PREG lyase reaction has been thought to stem from the ablation of proton dependent unproductive pathways (peroxide shunt and oxidase shunt) causing a decrease in uncoupling in reactions with deuterated components **(Figure 1.3)**. Resonance Raman spectroscopy is an impressive technique for investigating even minor changes in the vibrational modes of heme planar ring and more importantly in the diatomic ligands bound to the heme iron, information that is very useful for probing the mechanistic intermediates in the P450 cycle. Resonance Raman studies with CYP17A1 oxy-complex bound to OH-PREG and to OH-PROG showed that owing to different functional groups at 3β position in the A ring, the resulting conformation of these substrates near the O–O ligand bound to the iron is different, which may translate into major differences in the mechanism of catalysis of these two substrates (Gregory et al., 2013a). Moreover, OH-PREG was observed to be positioned such that the 17α-OH group donates a hydrogen bond to the proximal oxygen of the oxy-complex, whereas in the

case of OH-PROG a hydrogen bond was formed with the distal oxygen. This positioning of OH-PREG causes the distal oxygen of the oxy-complex to be in a position conducive to perform a nucleophilic attack on the carbonyl-20 of the substrate which would result in the formation of an acyl peroxo-iron (hemiketal) intermediate. Further indication came from optical spectroscopic investigation of reaction intermediates following thermal annealing of cryo-trapped peroxo-anion intermediate bound to OH-PREG, which strongly suggested that OH-PREG lyase chemistry does not proceed through Cpd I like PREG does, but rather through a different intermediate with an absorbance maximum at 405 nm (Mak et al., 2015).

Final proof that peroxo-anion species forms a hemiketal intermediate in OH-PREG chemistry came from resonance Raman measurements of thermally annealed cryo-trapped peroxo-anion intermediate bound to OH-PREG. While PREG bound peroxo-anion intermediate quickly proceeded to hydroperoxo species even at 77 K, with OH-PREG there was no hydroperoxo observed even at 165K. In order to follow the peroxo-anion in this case, a 406 nm excitation laser was used, a wavelength closer to the absorbance maximum of the new intermediate observed in optical annealing experiments. With this laser, a new intermediate was observed, which was H/D exchange independent and exhibited O–O vibrational modes similar to acyl-peroxo iron(III) species isolated in some non-heme reactions by Que and coworkers (Oloo et al., 2014). Definitive characterization of this intermediate as the proposed hemiketal intermediate came from oxygen isotope scrambling experiments, with a mixture of $^{16}O_2$, $^{16}O^{18}O$ and $^{18}O_2$. Using this gas mixture, it was convincingly shown that both the oxygen atoms in the proposed hemiketal intermediate came from an unbroken oxygen molecule. Had this intermediate been a result of ferryl-oxo mediated H-abstraction from 17α-OH, there wouldn't be a ^{18}O–^{18}O vibrational mode at all (Mak et al., 2015).

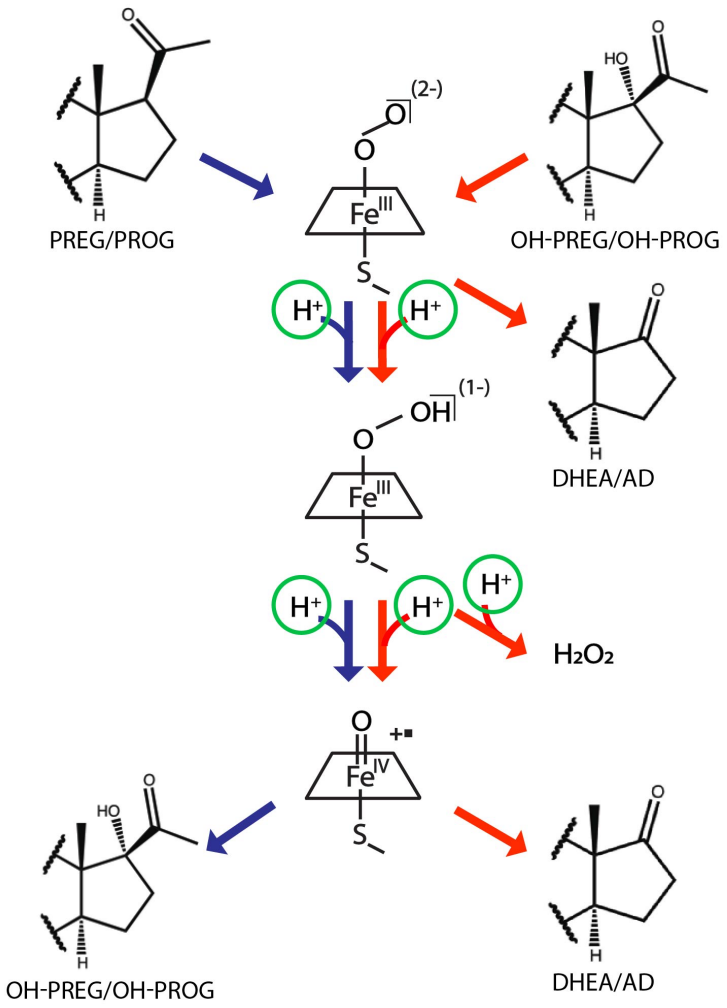

Figure 1.3: Distinction between CYP17A1 mediated mechanism of hydroxylation and lyase reactions highlighting the proton dependent steps. The blue arrows represent hydroxylase mechanism starting from peroxo-anion species resulting in the formation of compound I that forms the hydroxylated product and requires two protons. The red arrows represent the two possible hypotheses for lyase mechanistic pathway. The androgen product can be formed from peroxo-anion directly via a proton independent mechanism, or by the conventional compound I intermediate.

As mentioned above, in contrast to OH-PREG bound oxy-complex, OH-PROG bound oxy-complex has a different hydrogen bonding conformation. While the distal oxygen is free to attack the carbonyl-20 of OH-PREG, in OH-PROG the distal oxygen of the peroxo-anion would be less amenable for a similar reaction. This observation might have defining effects on the mechanism of OH-PROG lyase reaction, which might proceed through a Cpd I intermediate. Similar studies investigating the active intermediate in OH-PROG lyase reaction are lacking with homogeneous membrane bound full length human CYP17A1, whether this reaction follows a peroxo-anion mediated mechanism like OH-PREG, or if it proceeds through a conventional Cpd I intermediate.

1.3.3. Mechanism of cyt b_5 mediated modulation of androgen synthesis:

Another particularly intriguing aspect of CYP17A1 reactivity is its selective dependence on the membrane bound form of cyt b_5 for the lyase reaction, whereas hydroxylation reactions remain barely affected. Immuno-histochemical studies of the adrenal cortex have shown that cyt b_5 is expressed along with CYP17A1 in zona reticularis, the site that produces androgens but not corticosteroids, and not in zona fasciculata, where only corticosteroids are produced (Dharia et al., 2004; Suzuki et al., 1992). Additionally, the expression of cyt b_5 increases at the onset of adrenarche, correlated with increase in androgen production at these sites. The presence of membrane bound form of cyt b_5 has been known to selectively and significantly enhance the rate of the lyase reaction and is therefore important for maintaining normal levels of androgens (Sergeev et al., 2014). Mutations of R347, R358 and R449, the CYP17A1 surface residues involved in cyt b_5 binding results in impairment of lyase activity (Lee-Robichaud et al., 1998). Mice models with testicular Leydig cells lacking cyt b_5 show considerable loss of lyase activity (Sondhi et al., 2016). It is also known that male subjects lacking functional cyt b_5 present with pseudo hermaphroditism, while high cyt b_5 levels in adrenocortical

adenomas in Cushing's syndrome patients correlate with increased androgen synthesis (Sakai et al., 1994).

Cytochrome b_5 has been known to play a significant role in many P450 mediated reactions, fatty acid biosynthesis and hepatic drug metabolism (Oshino et al., 1971). For instance, Sato and co-workers suggested that the binding of cytochrome b_5 (cyt b_5) to cytochrome P450 elicited a structural change in the enzyme which activated product turnover, either by increasing the inherent catalytic rate or by inhibiting non-productive auto-oxidative shunt processes (Imai and Sato, 1977). Alternatively, as cyt b_5 contains a bis-imidazole coordinated heme, direct transfer of electrons from cyt b_5 to P450 has been proposed (Bonfils et al., 1981; Imai and Sato, 1977). In this role, the relatively high redox potential of cyt b_5 i.e. ~0 mV versus Normal Hydrogen Electrode (Rodgers and Sligar, 1991) suggests that electron transfer to ferric P450 (redox potential ~300 mV vs. NHE) is unfavorable. Hence it was suggested that the redox function of cyt b_5 involved electron transfer to the ferrous dioxygen intermediate which has a redox potential near 0 mV (Lipscomb et al., 1976) thus providing the second electron in the reaction chemistry. To differentiate between these two roles, Coon and co-workers reconstituted apo cyt b_5 with manganese protoporphyrin IX (Morgan and Coon, 1984). They found cytochrome P450 reductase (CPR) and NADPH could not reduce the manganese substituted cyt b_5, whereas iron cyt b_5 was rapidly reduced. Hence Mn b_5 is incapable of any electron transfer to the P450. They concluded that cyt b_5 effects depend on the specific P450 in question, the substrate being examined, and molar ratio of CPR to P450. This suggested that their observations could not be explained solely by a simple electron transfer role and some effects may also be caused by possible conformational changes caused by cyt b_5 binding.

The nature of this CYP17A1–cyt b_5 interaction has been controversial (Estrada et al., 2013; Im and Waskell, 2011; Sergeev et al., 2014; Zhang et al., 2007). Auchus and coworkers used apo b_5 and observed that it stimulated the lyase reaction in recombinant yeast, leading these workers to conclude that there is no redox role (Auchus et al., 1998). On the other hand, Estabrook and others

demonstrated in an in vitro reconstituted system in the presence of lipids that a zinc substituted cyt b_5 did not stimulate the lyase activity of CYP17A1, and that the previous reports of rate enhancement by apo b_5 are the result of transfer of the heme group from the P450 to apo b_5 forming the holoenzyme (Guryev et al., 2001). Conceivably, better understanding of this interaction between CYP17A1 and cyt b_5 is valuable from a therapeutic interest standpoint to specifically target androgen synthesis in diseased states.

Using solution NMR on soluble forms of both proteins and with the help of earlier mutagenesis experiments by the Akhtar group and others, Scott and co-workers have identified the cyt b_5 putative binding site on CYP17A1 surface (Estrada et al., 2013; Lee-Robichaud et al., 2004; Naffin-olivos and Auchus, 2006). As is the case with other P450s like CYP2B4, cyt b_5 is believed to occupy a binding site that is partially overlapping with that of CPR (Zhang et al., 2007). This finding raises interesting possibilities. If cyt b_5 is just an allosteric modulator, this would entail that when it binds to the CYP17A1 molecule, the associated conformational changes occur, but for catalysis to move forward, cyt b_5 has to be displaced by the CPR molecule to perform reduction of the P450. This would require that the CYP17A1 somehow 'remembers' the cyt b_5 modulated conformational changes even after the latter is unbound. On the other hand, if cyt b_5 acts as an electron partner for the second reduction, after CPR has carried out the first reduction, cyt b_5 could bind and along with any associated conformational changes, reduce the oxy-complex and result in a faster turnover cycle. In chapters 4 and 5, I have tried to answer this long-debated question, whether in CYP17A1 mediated lyase chemistry, cyt b_5 acts as a redox partner, an allosteric effector, or does it carry out a combination of both functions.

1.3.4. CYP19A1 mediated estrogen synthesis and mechanistic questions:

CYP19A1 (aromatase) enzyme, primarily expressed in ovaries, testes and brain, catalyzes the synthesis of estrogens from androgens in a three-step process. During this process, it consumes three

molecules each of NADPH and dioxygen per estrogen product molecule. CYP19A1 acts on a total of three androgenic substrates: androstenedione, testosterone and 16α-hydroxy-testosterone to produce the estrogenic products estrone, 17β-estradiol and estriol, respectively. Inactivating mutations of CYP19A1 have been known to result in pseudo-hermaphroditism in females and tall stature and delayed skeletal maturation in males (Jones et al., 2007). These symptoms can be reversed by estrogen replacement therapy. Mutations resulting in over activation of CYP19A1 are known to cause gynecomastia in males and a premature growth spurt but a decreased adult height (Shozu et al., 2003). Genetic mutations in CYP19A1 affecting estrogen synthesis are very rare. From the clinical standpoint, a more significant role of CYP19A1 lies in its involvement in estrogen dependent breast cancers in post-menopausal females.

After menopause occurs, the ovary is no longer the primary location of estrogen synthesis, instead the endothelial tissue, smooth muscle cells, skin and adipose tissue including the adipose tissue of breast take on this role. The estrogens synthesized here act in an autocrine or paracrine manner. Therefore, despite low circulating levels, the concentration of estrogen in the breast tissue of post-menopausal patients is several fold-higher than that in pre-menopausal women. Abnormally high estrogen levels in the breast can cause over-activation of estrogen receptor, which in turn can result in tumorigenesis. Majority of all breast cancers are either estrogen receptor dependent (ER+), or progesterone receptor dependent or both. In order to intervene ER+ cancers, ER antagonists such as Tamoxifen have been in clinical use for about 4 decades (Willis et al., 1977). Unfortunately, Tamoxifen therapy suffers from severe side effects, viz. increased risk for endometrial cancer, thromboembolism and stroke, and patients have been seen to relapse even decades after their initial treatment. Another therapeutic strategy is to inhibit CYP19A1 using exemestane, anastrozole or letrozole, a class of compounds that act as competitive inhibitors of the enzyme by binding irreversibly in the active site. CYP19A1 inhibitors have fewer side effects as compared to Tamoxifen therapy, but the patients are still at risk for heart disease and osteoporosis. Increased understanding of CYP19A1 molecular mechanism will help guide

efforts towards better mechanism based CYP19A1 inhibitors for improving prognosis in ER+ breast cancers.

Each CYP19A1 mediated estrogenic reaction proceeds through three sequential steps as depicted in **Figure 1.4.** Step I involves hydroxylation at the C-19 position, step II is another hydroxylation on C-19 position, the resulting geminal hydroxy product undergoes dehydration to form a 19-aldehyde. Step III comprises scission of C10–C19 bond, resulting in aromatization the A-ring of the steroid substrate and loss of C19 as a molecule of formic acid (Akhtar and Skinner, 1968; Akhtar et al., 1993; Braselton et al., 1974; Ghosh et al., 2010; Lo et al., 2013; Thompson Jr. and Siiteri, 1974). Similar to CYP17A1, the CYP19A1 mediated hydroxylations during the step I and II reactions are generally believed to proceed through the conventional high-valent Fe(IV)–O species, Cpd I. However, the mechanism of the third step has been controversial.

There are two hypotheses: a conventional Cpd I intermediate formed as a result of two subsequent protonations of peroxo-anion species would abstract 1β-hydrogen from the A-ring of 19-oxo substrate, this would initiate aromatization and loss of formic acid side product after C10–C19 bond scission. Alternatively, a mechanism involving direct interaction of peroxo-anion with the 19-aldehyde functionality has been proposed, in which the peroxo-anion is stabilized by the electrophilic carbonyl-19 of the substrate **(Figure 1.5)**. It is proposed that 19-oxo substrate binding causes some displacement of the Thr 310 of the “acid-alcohol pair”, which in turn results in disruption of proton delivery to the peroxo-anion (Graham-lorence et al., 1995). The latter species, now transiently stabilized, could carry out a nucleophilic attack on C19, making a peroxide adduct that would undergo decomposition resulting in aromatized A-ring of the substrate and release of formic acid side product (Akhtar et al., 1982).

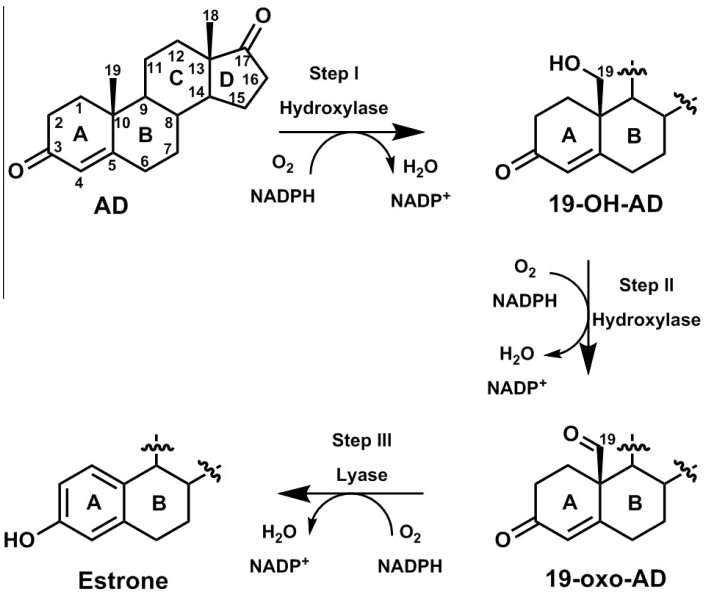

<u>Figure 1.4:</u> CYP19A1 mediated synthesis of estrogen from androgen precursor involves three steps: hydroxylation at C-19 (step I); second hydroxylation at C-19 followed by dehydration (step II); C10–C19 bond scission (step III).

(Khatri et al., 2014a)

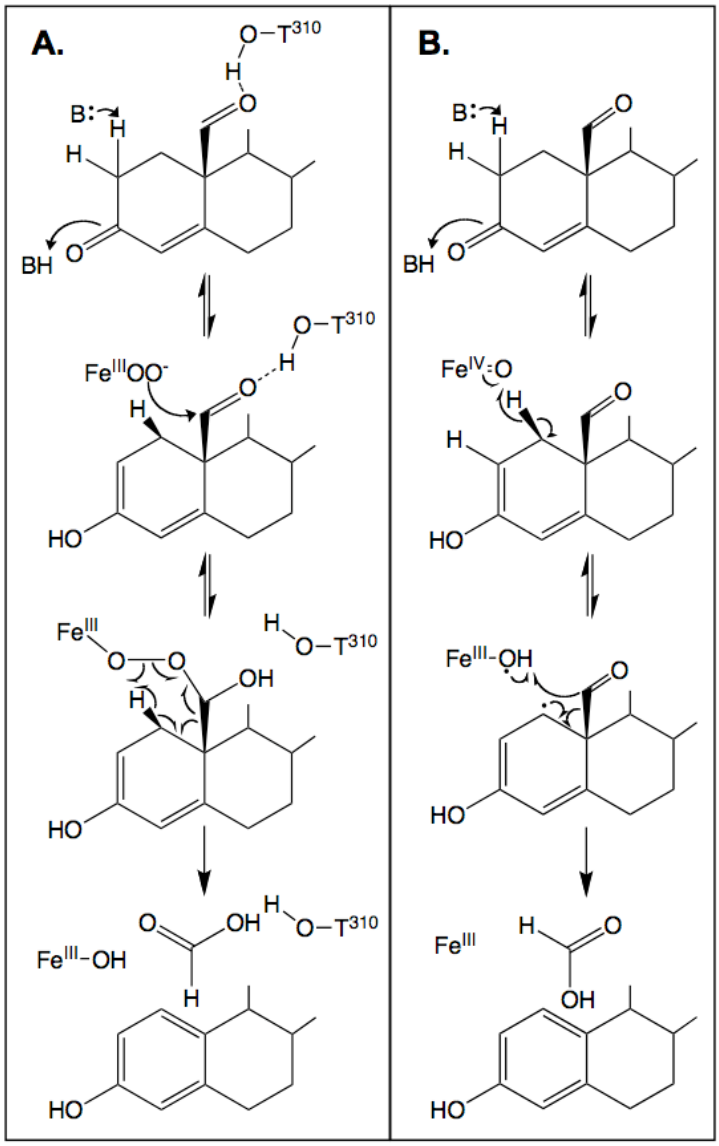

Figure 1.5: Possible hypotheses for the mechanistic pathway in CYP19A1 mediated estrogen synthesis: Peroxo-anion mediated mechanistic pathway (A); Compound I mediated mechanistic pathway (B).

(Luthra, 2015)

Considering the significance of the reactions catalyzed by CYP19A1 for human health, and its similarity to CYP17A1 lyase chemistry, I decided to investigate reaction mechanism for CYP19A1 lyase reaction, whether the key mechanistic intermediate in this reaction is Cpd I or peroxo-anion species (Cpd 0).

1.4 Nanodisc technology

1.4.1. Challenges in the study of membrane proteins:

Membrane proteins are involved in a variety of essential cellular processes, including signal transduction, cell adhesion, metabolite transport, oxidative phosphorylation and ATP synthesis, lipids and steroid biosynthesis, and xenobiotic detoxification among other roles. In vitro study of membrane proteins has proven to be challenging historically, major reason being the problems caused by working outside of the native membrane environment. Most biophysical tools like X-ray crystallography, optical spectroscopy, NMR, circular dichroism, ligand binding assays etc. that have been applied widely and easily to soluble proteins, fail in the case of membrane bound proteins, on account of their limited solubility in aqueous solutions. For ease of purification as well as application to the aforementioned biophysical and biochemical techniques, a solubilized state of the protein of interest is desirable. To this end, a variety of methods have evolved over the years.

One strategy to employ these techniques on insoluble membrane proteins is by expressing the protein devoid of its membrane anchor region, or by making use of agents that can help solubilize the membrane proteins. Clearly, a membrane protein devoid of its membrane anchor does not present as a perfect model for the native membrane associating, lipid interacting protein. Moreover, recent research has provided mounting evidence that membrane lipids and proteins are not randomly distributed, but are found in highly organized domains that are central to the functions of the membrane

proteins (Kusumi et al., 2012). However, while the use of detergents helps to maintain the complete protein in a solubilized state and often eliminates the undesirable oligomerization, this system is a poor mimic of the native lipid environment of the membrane proteins. Furthermore, although some membrane proteins retain native like activity in detergent micelles, oftentimes detergents can be destabilizing and cause protein denaturation. In the case of P450s, some detergents with structures similar to the native substrates can bind in the active site and interfere with ligand binding and turnover assays (Annalora et al., 2010; Shah et al., 2016). Another challenge in designing an in vitro system that is a good model for the native biology of membrane proteins is the role of phospholipids in the activity and downstream functions of the proteins. Examples of such critical protein-lipid interactions include interaction of membrane proteins with anionic lipids to activate blood coagulation events, signaling processes, cell migration among others (Shaw et al., 2007; Tavoosi and Morrissey, 2014; Ye et al., 2016a, 2016b). Furthermore, membrane proteins devoid of a membrane environment may display lack of, or altered activities. For this reason, several systems incorporating lipids in contact with the membrane proteins have been developed over the years. The simplest of these are mixed lipid detergent systems, in which the hydrophobic regions of the membrane proteins are solubilized in contact with the hydrophobic chains of lipid solution in detergent. Although an improvement over the use of only detergent micelles/bicelles, this system is far from perfect, in that some aggregation events may still occur causing decrease in protein activity, making this system less reproducible.

Phospholipid vesicles (liposomes) have been used to reconstitute membrane proteins in a membrane environment. These have proven to be useful for larger protein complexes in which mobility within a membrane is essential, and removal of detergents results in better stability of the reconstituted proteins. However, the use of liposomes comes with some caveats, the resultant solutions in many cases are turbid and viscous, and may result in precipitation over time. Moreover, in the case of integral membrane proteins, vesicles only provide access to one side of the protein and it is very difficult to control stoichiometric ratios of reacting proteins in this system. Despite these challenges, study of

membrane proteins remains an active field owing to their significant roles in a huge number of biological processes and being a target of >50% of drugs in the market (Bull and Doig, 2015).

1.4.2. Nanodiscs to incorporate functional membrane protein complexes:

Nanodiscs provide an exceptional alternative to the aforementioned reconstitution systems for membrane proteins. A nanodisc is a discoidal lipid bilayer encircled by a "membrane scaffold protein" (MSP) which is a derivative of naturally occurring amphipathic plasma lipoprotein ApoA-I. Since their inception in our lab ~15 years ago (Bayburt et al., 2002), nanodiscs have been applied to the studies of a variety of membrane proteins including cytochromes P450, G-protein coupled receptors, integrins, transporters, bacteriorhodopsin, blood coagulation factors, K-Ras and respiratory proteins (Gingras et al., 2013; Gregory et al., 2017; Lamichhane et al., 2015; Luthra et al., 2013; Morrissey et al., 2009; Ye et al., 2016a). Membrane scaffold proteins (MSPs) are α-helical proteins, the original sequences of which were derived from human ApoA-I lipoprotein. There are a variety of ways in which MSP sequences can be manipulated to achieve desired nanodisc size (from 8 nm to 17 nm), or selective labeling for fluorescence quenching experiments with removal of background fluorescence ("dark MSP") etc (Grinkova et al., 2010b). In addition to the many benefits of this technology, the procedure for their assembly is elegantly simple **(Figure 1.6)**. Purified (or partially purified) membrane protein target is incubated with lipids solubilized in the detergent of choice in the presence of desired MSP variant, and upon gradual removal of detergent using Biobeads or by dialysis, spontaneous formation of nanodiscs with membrane protein incorporated in the lipid bilayer in its correct conformation occurs.

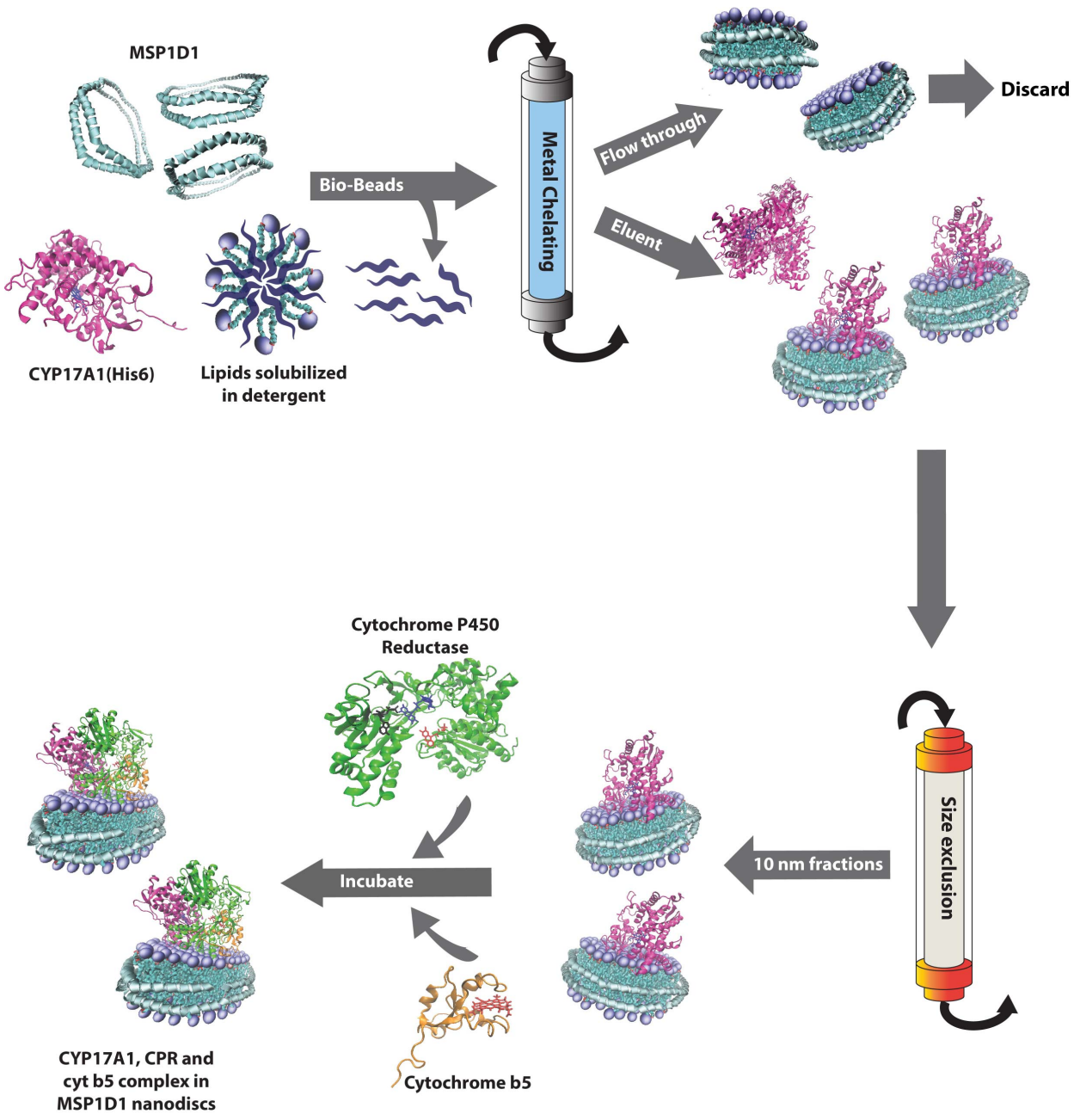

Figure 1.6: **Nanodisc assembly process to incorporate His-tagged CYP17A1 in POPC lipids encircled by MSP1D1 followed by complex formation with CPR and cytochrome b_5.**

A plethora of techniques can now be successfully applied to membrane proteins using this technology, including but not limited to: resonance Raman, optical absorption spectroscopy, NMR, EPR, membrane interaction studies using SPR, AFM, cryo-EM, small angle X-ray scattering, studies of membrane association effects on redox potentials of redox active proteins, and investigation of drug-drug interactions (Bayburt et al., 1998; Das et al., 2007; Denisov et al., 2005b; Efremov et al., 2014; Laursen et al., 2014; Mak et al., 2011; Sligar et al., 2007; Zhang et al., 2015). A few unconventional ways in which the nanodisc technology has been employed are their use as drug delivery agents, vaccines for influenza and personalized cancer immunotherapy, cell free expression of various membrane proteins, and optical imaging agents to monitor drug disposition (Bhattacharya et al., 2010; Carney et al., 2015; Duivenvoorden et al., 2014; Kuai et al., 2016; Rues et al., 2014). Given the many advantages of this system, we used nanodiscs to reconstitute the membrane bound forms of CYP17A1, cyt b_5, CPR and CYP19A1 in all our experiments. A depiction of an MSP1D1 nanodisc with the incorporated P450 in complex with CPR and cyt b_5 is shown in **Figure 1.7**.

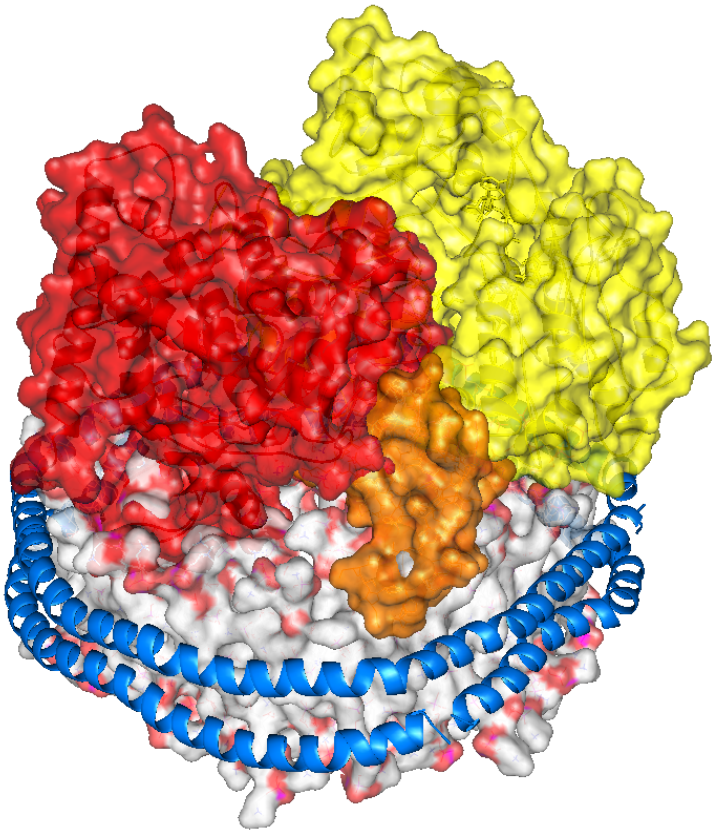

<u>Figure 1.7:</u> A depiction of MSP1D1 nanodisc with incorporated P450–CPR–cytochrome b_5 complex: P450: red, CPR: yellow, cyt b_5: orange, MSP1D1: blue helices.

(Ilia Denisov, unpublished)

Chapter 2

Mechanistic Investigation of CYP17A1 catalyzed Androstenedione Synthesis

2.1 Introduction

As described in section 1.3.1, CYP17A1 acts on 17-hydroxy-pregnenolone and 17-hydroxy-progesterone to form the androgenic products dehydroepiandrosterone (DHEA) and androstenedione (AD) respectively. It has been shown recently that in the case of OH-PREG, the reaction proceeds through an unconventional hemiketal intermediate formed as a result of nucleophilic attack of peroxo-anion on the carbonyl-17 (Mak et al., 2015). To investigate whether the alternate lyase reaction that involves the synthesis of AD from OH-PROG follows this unique chemistry, or the conventional Cpd I reactive intermediate, I measured kinetic solvent isotope effects on steady state product turnover of OH-PROG. From **Figure 1.1**, it is clear that the formation of Cpd I requires at least two protons whereas peroxo-anion species is formed independent of protons. The differential requirement of protons between the two potential reaction mechanisms is therefore exploited using this technique (Gregory et al., 2013b; Vidakovic et al., 1998).

In order to investigate the reaction mechanism, the various mechanistic intermediates around the P450 catalytic cycle can be explored by various spectroscopic techniques. By investigating the identity of species that appear following formation of peroxo-anion in CYP17A1 bound to OH-PROG, the active mechanistic intermediate can be determined. However, intermediates following the oxy-complex in the catalytic cycle are extremely short lived and accumulating these highly oxidizing species in amounts

sufficient to be amenable to biophysical characterization is not trivial. This obstacle was overcome by Symons and coworkers by the development of cryoradiolytic reduction (Kappl et al., 1985; Symons and Petersen, 1978), and further refined by other groups to be applied to various techniques including EPR, ENDOR, UV-Vis and most recently to resonance Raman spectroscopies (Davydov, 1980; Denisov et al., 2008; Makris et al., 2002). This technique involves freeze-trapping the oxy-complex in an aqueous solution containing glycerol, followed by irradiation with γ-rays at 77 K. This produces free electrons and organic radicals, of which only electrons are mobile at this temperature. Hence one electron reduction of the Fe–O–O fragment is achieved, giving rise to the peroxo-anion intermediate, which remains stable at 77 K while protons are generally immobilized. Upon gradual warming (thermal annealing) of the entrapped reactive complex, molecular mobility improves and the next intermediate in the pathway can be identified using spectroscopic techniques **(Figure 2.1)**. Using this method, considerable accumulation of highly reactive species can be achieved which can be then be applied for various mechanistic studies (Denisov et al., 2002). Here, I used UV-Vis spectroscopy to identify the species following peroxo-anion intermediate in substrate bound CYP17A1 on the basis of their optical signature.

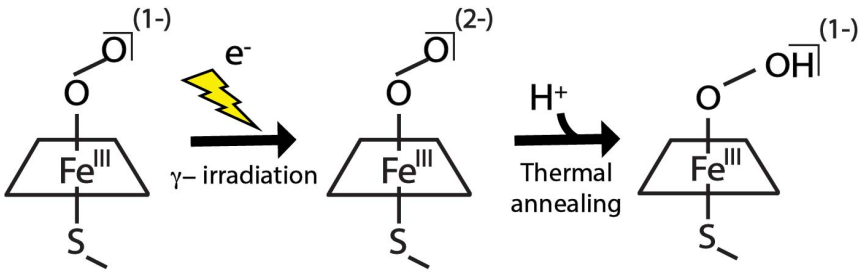

Figure 2.1: Schematic representation of cryo-radiolytic reduction of oxy-ferrous intermediate and thermal annealing. Upon γ-irradiation, reduction occurs resulting in the formation of peroxo-anion species. When temperature is increased, the next intermediate in the pathway is formed.

2.2 Materials and methods

2.2.1 Heterologous expression and purification of recombinant proteins:

- **CYP17A1:**

Full length human CYP17A1 synthetic gene with a His_6 tag at the C terminus was incorporated in pCWori vector with ampicillin resistance marker and co-transformed with GroEL/ES chaperone system (Takara Bio) into E. coli DH5α. Cells were grown in LB-agar (LA) plates with 100 μg/mL ampicillin and 20 μg/mL chloramphenicol following which transformation was confirmed by 1% agarose gel electrophoresis on overnight lysogeny broth (LB) cultures. A fresh LA plate was streaked and grown overnight, from which 50mL starter cultures were inoculated. After growing for 8-12 hours at 37 ^{o}C, 1 mL of this culture was used to inoculate 1 L of terrific broth (TB) medium with ampicillin, chloramphenicol, thiamine and Bracken's trace metal solution. The cells were grown at 37 ^{o}C until OD (600 nm) of 0.4 was attained. At this point, heme precursor δ-aminolevulinic acid (δ-ALA) was added at a final concentration of 1 mM and the culture transferred to 27-29 ^{o}C. When OD of 0.7-0.9 was reached at 600 nm, 1 mM isopropyl-β-D-1-thiogalactopyroside (IPTG) and 4 mg/mL L-arabinose were added as inducers of CYP17A1 and GroEL/ES respectively. The culture was then grown for 48 hours after which the cells were pelleted by centrifugation and stored at -80 ^{o}C.

Frozen cell pellet was broken and re-suspended in lysis buffer containing 0.1 M KPi (pH 7.4), 50 mM NaCl, 20% v/v glycerol, 50 μM progesterone, 10 mM β-ME, 0.5 mM PMSF, 0.1 mg/mL lysozyme, 0.1 mg/mL DNase and RNase. This solution was stirred at 4 ^{o}C for 30-60 min. Following this, the sphaeroplasts obtained were lysed by sonication for 15 min using 0.5 cm tip, 0.6 power and 70% duty cycle. The membranes were pelleted by ultracentrifugation at 30,000 rpm for 30 min. at 4 ^{o}C and re-suspended in membrane solubilization buffer containing 0.1 M KPi (pH 7.4), 0.5 M NaCl, 20% v/v glycerol, 50 μM progesterone, 10 mM β-ME, 0.5 mM PMSF and 1% Triton X-100. This suspension

was stirred at 4 ^{o}C for 1-2 hours. Insoluble fraction was pelleted by ultracentrifugation at 30,000 rpm for 30 min. The supernatant was applied to charged Ni-NTA resin equilibrated with 0.1 M KPi (pH 7.4), 0.5 M NaCl, 20% glycerol, 50 μM progesterone, 10 mM β-ME and 1% Triton X-100. The column was then washed with buffer A containing 0.05M Tris (pH 7.4), 0.3 M NaCl, 20% v/v glycerol, 50 μM progesterone, 10 mM β-ME and 0.02% v/v Emulgen 913 to remove unbound materials. A second wash with buffer B containing 20mM $MgCl_2$, 5 mM ATP and 50 mM Imidazole in buffer A was done to remove chaperones bound to CYP17A1 and non-specific binding agents. Following this step, CYP17A1 was eluted using buffer E containing 300mM imidazole in buffer A and colored fractions collected, pooled and dialyzed against 100x volume of buffer D containing 0.1 M KPi, 50 mM NaCl, 20% v/v glycerol, 50 μM progesterone and 10 mM β-ME (3 exchanges). The dialyzed protein was then concentrated using Amicon centrifugal concentrators with 10,000 MWCO and flash frozen before being stored at -80 ^{o}C. Purity of CYP17A1 was ascertained by the observation of a single band in SDS-PAGE and quantification done using UV-Vis spectroscopy with extinction coefficient of 100 $mM^{-1}cm^{-1}$ at 390 nm for PROG bound CYP17A1.

- **Cytochrome P450 reductase (CPR):**

Rat full length CPR in pOR262 plasmid obtained from Dr. Todd D. Porter (University of Kentucky, Lexington, KY) was expressed and purification was performed as described elsewhere (Shen et al., 1989). Briefly, after sonication of lysozyme treated cells, membrane fraction was obtained by ultracentrifugation and then lysed with 0.2% w/v Triton X-100 in buffer containing to 50 mM Tris (pH 7.7), 0.5 M NaCl, 0.1 mM DTT, 0.1 mM EDTA and 20% v/v glycerol. Supernatant obtained upon ultracentrifugation of this suspension was applied to ADP-agarose column equilibrated with column buffer containing 50 mM Tris (pH 7.7), 0.1% w/v Triton X-100, 0.1 mM DTT, 0.1 mM EDTA and 20% v/v glycerol. The column was washed with 2.5 mM Adenosine in column buffer and CPR was eluted

with 2 mM AMP in column buffer. The eluent was then applied to DEAE-sepharose column and washed with DEAE buffer (10 mM Tris pH 7.7, 0.1 mM EDTA, 0.1 mM DTT and 20% v/v glycerol) to eliminate Triton X-100 by monitoring OD of eluent at 275 nm. Following complete removal of detergent, CPR was eluted by using 0.4 M NaCl in DEAE buffer and yellow colored fractions obtained. Pooled fractions were rigorously dialyzed against buffer containing 50 mM KPi (pH 7.4), 20% v/v glycerol and 0.1 mM DTT. Spectroscopic characterization of purified CPR was done by using Rz ratio (A276 nm/A456 nm) of 8.7 and concentration was determined using an extinction coefficient of 24.1 $mM^{-1}cm^{-1}$ at 456 nm (Porter et al., 1987; Vermilion and Coon, 1978).

- **Cytochrome *b_5* and Membrane scaffold protein (MSP1D1):**

Full length rabbit cytochrome *b_5* and MSP1D1 were expressed and purified as described (Baas et al., 2004; Denisov et al., 2004; Mulrooney and Waskell, 2000)**.**

2.2.2 Incorporation of CYP17A1, CPR and cyt *b_5* in nanodiscs:

Purified CYP17A1 was incorporated into POPC nanodiscs as reported previously (Gregory et al., 2013a). For KSIE measurements, four times molar excess excesses of CPR and cyt *b_5* were used to incorporate into the CYP17A1 containing nanodiscs as described (Grinkova et al., 2010a). In order to test whether the presence of cyt *b_5* affects the KSIE for OH-PROG, reactions were carried out both in the presence and absence of cyt *b_5*, and then compared to the control reaction set with the hydroxylation substrate PROG. For CYP17A1 reactions with OH-PROG as substrate without cyt *b_5* present, co-incorporation of redox partners was done using 430.5 pmoles of CYP17A1 in nanodiscs incubated with 1722 pmoles of CPR, and in reactions with cyt *b_5*, the 242.8 pmoles of CYP17A1 was incubated with 971.2 pmoles each of CPR and cyt *b_5*. For the PROG reactions without cyt *b_5*, 419.4

pmoles of CYP17A1 was mixed with 1678 pmoles CPR whereas for reactions with cyt b_5, 209 pmoles of CYP17A1 was incubated with 838.8 pmoles each of CPR and cyt b_5.

2.2.3 Determination of steady state kinetic solvent isotope effect on CYP17A1 catalysis:

Briefly, 1 mL of CYP17A1 nanodiscs with co-incorporated redox partners in 0.1 M potassium phosphate buffer pH/pD 7.4, 50 mM NaCl with 50 μM of corresponding substrate (PROG or OH-PROG) was taken in a 1 mL stirred quartz cuvette with a path length of 0.4 cm. For deuterated buffers, pH value was corrected as pD = pH + 0.40 (Glasoe and Long, 1960). The sample was brought to 37 ^{o}C and reaction was initiated by addition of 600 nmoles NADPH. The reaction was allowed to proceed for 15 min while monitoring NADPH consumption using absorbance at 340 nm. At this point, the reaction was quenched by adding 8.9 N sulfuric acid, transferred to a 1.5 mL tube, flash frozen in liquid nitrogen and stored at -80 ^{o}C until analysis. When ready for analysis, 1.5 μL of 10 mM cortexolone solution in methanol was added as an internal standard to 800 μL each of the thawed samples. The tubes were vortexed for 30 seconds to ensure complete mixing, and extraction of organics was done by adding 2 mL dichloromethane. Upon phase separation, lower organic phase was aspirated, transferred to a fresh tube, and the solvent dried under a stream of nitrogen. The dried analytes for PROG reactions were dissolved in 100 μL methanol and 40 μL of this solution was injected to an equilibrated ACE-3 C-18 column (150 x 2.1mm) on HPLC (Waters) and resolved using 45% each of methanol and acetonitrile in water as mobile phase at a flow rate of 0.2 ml/min. The product OH-PROG was separated on a linear gradient of methanol and acetonitrile from 20% to 80% and detected at 240 nm. Peak integration was done in Millennium software (Waters). For analysis of AD product from reactions starting with OH-PROG substrate, similar extraction procedure was followed, except that the product analysis was done using HPLC system (Shimadzu) and peak integration performed using

LabSolutions software (Shimadzu). KSIE was calculated as the ratio of product turnover rate in protiated buffer to that in deuterated buffer.

2.2.4 Cryo-radiolysis and optical annealing to follow reaction intermediates:

CYP17A1 nanodiscs sample in 0.1 M potassium phosphate (pH 7.4), 15% v/v glycerol and 400 μM substrate (PROG/OH-PROG) was taken and deaerated under a stream of argon. The sample was then reduced anaerobically with 1.5-fold excess of sodium dithionite in the presence of $1/40^{th}$ molar amount of methyl viologen as redox mediator. Complete reduction of the samples was ensured by monitoring optical spectra using Ocean Optics spectrophotometer placed inside the anaerobic chamber. The ferrous samples were then rapidly injected into oxygen saturated solution of 67.5% v/v glycerol in 0.1 M KPi pH 7.4 in a methacrylate cuvette kept at 243 K in a dry ice-ethanol bath. The final concentration of CYP17A1 was ~30 μM and glycerol was 60% v/v. After mixing for 25 seconds, the cuvette was transferred to a second dry ice-ethanol bath maintained at 213 K. The cuvette was then transferred to our house-made cryostat **(Figure 2.2)** maintained at 77 K with liquid nitrogen and fit into a Cary 300 spectrophotometer. The visible spectrum was recorded to confirm efficient production of the oxy-complex. The cuvette with frozen oxy-complex was stored immersed in liquid nitrogen. This temperature is much lower than the glass transition temperature of the solvent, and the samples at this temperature remain stable for months. These were then irradiated with 4 Mrad dose of γ-rays in a Gammacell 200 ^{60}Co source on campus while immersed in liquid nitrogen. Radiolytic fragmentation of solvent molecules results in formation of hydrogen atoms, hydroxyl radicals, hydrated electrons, CO, aldehydes, ketones, alkanes and alkenes through spur reactions. At 77 K, except the hydrated electrons, all the radiolytic products are immobilized. It has been shown previously that the solvated electrons produced following 4-6 Mrad doses are optimal for cryolytic reduction of metalloproteins (Denisov et al., 2007a).

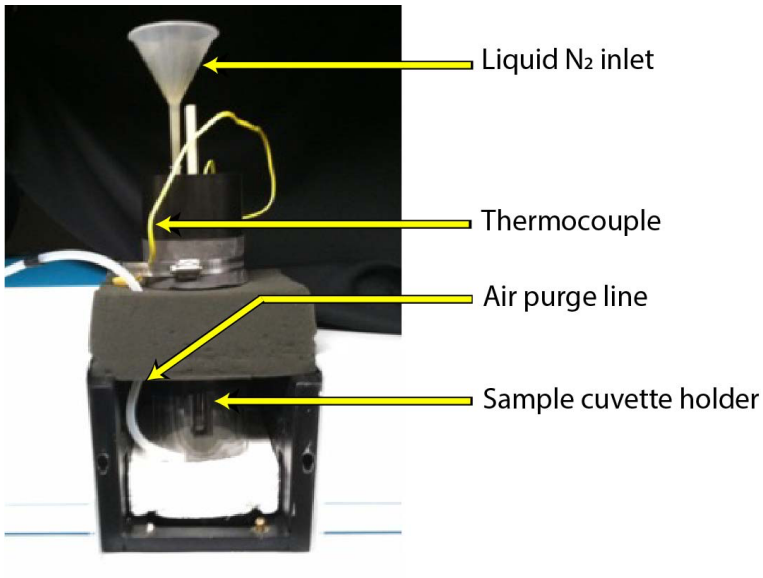

Figure 2.2: Home built cryostat setup fit into Cary 300 spectrophotometer for optical annealing experiments. Assembled by Dr. Ilia Denisov as described elsewhere (Denisov et al., 2002).

The samples while still immersed in liquid nitrogen were photo-bleached for ~5 min using a 100 W tungsten-halogen lamp. The cuvette was then transferred to cryostat maintained at 77 K and spectra were collected with Cary 300 spectrophotometer as the temperature was gradually increased.

2.3 Results

2.3.1 Effect of H_2O vs. D_2O on the steady state turnover in CYP17A1 catalysis:

When PROG was used as the substrate without any cyt b_5, the hydroxylated product OH-PROG was produced at a rate of 4.63 ± 0.05 min^{-1} in reactions with protiated buffer, and at a rate of 3.12 ± 0.06 min^{-1} in deuterated reactions. When cyt b_5 was present in PROG hydroxylation reactions, the product OH-PROG was obtained at a rate of 4.01 ± 0.01 min^{-1} in protiated reactions, and at a rate of 2.40 ±

0.01 min^{-1} in deuterated reactions. These turnover numbers translate to a KSIE of 1.5 in reactions without cyt b_5, and 1.7 in reactions with cyt b_5 **(Figure 2.3)**. This is an expected result, since the CYP17A1 mediated hydroxylation of PROG is generally accepted to proceed through the proton dependent Cpd I pathway.

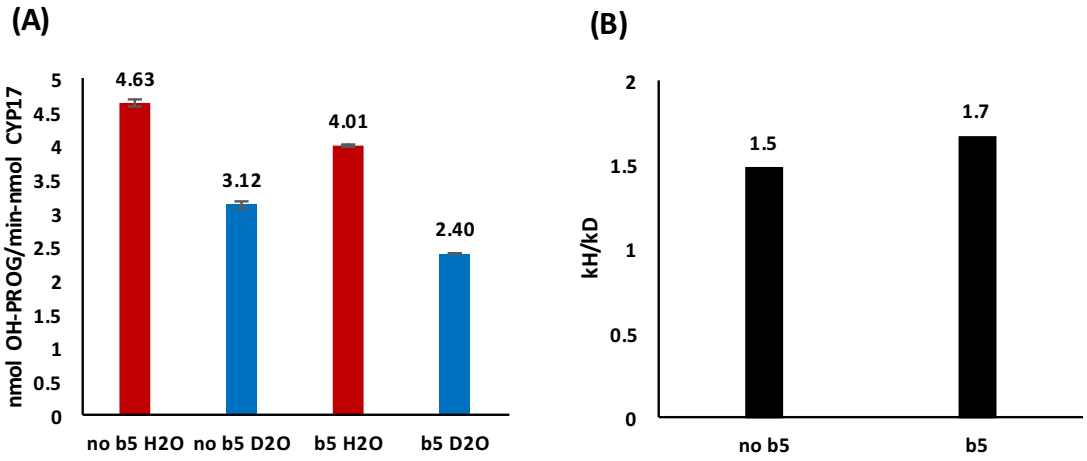

Figure 2.3: Product turnover rates expressed as nmol product formed per nmol CYP17A1 per min. for PROG hydroxylation in H_2O and D_2O in the absence and presence of cyt b_5 (A); Kinetic solvent isotope effect calculated as k_H/k_D in the absence and presence of cyt b_5 (B).

On the other hand, for reactions using OH-PROG as starting substrate without cyt b_5, the product AD was obtained at a rate of 0.11 ± 0.005 min^{-1} in protiated reactions, and at a rate of 0.12 ± 0.006 min^{-1} in deuterated reactions. For reactions with OH-PROG in the presence of cyt b_5, product AD was obtained at 0.26 ± 0.008 min^{-1} in protiated reactions, and at a rate of 0.32 ± 0.009 min^{-1} in deuterated reactions. These observations amount to a KSIE of 0.9 in reactions without cyt b_5, and 0.8 for reactions with cyt b_5 for OH-PROG lyase reaction **(Figure 2.4)**.

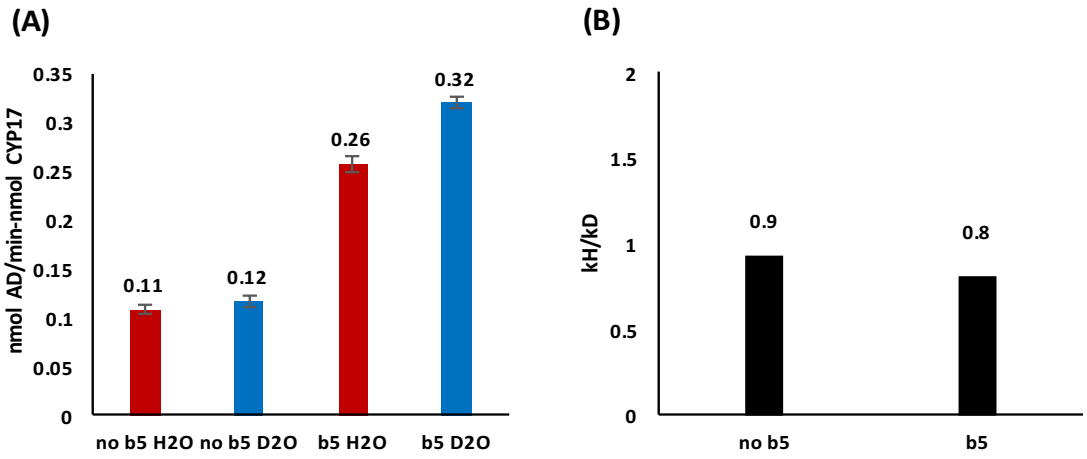

Figure 2.4: Product turnover rates expressed as nmol product formed per nmol CYP17A1 per min. for OH-PROG lyase in H_2O and D_2O in the absence and presence of cyt b_5 (A); Kinetic solvent isotope effect calculated as k_H/k_D in the absence and presence of cyt b_5 (B).

2.3.2 Optical spectroscopic isolation of active intermediate in androstenedione synthesis:

Optical spectra were obtained upon thermal annealing of PROG or OH-PROG bound CYP17A1 peroxo-anion species from 77 K to 185 K. It is expected that any hydroperoxo- species present would have an absorption maximum similar to that of peroxo- species, i.e. ~440 nm (Denisov et al., 2001). The results for PROG bound samples are depicted in the form of difference spectra from 160 K to 185 K with negative absorption band at 439 nm, corresponding to the disappearance of peroxo-anion species, with a positive absorption band at 413 nm concomitant with the appearance of a ferric like species (**Fig. 2.5 left panel**). When OH-PROG bound peroxo-anion species was annealed, the disappearance of peroxo-anion intermediate was accompanied by appearance of a very distinct species with absorption peak at 407nm (**Fig. 2.5 right panel**).

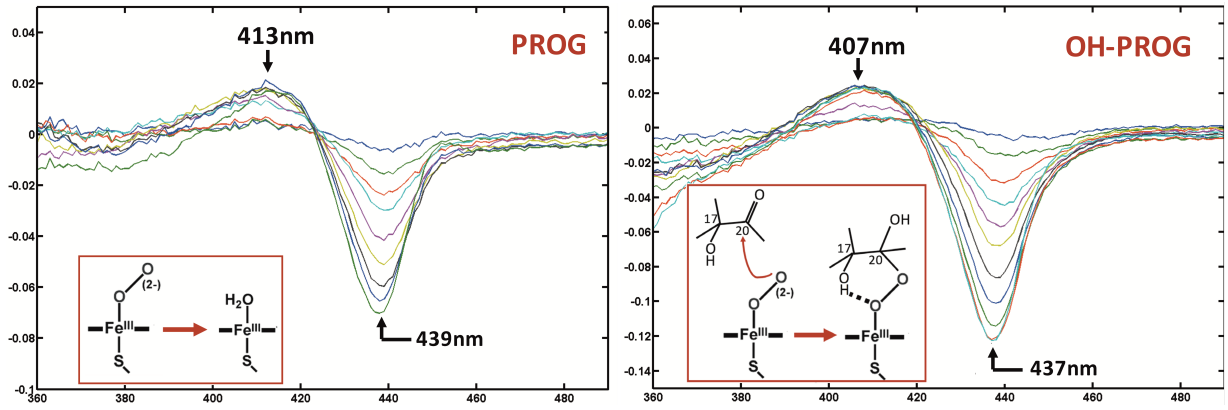

Figure 2.5: Difference spectra obtained from 160K to 185K from optical annealing following cryolytic reduction of oxy-ferrous intermediate for PROG hydroxylation and OH-PROG lyase reaction. [Insets: mechanistic processes resulting in the spectroscopic observations depicted].

2.4 Conclusions

We observed a normal KSIE value of 1.5 and 1.67 for PROG hydroxylation, consistent with the understanding that CYP17A1 mediated hydroxylation reactions proceed through proton dependent Cpd I intermediate. From KSIE results with OH-PROG lyase reaction of 0.9 and 0.8, it can be reasonably concluded that OH-PROG lyase follows a different chemical mechanism than PROG hydroxylation. The mildly inverse value of KSIE in this case, which does not get affected by the presence or absence of cyt b_5, is suggested to stem from the ablation of proton dependent uncoupling pathways viz. peroxide and oxidase shunts in deuterated water reactions as depicted in **Figure 1.3**. It therefore indicates that OH-PROG lyase reaction might also follow peroxo-anion mediated mechanism, similar to OH-PREG (Gregory et al., 2013b). The lower magnitude of inverse KSIE in OH-PROG (0.8) as compared to large inverse KSIE (0.4) in OH-PREG might suggest that OH-PROG lyase reaction is mostly uncoupled through autoxidation.

Using cryo-reduction and optical annealing, PROG bound CYP17A1 peroxo- intermediate was observed to convert to a ferric like species, whereas OH-PROG bound samples showed the appearance of a novel intermediate absorbing at 407nm. This intermediate is similar to the 405 nm intermediate observed during OH-PREG catalysis (Mak et al., 2015).

Taken together, the inverse KSIE values and the appearance of a 407nm intermediate upon thermal annealing suggest that CYP17A1 catalyzes the lyase reaction of OH-PROG through peroxo-anion mediated mechanism, similar to the mechanism described for lyase reaction with OH-PREG (Mak et al., 2015).

Chapter 3

Resonance Raman Spectroscopy to Probe the Mechanism of CYP17A1 Mediated Androstenedione Synthesis

3.1 Introduction

Resonance Raman spectroscopy (rR) has emerged as a powerful technique for probing structural characteristics of heme-bound enzymes both in their stable resting states and more importantly, in their fleeting intermediate states. Raman spectroscopy is a vibrational spectroscopy that uses any excitation frequency to observe inelastic scattering from a molecule, the magnitude of the inelastic shift informs vibrational, rotational and other low frequency transitions. In the case of colored molecules such as heme proteins, the resultant Raman spectrum may be contaminated with strong fluorescence, and the useful Raman signal may be too weak in intensity. For this reason, rR spectroscopy makes use of carefully chosen excitation frequency which crosses the frequency of the excited electronic states and resonates with them. This results in enhancement of the Raman active modes in the chromophore, since it absorbs the maximum amount of light, thereby reducing the background noise and causing an increase in intensity of observable Raman bands by 10^2-10^5 fold (Mak, 2016).

Using the impressive power of rR, a lot of information regarding the heme environment can be obtained. The high frequency modes reveal changes in oxidation state, spin state and coordination number of the heme iron (Mak and Denisov, 2017). Low frequency markers inform changes in heme planarity and the linkages of the porphyrin peripheral groups to the protein cavity by detecting changes in propionate and vinyl bending modes. Furthermore, valuable information regarding exogenous

ligands bound to the heme iron such as O_2, CO, NO, CN^- as well as axial linkages with the protein (Cys or His) is also obtained (Podstawka et al., 2000). This technique has long been in use for studying mechanism of P450s ranging from the simplest CYP101A1 to the complex mammalian P450s (Denisov et al., 2008; Mak, 2016; Mak and Denisov, 2017; Mak et al., 2011, 2012, 2014a). It has been successfully applied to CYP17A1 reconstituted into nanodiscs, and has provided a remarkable amount of information regarding the substrate induced changes in the active site, and the heme oxygen adduct formed during substrate catalysis, and characterizing the peroxo- intermediate formed in OH-PREG chemistry.

Using rR spectroscopy on CYP17A1 oxy-ferrous complex with OH-PREG and OH-PROG, Gregory and coworkers made a seminal discovery (Gregory et al., 2013a). They found that the orientation of the D-ring of the substrates was slightly different near the heme iron, which translated into differential hydrogen bonding pattern from the 17α-OH- group to the oxy-complex. When the protein was bound to OH-PREG, the hydroxyl group donates a hydrogen bond to the proximal oxygen atom, O_P in the Fe-O-O fragment, whereas in the case of OH-PROG, this hydrogen bonding interaction is towards the distal oxygen atom, O_D. This H-bonding pattern is expected to persist in the peroxo- intermediate as well, suggesting that the H-bond interaction with the proximal O in the case of OH-PREG would prevent the scission of O-O linkage, and allow the distal O to perform nucleophilic attack on the carbonyl-20, giving rise to the hemiketal intermediate before decaying into the products DHEA and acetic acid. The impact of differential H-bonding on the involvement of a specific mechanistic intermediate has been previously observed in the case of nitric oxide synthase (Li et al., 2007). On the other hand, the observed H-bonding pattern in OH-PROG bound to oxy-ferrous CYP17A1 could result in rapid cleavage of O-O linkage and formation of Cpd I. The observation that OH-PREG is catalyzed more efficiently than OH-PROG could be explained by this differential pattern of H-bonding (Flück et al., 2003).

In the case of OH-PREG, the former scenario was confirmed when thermal annealing of trapped peroxo-anion intermediate revealed a novel intermediate that was dramatically different than a Cpd I species. Using rR, this intermediate was discovered to be an acyl peroxo- like species and was confirmed to be hemiketal intermediate resulting from peroxo-anion by employing scrambled oxygen (Mak et al., 2015). As explained above, the differential H bonding pattern to the oxy-complex in OH-PROG could indicate that this substrate goes through a Cpd I mediated mechanism, since the electrophile distal oxygen is not involved in the H bond with C17-OH- moiety. On the other hand, as described in section 2.4, steady state KSIE values obtained for the lyase reaction suggest that this reaction does not require protons and therefore Cpd I must not be involved. In order to definitively answer this question, rR spectroscopy on cryo-radiolytically reduced samples of CYP17A1 in nanodiscs bound to PROG or OH-PROG was performed. Samples were prepared in both H_2O and D_2O in order to confidently inform the identity of intermediates as observed, based on whether they are H/D senstitive or not. The difference traces between $^{16}O_2$ and $^{18}O_2$ were used for analysis, this helps to cancel out heme vibrational modes, which would otherwise clutter the raw spectra and hinder the characterization of O–O and Fe–O modes.

This work was performed in collaboration with Dr. Piotr Mak in the laboratory of Prof. James R. Kincaid at Marquette University.

3.2 Materials and methods

3.2.1 CYP17A1 expression, purification and incorporation into nanodiscs:

The expression, purification and incorporation of CYP17A1 into POPC nanodiscs was performed as previously described in section 2.2.

3.2.2 Preparation of cryolytically reduced rR samples:

As described in section 2.2, purified CYP17A1 was assembled in nanodiscs and substrate PROG/OH-PROG added. The final composition of the samples was ~40 nmoles CYP17A1:ND in 30% v/v double distilled glycerol, 6.25 μM methyl viologen, 450 μM substrate, 0.1 M potassium phosphate pH 7.4, 230 mM NaCl and 5% v/v methanol. Four such samples were prepared, both protiated and deuterated for each substrate. After anaerobic preparation of oxy-complex, cryo-radiolytic reduction was performed and the samples kept at 77 K until ready for rR experiments.

3.2.3 rR spectroscopy of substrate bound peroxo-ferric CYP17A1:

The trapped peroxo- samples at 77 K were excited using a 441.6 nm line by a He-Cd laser (IK Series He-Cd laser; Kimmon Koha Co.), and the samples annealed to 190 K were measured with 406.7 nm excitation lines from a Kr^+ laser (Coherent Innova Sabre Ion Laser). All measurements were done with Spex 1269 spectrometer equipped with Spec-10 LN-cooled detector (Princeton Instruments). The slit width was 150 μm and 1,200 g/mm grating was used with which the resultant spectral dispersion is 0.46 cm^{-1} per pixel. The laser power was maintained at ≤1mW to prevent photo-dissociation. In order to avoid laser-induced heating and protein degradation, the samples were contained in spinning NMR tubes (5mm outside diameter, WG-5 ECONOMY; Wilmad). The 180° backscattering geometry was used for all measurements and the laser focused onto the sample using a cylindrical lens (Shriver and Dunn, 1974). The NMR tubes were positioned into a double-walled quartz low-temperature cell filled with liquid nitrogen. All measurements were done at 77 K, and total collection time was around 6 hours for the irradiated samples and ~8-9 hours for the annealed samples. Spectra were calibrated with fenchone (Sigma–Aldrich) and processed with GRAMS/32 AI software (Galactic Industries).

3.3 Results

3.3.1 rR measurements of irradiated oxy-complex bound to PROG/OH-PROG:

The irradiated PROG-bound H_2O and D_2O samples at 77 K were excited using 441.6 nm line and the spectra obtained are depicted as $^{16}O–^{18}O$ difference spectra in **Figure 3.1 A, B.** A strong positive band at 772 cm^{-1} was observed which showed an expected downshift to 735 cm^{-1} upon $^{18}O_2$ substitution. The 772 cm^{-1} mode appears very similar to the hydroperoxo-ferric ν(O–O) in the case of PREG bound samples (775 cm^{-1}). Significantly, this mode exhibited a 4 cm^{-1} downshift in D_2O samples. Hence, on the basis of H/D sensitivity and its frequency, this band was assigned to the ν(O–O) stretching mode for hydroperoxo-ferric intermediate. The corresponding ν(Fe–O) mode was observed at 575 cm^{-1} and was found to be downshifted to 549 cm^{-1} in $^{18}O_2$ and by 3 cm^{-1} in D_2O. Clearly, all of the PROG bound peroxo-ferric intermediate got protonated to form the hydroperoxo- species even at 77 K, suggesting that unlike in PREG bound samples, proton transfer in PROG bound CYP17A1 is more facile (Mak et al., 2015). This is an expected result, considering PROG reaction is believed to follow Cpd I mechanism, and since the samples had no peroxo- form even at 77 K, they were not annealed further.

Similar experiment with OH-PROG bound samples exhibited two sets of oxygen sensitive modes as shown in **Figure 3.1 C, D**. A band at 790 cm^{-1} that shifted to 753 cm^{-1} in $^{18}O_2$ did not exhibit H/D sensitivity, while the second oxygen sensitive mode at 771 cm^{-1} shifted to 734 cm^{-1} in $^{18}O_2$ and downshifted to 768 cm^{-1} in D_2O buffer. The former was most reasonably assigned to a peroxo- species (790 cm^{-1}) and the latter mode was assigned to the hydroperoxo- (771 cm^{-1}) species. The corresponding ν(Fe–O) modes were observed at 562 cm^{-1} (peroxo- species with 25 cm^{-1} sensitivity to $^{18}O_2$ and no sensitivity to H/D exchange) and 576 cm^{-1} (hydroperoxo- species with 26 cm^{-1} sensitivity to $^{18}O_2$ and 2 cm^{-1} sensitivity to H/D exchange). These results have a prominent distinction in comparison to rR results of OH-PREG bound samples where only the peroxo- intermediate was observed at 77 K.

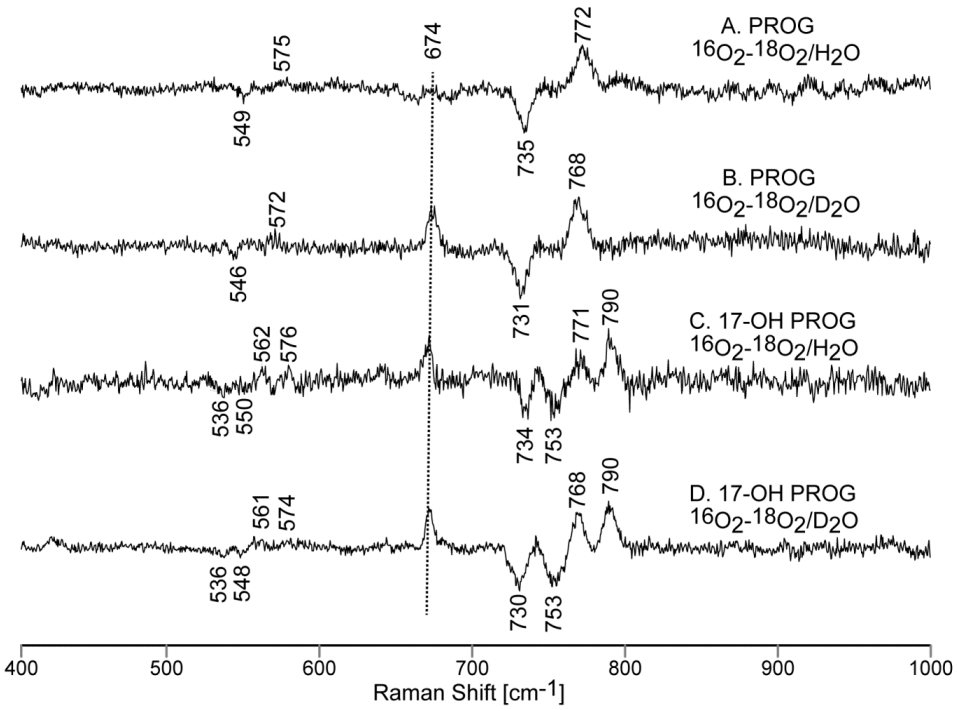

<u>Figure 3.1:</u> Resonance Raman results in the form of $^{16}O_2$–$^{18}O_2$ difference traces of irradiated samples of oxy-ferrous CYP17A1 bound to PROG in H_2O (A); D_2O (B); bound to OH-PROG in H_2O (C); D_2O (D). Excitation line 441.6 nm, total collection time for each rR spectrum used to generate the difference trace was 4.0-4.5 h. The subtraction was performed in a way to obtain the cleanest difference trace. In some traces, though, there is some positive band at around 674 cm^{-1}. Its arises most probably form higher intensity of the ν_7 mode in the $^{16}O_2$ samples, most probably caused by higher amounts of residual ferric form in these samples as compared to the $^{18}O_2$ samples.

Upon closer inspection of the relative positioning of the ν(Fe–O) modes, an important observation was made. While no peroxo- intermediate was observed for the PROG sample, it is reasonable to expect that its ν(Fe–O) mode would occur near 554 cm^{-1} (a frequency close to that observed for the peroxo form of the PREG sample). In this way, the observed ν(Fe–O) mode at 562 cm^{-1} of the peroxo- form

in OH-PROG sample, indicates an ~8 cm^{-1} upshift to higher frequency, which is consistent with H-bonding of the 17-OH fragment to the distal oxygen of the Fe–O–O fragment (Gregory et al., 2013a). Therefore, the differential hydrogen bonding pattern observed previously in OH-PROG bound oxy-complex (upshifted ν(Fe–O) in OH-PROG as compared to that in PROG) persists in the peroxo- forms. A similar persistence of H-bonding pattern from the oxy form to the peroxo- form was also seen in the case of OH-PREG (Mak et al., 2015).

3.3.2 rR measurement of OH-PROG bound peroxo- forms upon thermal annealing:

The OH-PROG samples were thermally annealed to 165 K and spectra recorded using 441.6 nm excitation line. **Figure 3.2** shows $^{16}O_2$–$^{18}O_2$ traces of these samples in H_2O and D_2O buffers. It was observed that a significant part of peroxo- intermediate (790 cm^{-1}) that was observed at 77 K disappears at 165 K. In order to explore the fate of the disappeared peroxo- form, 406.7 nm excitation line was used on OH-PROG samples. This wavelength was chosen to resonate with the intermediate observed during optical annealing experiments which was found to absorb at 407 nm (section 2.3.2).

The spectra at three different temperatures- 77 K, 165 K and 190 K were recorded using this excitation wavelength. OH-PROG samples annealed to 165 K and observed using 406.7 nm laser showed appearance of a new species at 785 cm^{-1} which shifted to 745 cm^{-1} in $^{18}O_2$ **(Figure 3.3)**. These modes were not seen at 77 K **(Figure 3.3A)**, and did not shift in deuterated buffer at all. These findings suggest that this new species is identical to the peroxo-hemiketal intermediate observed previously in the case of OH-PREG seen at 791 cm^{-1}. Using oxygen isotope scrambling experiment, it was observed that this intermediate originated from an unbroken O-O bond, hence its assignment to hemiketal was confirmed (Mak et al., 2015). Intensity of this peroxo-hemiketal species was seen to increase upon further increase in temperature to 190 K **(Figure 3.4)**.

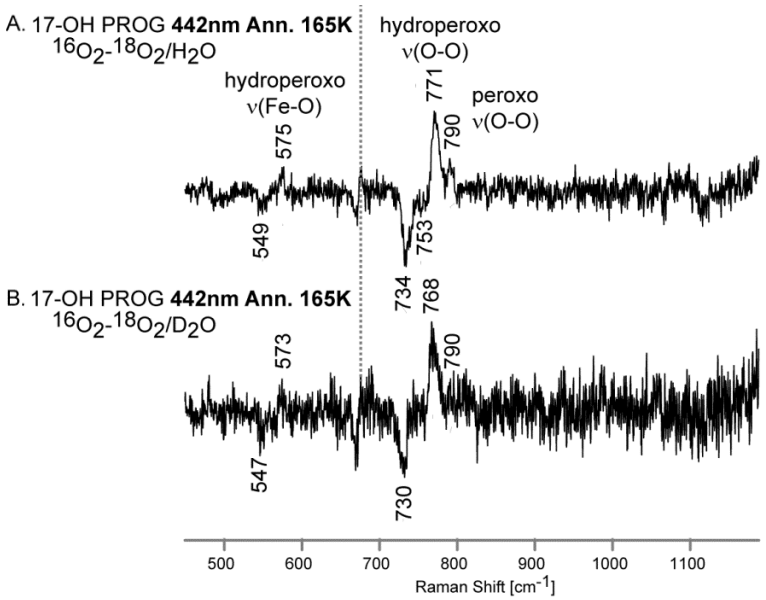

<u>Figure 3.2:</u> Resonance Raman results depicted as $^{16}O_2$–$^{18}O_2$ difference traces obtained upon annealing the irradiated oxy-ferrous samples bound to OH-PROG from 77 K to 165 K in H_2O (A) and in D_2O (B). Excitation line used 441.6 nm, total collection time for each rR spectrum used to generate the difference trace was 4.0-4.5 h.

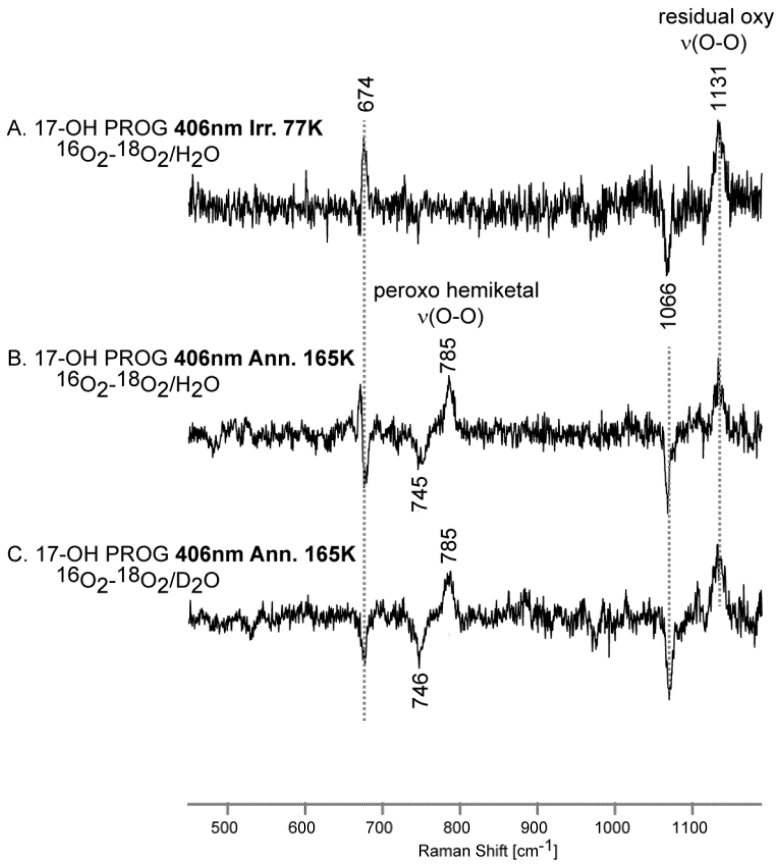

Figure 3.3: Resonance Raman results depicted as $^{16}O_2$–$^{18}O_2$ difference traces of irradiated oxy-ferrous samples bound to OH-PROG at 77 K obtained using 406.7 nm excitation (A); Upon annealing the irradiated oxy-ferrous samples bound to OH-PROG from 77 K to 165 K in H_2O (B) and in D_2O (C).

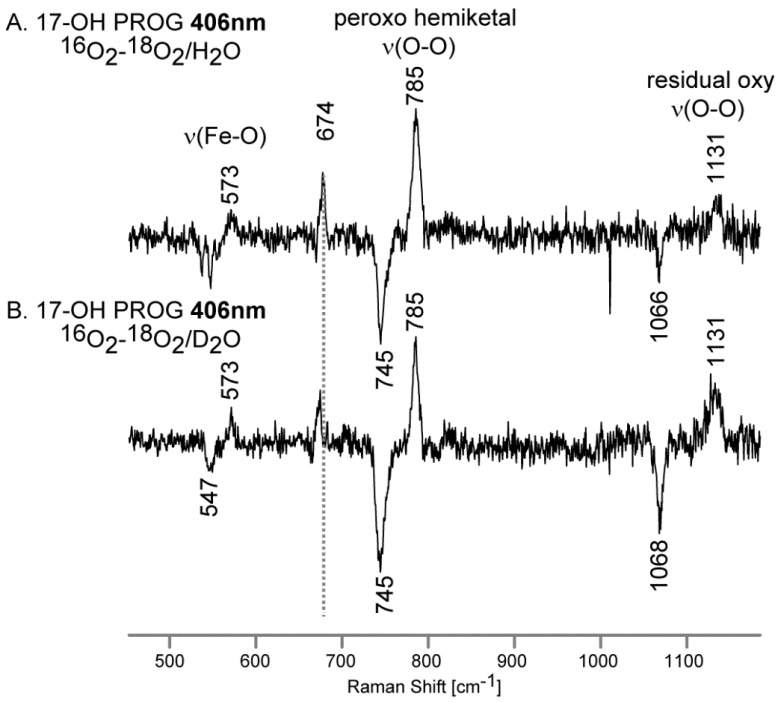

Figure 3.4: Resonance Raman results depicted as $^{16}O_2$–$^{18}O_2$ difference traces of irradiated oxy-ferrous samples bound to OH-PROG obtained upon annealing the irradiated oxy-ferrous samples bound to OH-PROG to 190 K in H_2O (A) and in D_2O (B). The new intermediate observed at 785 cm^{-1} is clearly seen to increase in amplitude in comparison to 165 K.

3.4 Conclusions

From our resonance Raman spectroscopy experiments with PROG bound CYP17A1 irradiated oxy-complex at 77 K, we observed that all the peroxo- species was converted to hydroperoxo. Similar experiment with OH-PROG sample showed both the peroxo- and hydroperoxo- forms. These observations are contrary to what was observed in the case of PREG and OH-PREG by Mak and coworkers, while PREG exhibited the presence of peroxo- and hydroperoxo- species, in the case of OH-PREG protonation of the peroxo- forms did not occur at all. This suggests that due to distinct

positioning of the Δ4 substrates (PROG and OH-PROG), proton transfer is more facile as compared to that for Δ5 substrates (PREG and OH-PREG). This difference in substrate positioning is known to stem from the differential hydrogen bonding interactions of the 3β keto/3β hydroxyl in the A ring of the substrate with the active site residues (Petrunak et al., 2014). Further annealing of PROG bound samples is expected to show increased intensity of the observed hydroperoxo- modes and then disappearance when this species forms Cpd I and subsequently, the hydroxylated product. Our rR results with PROG are completely consistent with a Cpd I mediated mechanism, as also evidenced by KSIE values and optical annealing experiments shown in section 2.3.

On the other hand, results with OH-PROG samples annealed to 165 K and then to 190 K exhibit a more complicated mechanism. While we saw both the peroxo- and hydroperoxo- species at 77 K, as the temperature was raised to 165 K, the peroxo- disappeared concomitant with appearance of a new species that could be identified using a 406.7 nm excitation laser. Upon further increase in temperature to 190 K, the intensity of this species was seen to increase. On the basis of its insensitivity to H/D substitution, and its similarity with the new intermediate observed in the case of OH-PREG, this intermediate was confidently assigned to be peroxo-hemiketal, derived from nucleophilic attack by the peroxo-anion on the carbonyl 20 of OH-PROG substrate **(Figure 3.5)**. Hence, we conclude that OH-PROG lyase catalysis, like OH-PREG proceeds through the peroxo-anion mediated mechanism. This result is entirely in-line with our previously performed KSIE and optical annealing experiments with OH-PROG (section 2.3).

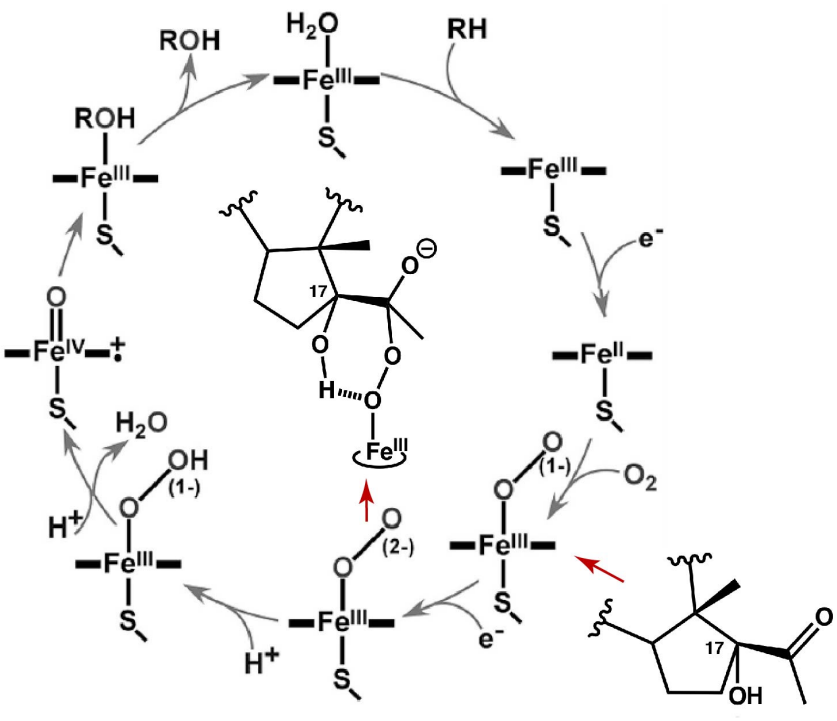

Figure 3.5: Updated P450 reaction cycle with CYP17A1 lyase mechanistic intermediate peroxo-hemiketal which is formed as a result of nucleophilic attack from peroxo-anion to the carbonyl-20 of substrate.

Chapter 4

Investigation of the Role of Cytochrome b_5 in Androgen Synthesis

4.1 Introduction

Cytochrome b_5 (cyt b_5) is a small hemeprotein which is known to affect the catalysis of a variety of P450s. While the primary function of cyt b_5 has been long known to be the electron transfer to fatty acid desaturase (Oshino et al., 1971), as of now cyt b_5 has also been shown to affect the catalysis of more than 20 isoforms of P450s, including the drug metabolizing CYP3A4, 2B6, 2C9, 2C19 and 2E1 (Mokashi et al., 2003; Pompon and Coon, 1984; Yamaori et al., 2003; Yamazaki et al., 1997, 2002). In the adrenal cortex, the spacio-temporal regulation of cyt b_5 expression gives compelling clues to its essential role in steroidogenesis. Cyt b_5 is expressed only in the zona reticularis, which is one of the primary sites for androgen synthesis, with the its levels steadily increasing with the progression of adrenarche (Auchus and Rainey, 2004; Nguyen et al., 2009). That cyt b_5 selectively enhances the androgenic lyase reaction catalyzed by CYP17A1, was first demonstrated in 1982 (Onoda and Hall, 1982). Indirect evidence also came from patients suffering from Cushing's syndrome, who were found to produce large amounts of cyt b_5 in the adenomas (Sakai et al., 1994). Conversely, patients presenting with isolated lyase deficiency were found to have disrupted interactions with cyt b_5 (Geller et al., 1997, 1999). Given that the only FDA approved CYP17A1 inhibitor suffers from complications

Reproduced in part with permission from

Duggal, R., Liu, Y., Gregory, M.C., Denisov, I.G., Kincaid, J.R., and Sligar, S.G. Evidence that cytochrome b5 acts as a redox donor in CYP17A1 mediated androgen synthesis. Biochemical and Biophysical Research Communications (2016) 477, 202–208. Copyright 2016 Elsevier. The published version may be found online at https://dx.doi.org/10.1016/j.bbrc.2016.06.043.

due to its blanket inhibition of both the reactions, the interaction of cyt b_5 with CYP17A1 presents with a very attractive therapeutic potential.

Various groups have identified the residues key to the CYP17A1–cyt b_5 interaction. Mutagenesis studies and NMR mapping experiments have confirmed that CYP17A1 surface residues R347, R358, R449 and cyt b_5 E48 and E49 are essential for a functional interaction (Estrada et al., 2014; Lee-Robichaud et al., 2004; Naffin-olivos and Auchus, 2006). Solution NMR with soluble forms of CYP17A1 and cyt b_5 has shown conformational changes in F, G and I-helices in CYP17A1, potentially indicating an allosteric role for cyt b_5. Another important feature of the cyt b_5 binding site on CYP17A1 surface is that it partially shares the area that binds CPR (Estrada et al., 2014, 2016).

It has long been debated whether the cyt b_5 mediated stimulation of lyase activity is due to its allosteric role potentially affecting ligand binding, or if there is an associated electron transfer role owing to the presence of a bis- imidazole coordinated heme. In the latter role, the relatively high redox potential of cyt b_5 (~0 mV versus Normal Hydrogen Electrode) implies that electron transfer to ferric P450 (redox potential ~ −300 mV vs. NHE) is strongly unfavorable (Rodgers and Sligar, 1991). Consequently, any redox transfer from cyt b_5 could only occur to the oxy-ferrous intermediate (redox potential ~0 mV) (Lipscomb et al., 1976). Extensive research on the mechanism of cyt b_5 mediated modulation of CYP2B4 catalysis has shown that in cyt b_5 competes with CPR to perform the second electron reduction of oxy-complex (Im and Waskell, 2011).

To identify whether cyt b_5 occupies a similar redox effector role in CYP17A1 mediated lyase catalysis, I made use of a manganese reconstituted of cyt b_5 (Mn b_5), which has been shown to be redox inactive in the presence of CPR (Morgan and Coon, 1984). Additionally, in order to investigate whether the conformational changes associated with cyt b_5 binding affect the heme functionality and the active site structure of CYP17A1, we performed resonance Raman spectroscopy on ferric CYP17A1 bound to lyase substrates, in complex with cyt b_5. As discussed in section 3.4 and in (Gregory et al., 2013a),

OH-PREG and OH-PROG bind in the CYP17A1 active site with different hydrogen bonding conformations to the dioxygen adducts of heme. This is suggested to impact the catalysis of these lyase substrates, by differentially making a peroxo-anion mediated nucleophilic attack more feasible in OH-PREG vs. OH-PROG. All the aforementioned studies with oxy-ferrous CYP17A1 bound to lyase substrates had been performed in the absence of b_5. Therefore, we decided to perform similar experiments with oxy-ferrous CYP17A1 in complex with cyt b_5, in order to probe potential catalytically significant effects of this interaction on the orientation of lyase substrates in the active site. In order to prevent spectroscopic interference from the heme moiety of cyt b_5, Mn b_5 was employed which has been shown previously to have an identical structure, but significantly lower spectral overlap in the Soret region (Gruenke et al., 1997; Mak et al., 2008). Finally, given the need for the cyt b_5 membrane anchor in its effects on P450s, Nanodisc reconstituted forms of full length proteins were employed for all experiments (Holmans et al., 1994; Sergeev et al., 2014). This system provides an additional advantage over other reconstitution systems such as detergent micelles in that the stoichiometric ratios of the interacting proteins can be controlled in the native like membrane environment.

The rR experiments described in this chapter were performed in collaboration with Dr. Yilin Liu in the laboratory of Prof. James R. Kincaid at Marquette University.

4.2 Materials and methods

4.2.1 Protein expression, purification and incorporation into nanodiscs:

The expression, purification and incorporation of CYP17A1, CPR and cyt b_5 into POPC Nanodiscs was performed as previously described in section 2.2.

4.2.2 Reconstitution of redox inactive manganese substituted cyt b_5 (Mn b_5):

Cyt b_5 prepared as described in section 2.2.1 was reconstituted with Mn protoporphyrin IX according to (Morgan and Coon, 1984), with the following changes: after removal of unbound Mn protoporphyrin IX by gel filtration using a G-25 column, the eluate was run through a DEAE-cellulose column which was equilibrated with 25 mM Tris acetate (pH 8.0), 1 mM EDTA and 10 mM sodium cholate. A linear salt gradient was formed using the equilibration buffer supplemented with 1 M NaCl. Mn b_5 fractions were characterized based on their Rz ratios, pooled, rigorously dialyzed against 100mM potassium phosphate buffer (pH 7.4) and flash frozen in liquid nitrogen before being stored at -80 ^{o}C until use. Mn b_5 was quantified using UV-visible spectroscopy **(Figure 4.1)** using ε_{368} = 50 ± 2 $mM^{-1}cm^{-1}$ and ε_{468}= 38 ± 1.5 $mM^{-1}cm^{-1}$ (Morgan and Coon, 1984). Purity and identity of reconstituted Mn b_5 was confirmed by denaturing gel electrophoresis and MALDI-mass spectrometry.

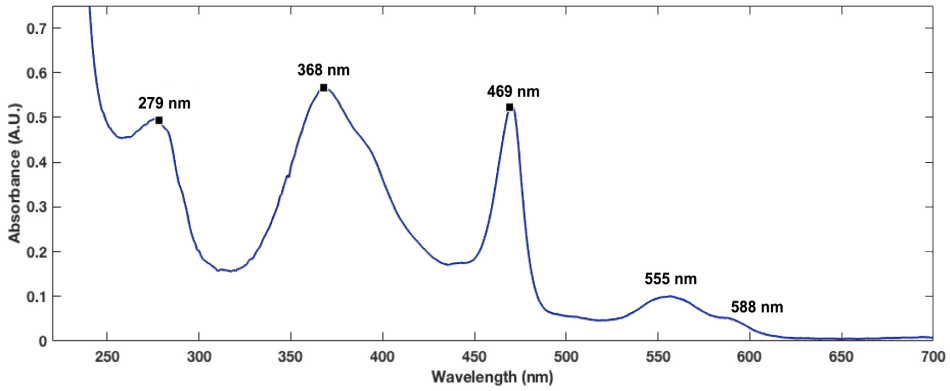

Figure 4.1: UV-visible spectrum of cytochrome b_5 reconstituted with manganese protoporphyrin IX. The characteristic peaks at 368 nm, 468 nm and 555 nm with a shoulder at 588 nm were observed.

4.2.3 Measurement of steady state NADPH consumption rates and androgen formation rates:

NADPH oxidation rates and product formation rates were determined with 365 pmoles of CYP17A1 in Nanodiscs reconstituted with 4-fold molar excess of CPR, and 4-fold molar excess cyt b_5 or Mn b_5. The solution was brought to 1 mL with 100 mM potassium phosphate (pH 7.4) containing 50 mM NaCl and 50 μM OH-PREG or OH-PROG (Sigma) in a stirred quartz cuvette with 0.4 cm path length. The solution was equilibrated at 37 ^{o}C for 5 min and reaction initiated with 600 nmoles of NADPH. The oxidation of NADPH was monitored by change in absorbance at 340 nm for 15 min. At this point, the reaction was quenched by adding 50 μL of 8.9 N sulfuric acid. Each reaction solution was transferred to a 1.5 mL tube, flash frozen in liquid nitrogen and stored at -80 ^{o}C until product analysis. These reactions were performed in Cary 300 spectrophotometer fitted with magnetic stirrer and Peltier temperature controller.

Frozen samples were thawed and extraction of analytes was performed as previously documented (Gregory et al., 2013b; Khatri et al., 2014b). The analysis for DHEA product from OH-PREG was performed by gas chromatography with a DB-17 phenol substituted siloxane column and a flame ionization detector on a Hewlett-Packard 6890 gas chromatograph, and the chromatograms were processed with Grams/32 AI software. Analysis for AD product from OH-PROG reactions was performed using C18 HPLC system (Shimadzu) with a linear gradient of methanol and acetonitrile as described in section 2.2.3.

4.2.4 Preparation of Raman samples of Mn b_5 complex with ferric and oxy-ferrous CYP17A1:

Purified CYP17A1 was assembled in nanodiscs (CYP17A1:ND) and substrate added as described in section 2.2. While all 4 substrates were investigated for ferric samples, only the lyase substrates OH-PREG and OH-PROG were probed for oxy-ferrous samples. The ferric CYP17A1 samples consisted of 85 μM CYP17A1:ND in 15% v/v double distilled glycerol, with 2-fold excess of Mn b_5 and 420 μM substrate. The final composition of the oxy-ferrous samples was 40 nmoles CYP17A1:ND in complex with 2-fold excess of Mn b_5 in 30% v/v double distilled glycerol, 6.25 μM methyl viologen, 400 μM OH-PREG/OH-PROG, 0.1 M potassium phosphate pH7.4, 200 mM NaCl and 5% v/v methanol. Preparation of oxy-complex and rR measurements at 77 K were performed as described (Gregory et al., 2013a).

4.2.5 rR spectroscopy of ferric and oxy-ferrous CYP17A1 in complex with Mn b_5:

We acquired resonance Raman spectra after adding 2-fold and 4-fold excess of Mn b_5. The high frequency spectra were acquired using the 406.7 nm excitation line from a Krypton ion laser (Coherent Innova Sabre Ion Laser) and changes in the Fe–S stretching mode were investigated using the 356.4 nm excitation line from the same laser, a wavelength known to selectively enhance this mode (Champion et al., 1982). The rR spectra of all samples were measured using a Spex 1269 spectrometer equipped with a Spec-10 LN liquid nitrogen-cooled detector (Princeton Instruments, NJ). The laser power was adjusted to ~10 mW at the sample. All samples were measured in a spinning NMR tube to avoid local heating and protein degradation. The spectra were collected using a 180° backscattering geometry, with the laser beam being focused as a line image on the sample tube using a cylindrical lens. The spectra for oxy-ferrous samples were measured at 77 K, using 413.1 nm excitation from Krypton ion laser, which enhances heme modes and internal modes of the Fe–O–O adduct. Spectra were calibrated with fenchone (Sigma-Aldrich, WI) and processed with Grams/32 AI software (Galactic Industries, Salem, NH).

4.3 Results

4.3.1 Effect of Mn b_5 on steady state turnover of CYP17A1 lyase reactions:

The rates of NADPH oxidation and product formation for OH-PREG in the presence of cyt b_5 and Mn b_5 were compared to the rates in the absence of any added cyt b_5. The presence of cyt b_5 increased the product formation rate ~5 fold, while the addition of Mn b_5 did not affect it at all **(Figure 4.2 A)**. NADPH consumption rates were close in value in all three cases, 54 ± 1.3 min^{-1} for cyt b_5, 51 ± 1.0 min^{-1} for Mn b_5 and 46 ± 1.9 min^{-1} for reactions in the absence of any b_5. The efficiency of coupling, calculated as the ratio of product formation rate to the rate of NADPH consumption, was seen to be maximal in the reactions with cyt b_5, while reactions with no b_5 and with Mn b_5 had similar coupling efficiency **(Figure 4.2 B)**. Turnover experiment using OH-PROG as the lyase substrate yielded similar results. In the presence of cyt b_5, AD formation occurred at a rate of 0.26 ± 0.008 min^{-1}, whereas when there was no b_5 added, this rate was expectedly slower, 0.11 ± 0.005 min^{-1}. In the presence of the redox inactive Mn b_5, AD formation occurred at a rate of 0.10 ± 0.013 min^{-1}, very similar to that when no b_5 was present. Therefore, while cyt b_5 enhanced the turnover rate of conversion of OH-PROG to AD 2.5 times, Mn b_5 had no effect on this reaction at all **(Figure 4.2 C)**.

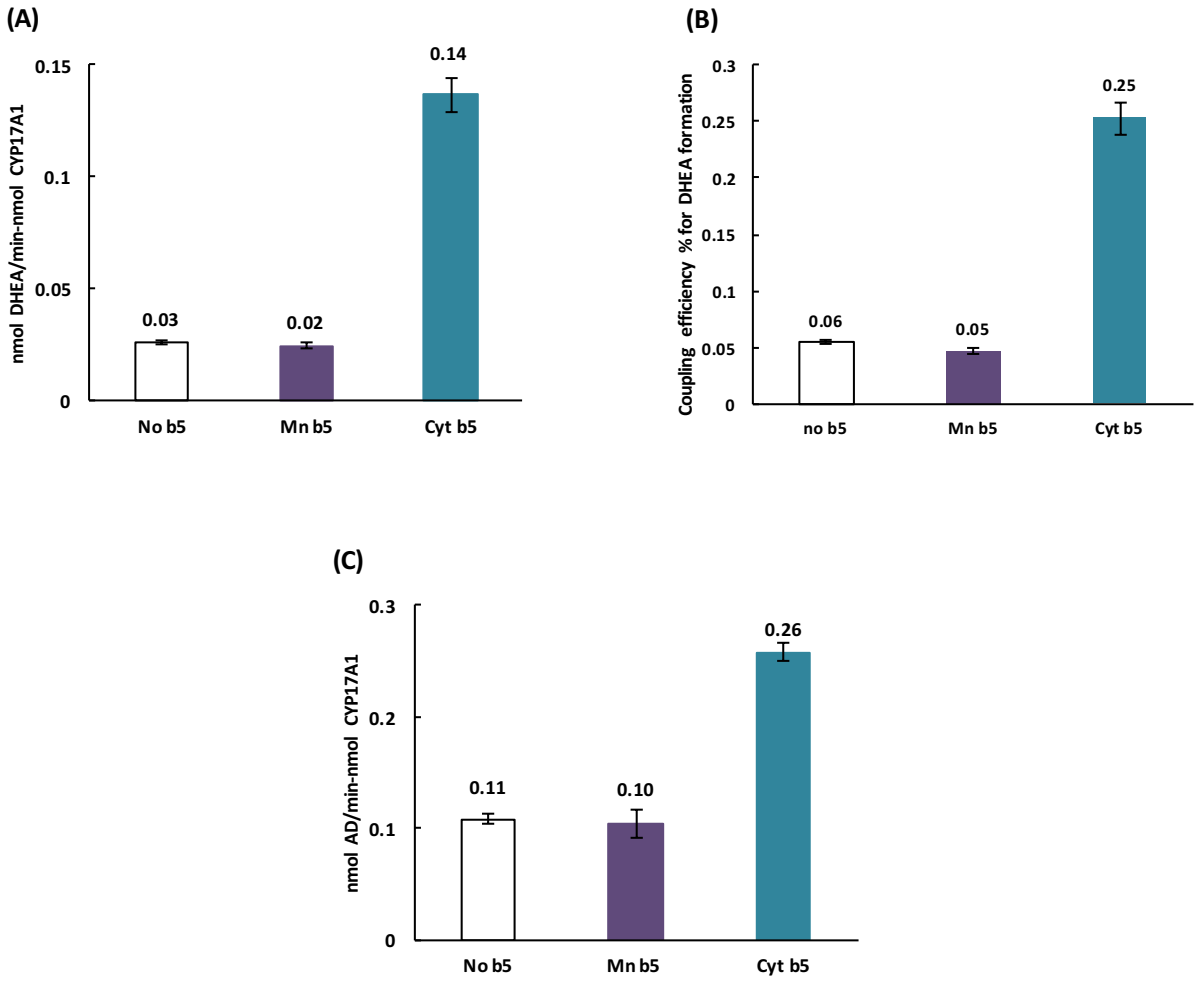

<u>Figure 4.2:</u> Effects of Mn b_5 on CYP17A1 mediated catalysis of lyase substrates OH-PREG and OH-PROG in comparison to cyt b_5. Rates of formation of DHEA product from OH-PREG (A); Efficiency of coupling for CYP17A1 mediated conversion of OH-PREG to DHEA (B); Rates of AD product formation form OH-PROG (C).

4.3.2 rR measurements to probe effects of Mn b_5 on ferric CYP17A1:

The presence of Mn b_5 in complex with substrate-bound forms of CYP17A1 showed minor changes in the spin states **(Figure 4.3)**. As can be seen in trace B, PREG bound CYP17A1 in complex with Mn b_5 showed an isolated ν3 mode at 1488 cm^{-1} and a small signal for LS population near 1500 cm^{-1}, features similar to that for the sample without Mn b_5 (trace A). The spin state population was estimated using the intensity ratio of I_{HS}/I_{LS} equal to 1.24, a procedure developed by (Mak et al., 2013). The HS population of PREG bound CYP17A1 in the presence of a 2-fold excess of Mn b_5 was 80%, close to the value observed in the absence of Mn b_5. In the case of OH-PREG samples, the HS component changed from ~57% to ~50% when a 2-fold excess of Mn b_5 was present (trace D). Similar results were obtained with PROG and OH-PROG bound CYP17A1 in the presence of 2-fold Mn b_5 **(Figure 4.4)**. These values remained the same even in the presence of 4-fold Mn b_5, indicating that all of CYP17A1 binding sites for cyt b_5 had been occupied with 2x excess of the redox partner.

It is important to note that the frequencies observed for both the low energy and high energy internal modes of the heme prosthetic group did not shift relative upon binding to Mn b_5, indicating that this interaction does not induce significant structural changes of the heme macrocycle or its peripheral substituents in the substrate-bound ferric CYP17A1. Importantly, when 356.4 nm excitation was used to selectively enhance the ν(Fe–S) stretching mode, it was observed that the binding of Mn b_5 increased the strength of Fe–S bond. As depicted in the insets for the low-frequency spectra in **Figure 4.3**, the ν(Fe–S) stretching modes in samples with Mn b_5 appeared at 350 cm^{-1}, as compared to 347 cm^{-1} in its absence as shown previously (Mak et al., 2014b). Similar effect on the ν(Fe–S) mode was observed when 356.7 nm excitation was used on PROG and OH-PROG bound ferric CYP17A1 samples (data not shown).

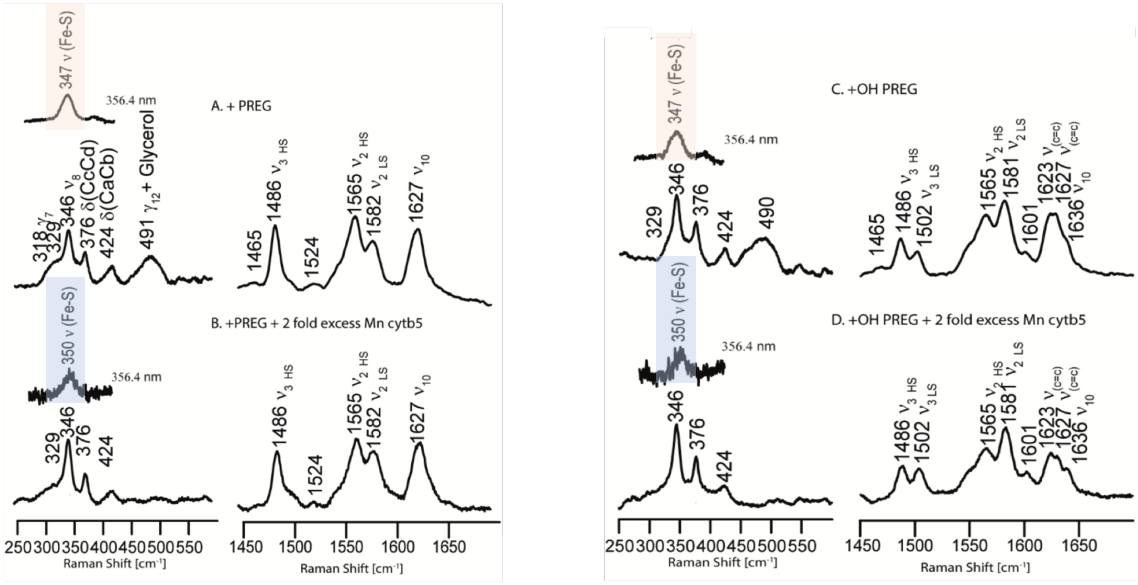

<u>Figure 4.3:</u> Low frequency (left panels) and high frequency (right panels) resonance Raman traces of PREG (A, B) and OH-PREG (C, D) bound to ferric-CYP17A1 in the absence and presence of Mn b_5. Excitation wavelength 406.7 nm. Inset bands in the low frequency region were acquired with the 356.4 nm excitation line from the same laser, a wavelength known to enhance the ν(Fe–S) stretching mode (highlighted in color). B and D traces were obtained after subtraction of spectra obtained for equivalent amount of Mn b_5.

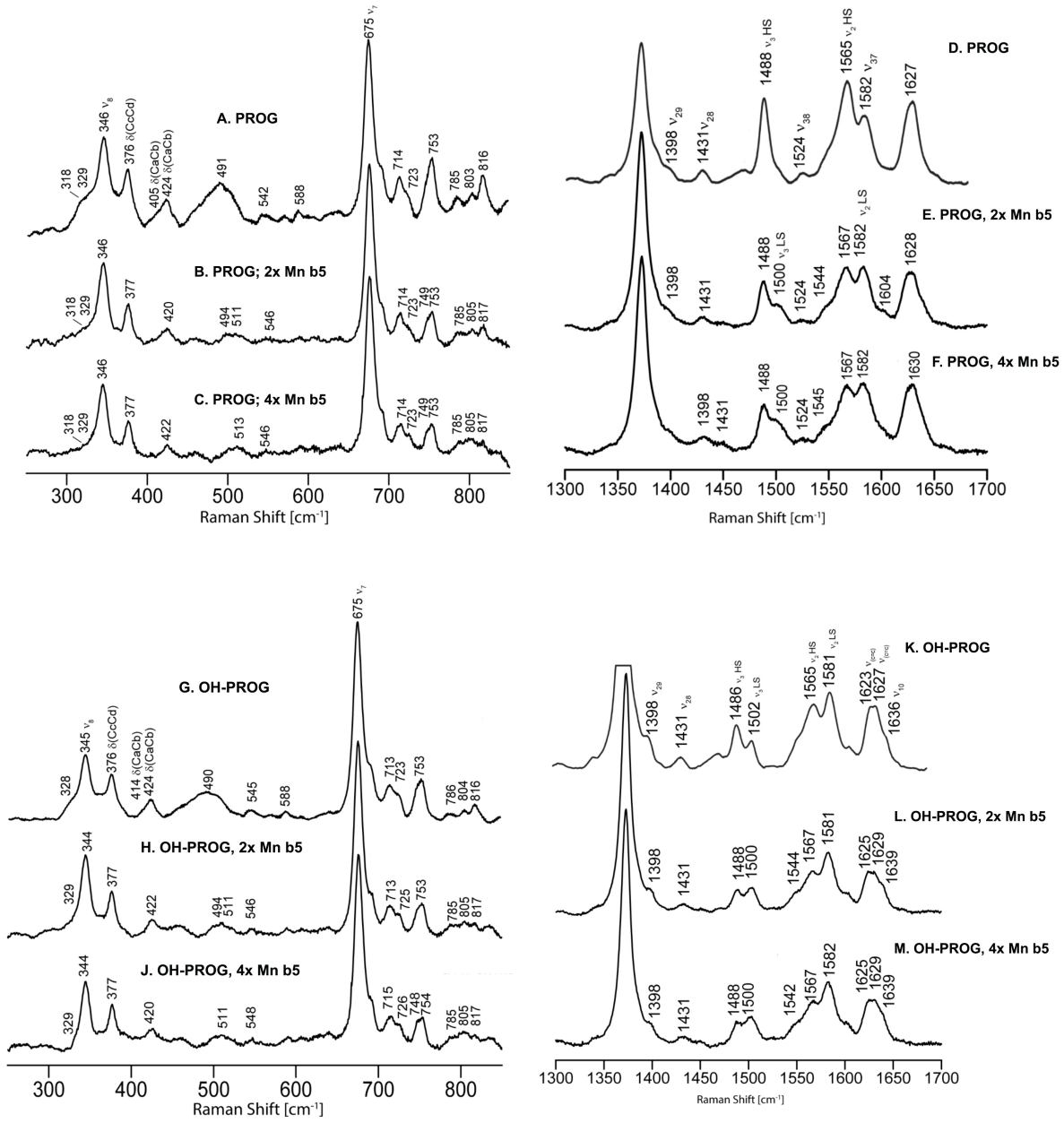

<u>Figure 4.4:</u> Low frequency (left panels) and high frequency (right panels) resonance Raman traces of ferric-CYP17A1 bound to PROG in the absence of Mn *b*$_5$ (A, D); in the presence of 2-fold Mn *b*$_5$ (B, E); in the presence of 4-fold Mn *b*$_5$ (C, F); ferric-CYP17A1 bound to OH-PROG in the absence of Mn *b*$_5$ (G, K); in the presence of 2-fold Mn *b*$_5$ (H, L); in the presence of 4-fold Mn *b*$_5$ (J, M). Excitation wavelength used 406.7 nm.

4.3.3 rR measurements to probe effects of Mn b_5 on oxy-ferrous CYP17A1:

Effects of Mn b_5 binding on oxy-complex was investigated with both the lyase substrates. When OH-PREG was bound to oxy-complex and 2-fold Mn b_5 added, the key $\nu(^{16}O–^{16}O)$ and $\nu(Fe–^{16}O)$ modes were observed at 1135 cm^{-1} and 526 cm^{-1} **(Figure 4.5)**. The corresponding oxygen isotope bands $\nu(^{18}O–^{18}O)$ and $\nu(Fe–^{18}O)$ appeared at 1070 cm^{-1} and 497 cm^{-1}. These modes are identical to previous measurements with OH-PREG bound oxy-ferrous CYP17A1 in the absence of Mn b_5 **(Figure 4.6)** (Gregory et al., 2013a). Therefore, the presence of Mn b_5 did not induce any changes to the conformation of OH-PREG near the dioxygen adduct of heme, suggesting that the origin of cyt b_5 mediated enhancement of OH-PREG turnover can be attributed to its electron transfer role alone.

When similar measurements were done on OH-PROG bound oxy-ferrous samples in complex with 2-fold Mn b_5, $\nu(^{16}O–^{16}O)$ mode was observed at 1131 cm^{-1} and $\nu(^{18}O–^{18}O)$ stretching mode was seen at 1068 cm^{-1} **(Figure 4.7)**. Upon expanding this spectral region and comparing it with the spectrum acquired with $^{18}O_2$, we saw a minor conformer of Fe–O–O fragment with the $\nu(^{16}O–^{16}O)$ mode occurring at 1140 cm^{-1}, which is identical to the OH-PROG spectra obtained in the absence of b_5 **(Figure 4.8)** (Gregory et al., 2013a). Significantly, we observed a new Fe–O–O conformer, with $\nu(Fe–^{16}O)$ mode at 530 cm^{-1} and corresponding $\nu(Fe–^{18}O)$ mode at 501 cm^{-1}. This suggests that the interaction of OH-PROG bound CYP17A1 with Mn b_5 causes partial transformation to a conformer with an H-bonding interaction with the proximal oxygen, similar to that of OH-PREG. This is expected to make the peroxo-anion mediated nucleophilic mechanism more conducive and hence favor the lyase reaction.

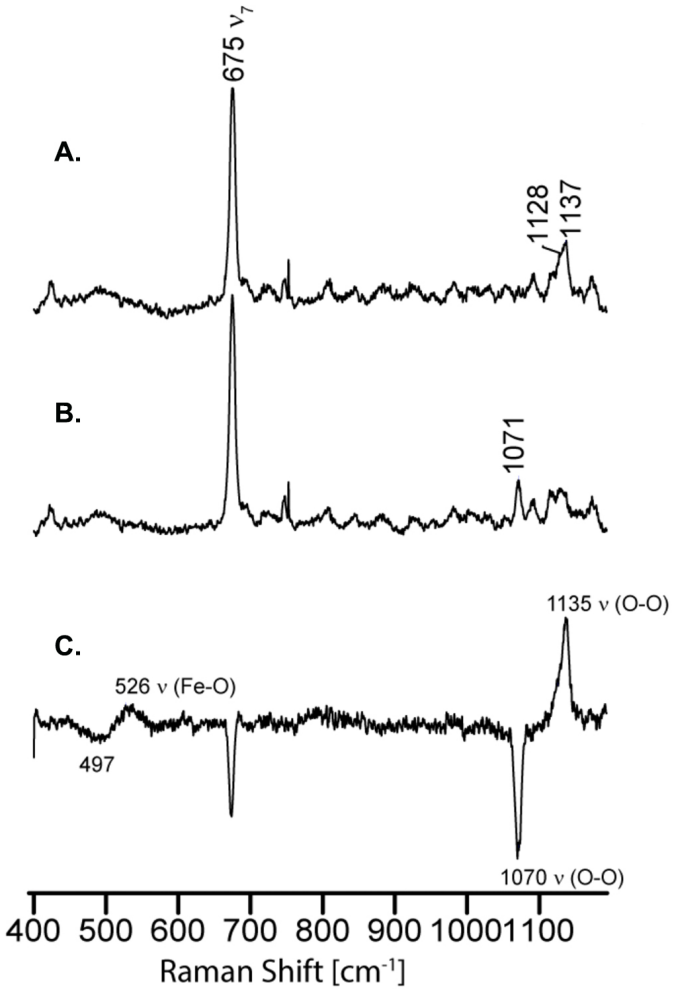

Figure 4.5: Resonance Raman traces of OH-PREG bound oxy-ferrous CYP17A1:ND in presence of 2-fold Mn b_5 in mid-frequency region. Spectra obtained when $^{16}O_2$ was used (A); Spectra obtained for $^{18}O_2$ complex (B); difference spectra obtained by subtracting $^{18}O_2$ trace from $^{16}O_2$. All measurements were done at 77 K and 413.1 nm excitation line was used.

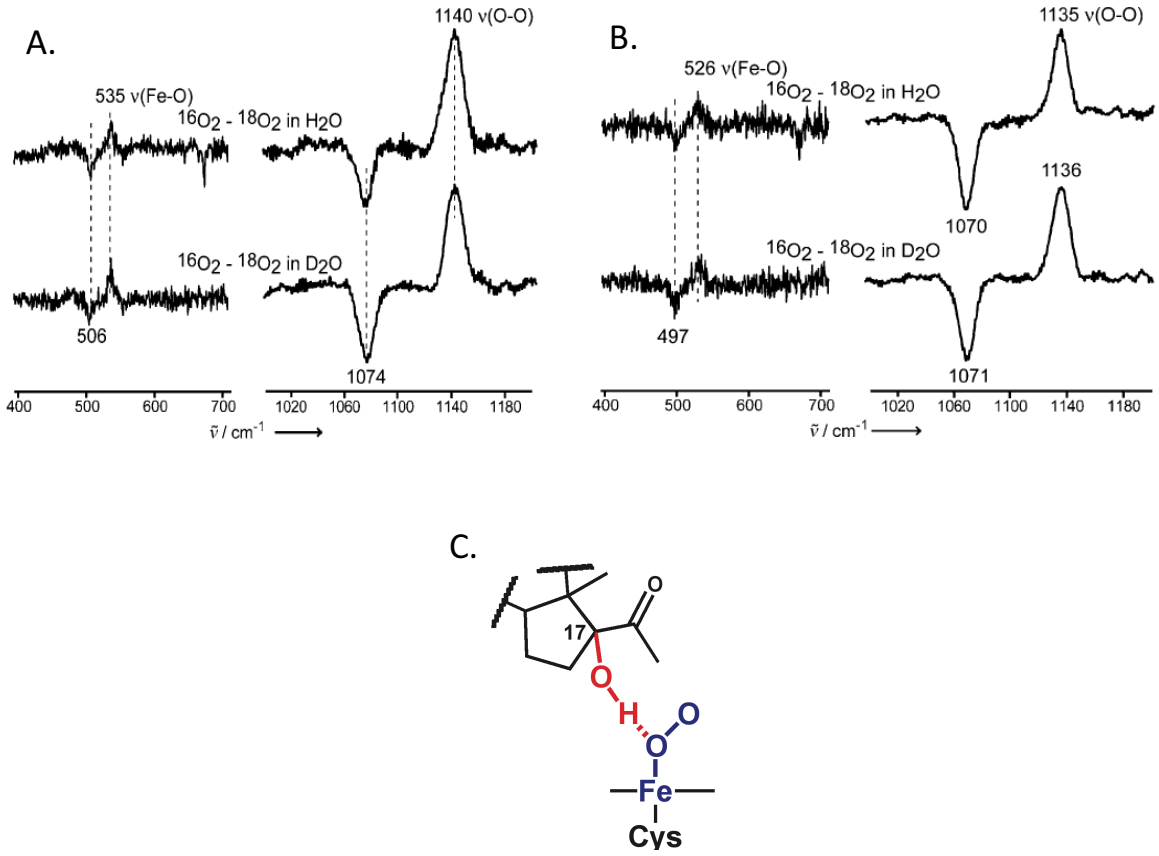

<u>Figure 4.6:</u> Resonance Raman spectra depicted as $^{16}O_2$–$^{18}O_2$ difference traces of PREG (A); and OH-PREG (B) bound oxy-ferrous CYP17A1:ND obtained using 413.1 nm excitation line. The downshifted ν(O–O) and ν(Fe–O) modes in OH-PREG samples are consistent with a hydrogen bonding interaction from the carbonyl-17 of the substrate to the proximal oxygen atom in the oxy-ferrous complex (C). Comparing to Figure 4.5, it is evident that binding of Mn *b_5* to OH-PREG bound oxy-complex does not induce any changes in the substrate orientation with respect to the dioxy-adduct of the heme.

(Gregory et al., 2013a)

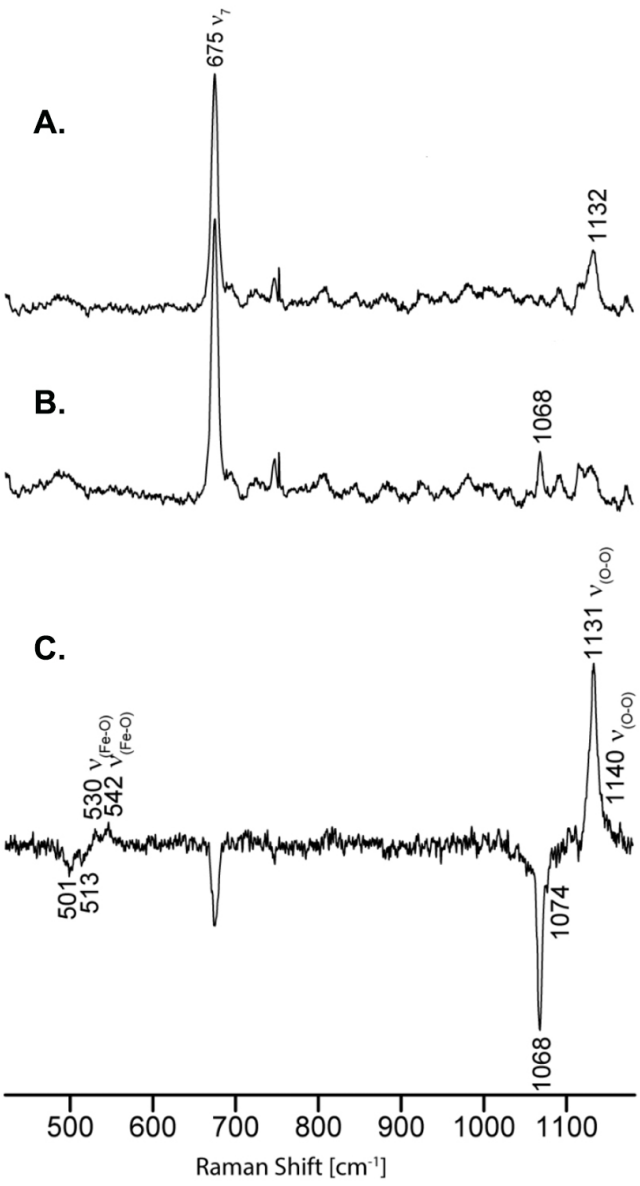

<u>Figure 4.7:</u> Resonance Raman traces of OH-PROG bound oxy-ferrous CYP17A1:ND in presence of 2-fold Mn *b_5* in mid-frequency region. Spectra obtained when $^{16}O_2$ was used (A); Spectra obtained for $^{18}O_2$ complex (B); difference spectra obtained by subtracting $^{18}O_2$ trace from $^{16}O_2$. All measurements were done at 77 K and 413.1 nm excitation line was used.

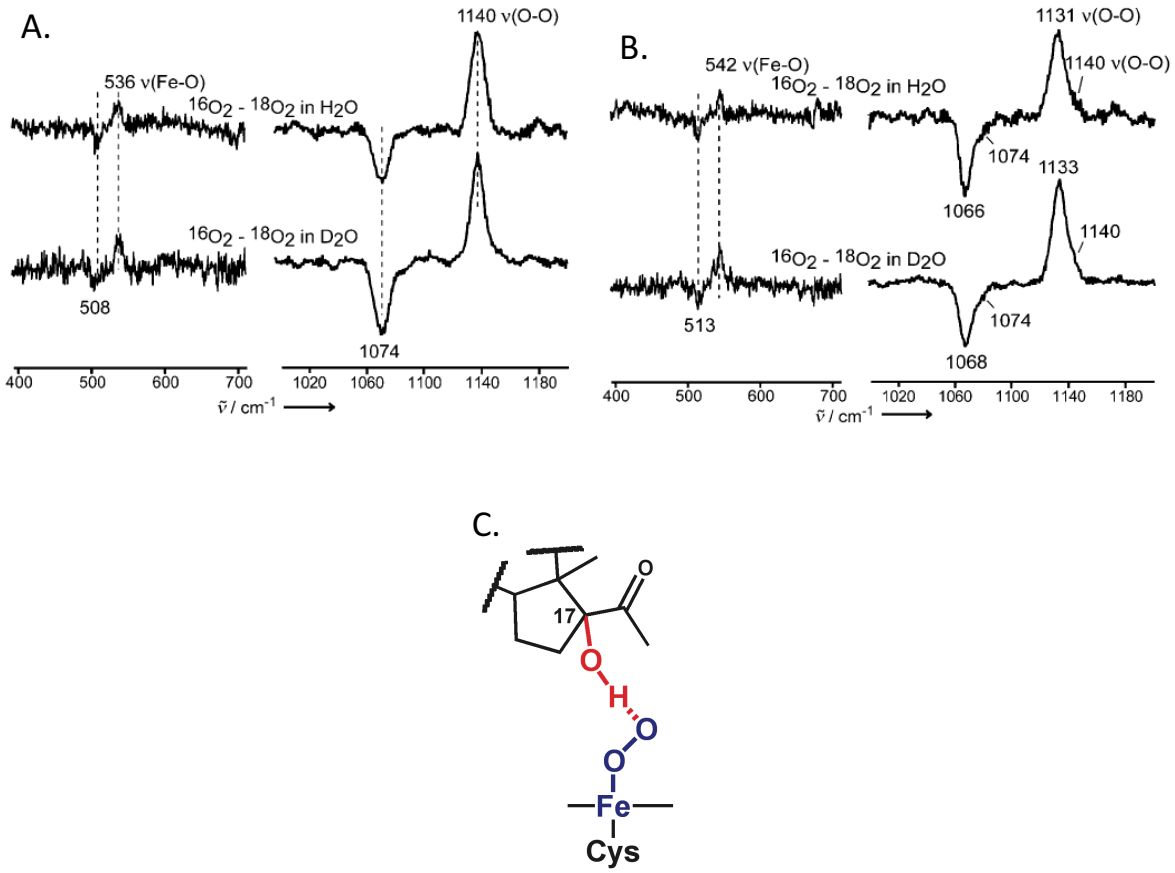

Figure 4.8: **Resonance Raman spectra depicted as $^{16}O_2$–$^{18}O_2$ difference traces of PROG (A); and OH-PROG (B) bound oxy-ferrous CYP17A1:ND obtained using 413.1 nm excitation line. The downshifted ν(O–O) and upshifted ν(Fe–O) modes in OH-PROG samples are consistent with a hydrogen bonding interaction from the 17-hydroxyl of the substrate to the distal oxygen atom in the oxy-ferrous complex (C). Comparing to Figure 4.7, it is evident that binding of Mn *b_5* to OH-PROG bound oxy-complex induces the transition to a conformer in which the substrate orientation is such that the 17-hydroxyl is shifted towards the proximal oxygen atom of the oxy-ferrous complex, possibly forming a hydrogen bond.**

(Gregory et al., 2013a)

4.4 Conclusions

In order to investigate whether cyt b_5 mediated enhancement of CYP17A1 lyase activity arises from a possible electron transfer interaction, I made use of redox inactive form of cyt b_5, in which the heme was replaced with Mn protoporphyrin IX. Mn b_5 failed to stimulate product turnover of either of the two lyase substrates, and also showed no effect on coupling efficiency. This indicates that for the stimulatory effect of cyt b_5 on CYP17A1 androgen synthesis reactions, an electron transfer from the former is critical. We then made use of the remarkable ability of rR spectroscopy to probe conformational changes near the active site occurring as a result of cyt b_5 binding. Experiments with ferric form of CYP17A1 in complex with Mn b_5 showed minor spin state changes and an increase in the bond strength of the Fe–S bond. Collectively, this suggests that while Mn b_5 forms a complex with substrate CYP17A1, it does not enhance lyase turnover due to its inability to perform electron transfer.

Upon application of rR on oxy-ferrous forms of CYP17A1 in complex with Mn b_5, interesting observations were made. When OH-PREG was present in the active site, the observed vibrational modes were identical to when no b_5 was present. The OH-PREG substrate retained the same hydrogen bonding conformation to the dioxygen moiety, which is now known to be favorable for peroxo-anion mediated catalysis on the basis of structural studies with X-ray crystallography, rR measurements as well as recently by DFT calculations (Bonomo et al., 2017; Gregory et al., 2013a; Petrunak et al., 2014). The observation that OH-PREG shows similar H-bonding pattern **(Figure 4.7)** when in complex with cyt b_5, lends further support to the hypothesis that in vivo OH-PREG lyase reaction proceeds through peroxo-anion mediated mechanism. Additionally, it also suggests that the stimulatory effect of cyt b_5 on OH-PREG catalysis to DHEA product arises predominantly from its electron transfer role, with cyt b_5 possibly providing a faster reduction route than CPR. This hypothesis was tested and is documented in chapter 5.

When OH-PROG bound oxy-ferrous CYP17A1 in complex with Mn b_5 was probed and compared to

spectra obtained in the absence of b_5, while the major modes remained unchanged, intriguing new Fe–O modes was observed. These correspond to appearance of a new Fe–O–O conformer, which only appears when Mn b_5 is bound. Based on the 12 cm^{-1} upshift in values of the new ν(Fe–O) modes, we believe that this new conformer has an OH-PREG like hydrogen bonding interaction, with the 17-OH group of the substrate donating an H-bond to the proximal oxygen of the ferrous-dioxygen adduct. This is a very exciting observation, in that cyt b_5 binding causes subtle conformational changes, depending on the identity of the substrate in the active site, and these conformational changes make OH-PROG bound CYP17A1 more amenable to the peroxo-anion mediated nucleophilic attack, thereby stimulating catalysis.

Chapter 5

Investigation of Cytochrome b_5 as Redox Partner for CYP17A1

5.1 Introduction

As described in section 4.4, using redox inactive form of cyt b_5 we found that for it to exert its stimulatory effect on lyase activity, it's electron transfer ability is critical. Our resonance Raman spectroscopy experiments revealed that in the case of OH-PREG bound CYP17A1, aside from minor changes to Fe–S mode, binding of cyt b_5 does not result in detectable perturbations to the heme prosthetic group or to the active site (section 4.4). A recent study by Waskell and coworkers demonstrated that cyt b_5 improves coupling efficiency in CYP17A1 lyase chemistry (Peng et al., 2016). Similar observations were made by us: while cyt b_5 improves coupling efficiency in OH-PREG lyase reaction, Mn b_5 does not, indicating that the effect of cyt b_5 on overall coupling stems from its electron transfer interaction with the oxy-complex (section 4.4).

In the CYP17A1 lyase reaction cycle as depicted in figure 3.4, starts when ferric form of the P450 binds the lyase substrate, partially changing the spin state of the heme from low spin to high spin owing to the displacement of aquo- axial ligand. The high spin heme iron then gets reduced by CPR to form the ferrous species, which then binds a molecule of atmospheric oxygen and forms the oxy-ferrous complex. The oxy-ferrous species has been shown to be involved in hydrogen bonding interactions with the C17-OH group of both lyase substrates, OH-PREG and OH-PROG, albeit in different patterns (Gregory et al., 2013a). The oxy-complex can either autoxidize back to ferric by releasing a superoxide ion, or it can get reduced by cyt b_5 or by CPR to produce the peroxo-anion intermediate. This intermediate is now confirmed to play a key role in the lyase mechanism, by initiating

a nucleophilic attack on carbonyl-20 of the lyase substrates, forming the hemiketal intermediate (Mak et al., 2015, section 3.4). Steps 1 through 3, which are also shared by P450s catalyzing the canonical mono-oxygenation reactions, have been studied in great detail and usually are not the rate determining steps of catalysis. Steps 4 and onwards, on the other hand, are each good candidate for being the rate limiting step. In the case of CYP101A1 mediated conversion of camphor to 5-exo-hydroxycamphor, the second electron transfer from the redox partner putidaredoxin to the oxy-ferrous CYP101A1 was found to be the rate determining step (Brewer and Peterson, 1988). Considering that the stimulatory effect of cyt b_5 relies completely on its ability to carry out electron transfer, and that based on the redox potentials, the only feasible electron transfer interaction between the two proteins is the reduction of the oxy-complex (Lipscomb et al., 1976; Rodgers and Sligar, 1991), we hypothesized that the second reduction in the case of lyase substrate OH-PREG may be at least a partially the rate limiting step of the reaction, and cyt b_5 accelerates this step by providing a faster reduction route than CPR.

It is known that in human androgen synthesis, OH-PREG is the preferred substrate over OH-PROG (Flück et al., 2003). Therefore, we decided to investigate the reduction rate of oxy-ferrous CYP17A1 bound to OH-PREG by cyt b_5 and compare with the rate of reduction by CPR. We also determined the effects of these redox partners on the autoxidation rate of oxy-ferrous CYP17A1. Because CYP17A1, as well as CPR and cyt b_5 are incorporated in the membrane, which plays an important role in defining their mutual orientation and interactions (Sergeev et al., 2014), we employed Nanodisc technology to reconstitute active complexes of these proteins in a native-like membrane environment. Furthermore, since the presence of lipids affects the reduction potential of cyt b_5 (Kawai et al., 1963), nanodiscs present as a perfect model system for determination of rates by which reduction occurs during in vivo reactions. In order to compare the rates of oxy-complex reduction with cyt b_5 and with CPR, we performed rapid mixing experiments of oxygen-saturated buffer with OH-PREG bound ferrous CYP17A1 reconstituted in nanodiscs with reduced redox partners. Immediately after mixing, visible

spectrum was monitored using photodiode array detector with millisecond resolution over the course of 50-200 seconds. To be able to compare the effects of each redox partner on the autoxidation rate of substrate bound oxy-ferrous CYP17A1, we also measured the autoxidation rate of oxy-ferrous complex of CYP17A1 and oxidation rates of cyt b_5 and CPR separately.

5.2 Materials and methods

5.2.1 Protein expression, purification and incorporation into nanodiscs:

The expression, purification and incorporation of CYP17A1 into POPC nanodiscs was performed as previously described in section 2.2.

5.2.2 Preparation of reduced samples of CYP17A1 and redox partners:

Purified nanodiscs assembled with CYP17A1 were taken and incorporation of CPR and/or cyt b_5 was performed by direct addition in 1.1-1.3 fold molar excess of these proteins. The following samples were prepared:

1) Nanodisc reconstituted CYP17A1 (CYP17A1:ND)

2) Cytochrome P450 reductase

3) Cytochrome b_5

4) CYP17A1:ND in complex with 1.3 times molar excess CPR

5) CYP17A1:ND in complex with 1.1 times molar excess cyt b_5

6) Ternary complex of CYP17A1:ND with cyt b_5 and CPR

After addition of 50 μM OH-PREG to each, the samples were deaerated under a constant stream of Argon for 10 minutes. The samples were then transferred to an anaerobic chamber, where they were reduced by adding a small excess of sodium dithionite solution at a known concentration (measured spectroscopically using ε_{314} = 8 $mM^{-1}cm^{-1}$) and methyl viologen (1:20 molar ratio to CYP17A1) to facilitate reduction. Complete reduction was confirmed by the appearance of single peak for ferrous form of CYP17A1 at 410 nm using an Ocean Optics spectrophotometer housed inside the anaerobic chamber.

5.2.3 Stopped flow spectroscopy to follow reaction kinetics:

All experiments were performed on an Applied Photophysics SX.18MV stopped flow spectrophotometer using 75 μL mixing volumes with dead time of 1.5 msec. Each anaerobic sample prepared in section 5.2.2 above was taken in a gastight syringe. In the second syringe oxygen saturated buffer containing the same concentration of OH-PREG was taken. Both these solutions were rapidly mixed in 1:1 ratio following which a thousand spectra were collected on a logarithmic time scale at 298 K at 0 - 50 sec or 0 - 200 sec time intervals using a diode array detector.

5.2.4 Data Analysis

The spectra obtained from each sample were arranged in a matrix and the spectrally different components and the kinetics of their appearance or disappearance were determined by using singular value decomposition (SVD). For autoxidation processes of reduced CYP17A1 and CPR, two distinct kinetic processes were identified. In the case of oxidation of reduced cyt b_5 only one slow process was

observed. For samples containing binary or ternary complexes of proteins, at least three distinct kinetic phases were identified and rate constants for all the processes were calculated using single-exponential or double-exponential fitting subroutines written in MATLAB (Mathworks, US). Because three kinetic phases were well separated in time, in most cases they could be analyzed separately, i.e. in the time intervals 0 - 0.3 s, 0.5 - 5 s and 5 - 50 or 5 - 200 s.

5.3 Results

5.3.1 Determination of autoxidation rates of oxy-ferrous CYP17A1, cyt b_5 and CPR:

Using OH-PREG bound reduced CYP17A1, we determined the rate of unproductive decay of OH-PREG bound CYP17A1 by autoxidation in the absence of any redox partners. A fast process occurring at a rate of ~20 s-1 at 298 K was identified, corresponding to formation of oxy-complex. This oxygen binding rate was similar to the previously reported for other cytochromes P450 (Denisov et al., 2006, 2007b). This fast process was followed by a slower process comprising the autoxidative decay of oxy-complex back to ferric state and simultaneous release of superoxide ion. The rate constant for this slow process was determined to be 0.02 s^{-1} **(Figure 5.1A)**. When only reduced form of cyt b_5 was rapidly mixed with oxygen, the oxidation process was observed to be very slow, occurring at a rate of 0.01 s^{-1} **(Figure 5.1B)**. The oxidation of CPR alone was found to be a multiphasic process, comprising of four kinetic processes corresponding to the two-electron oxidations of the FAD and FMN cofactors. A fast phase in the initial 500 ms with a rate constant of 6 s^{-1} was followed by an intermediate phase from 0.5 to 5 s with a rate constant of 1.5 s^{-1}. Following this, a slow phase (0.08 s^{-1}) and a very slow phase with a decay constant of 0.0006 s^{-1} were identified **(Figure 5.1C)**. This is in agreement with earlier results with oxidation of fully reduced CPR by Coon and coworkers (Oprian and Coon, 1982).

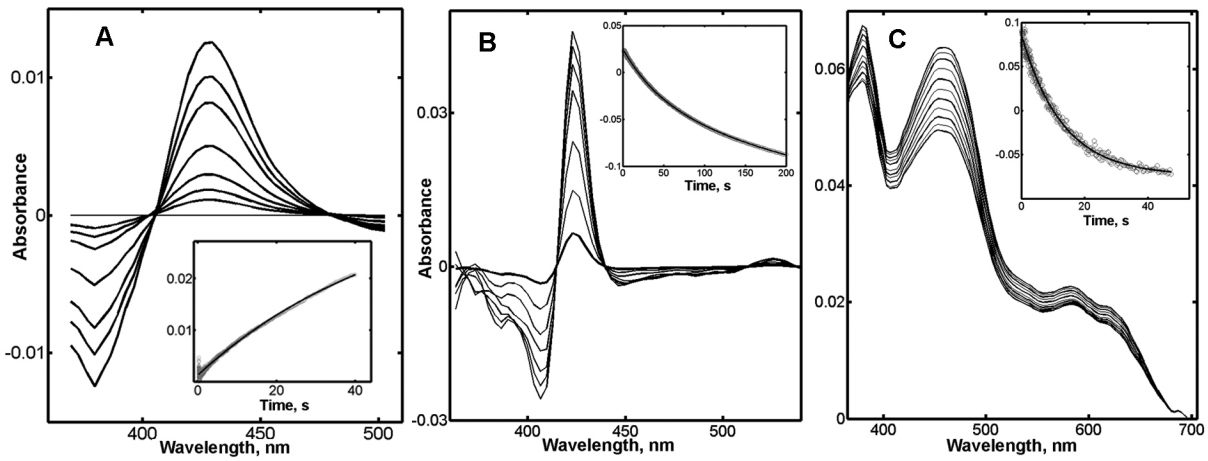

Figure 5.1: Difference spectra depicting autoxidation spectra of OH-PREG bound CYP17A1 (A); oxidation of cyt b_5 (B); and oxidation of CPR (C) obtained upon rapid mixing of oxygen saturated buffer containing OH-PREG with anaerobically reduced proteins. [Insets showing exponential fits for the autoxidative process in A, decay of reduced cyt b_5 component in B and decay of reduced CPR component in C].

5.3.2 Determination of rates of reduction of oxy-ferrous CYP17A1 by redox partners:

In the binary complex of CYP17A1 and CPR, three kinetic phases were identified. The fast phase attributed to the formation of oxy-complex proceeded with a rate of 18 s^{-1}, and occurred during the first 500 ms after mixing. This was followed by an intermediate phase with a decay constant of 0.09 s^{-1} was followed by a slow phase with a decay constant of 0.01 s^{-1} **(Figure 5.2)**. Approximately 85% of the decay was observed to proceed in the slow phase. Fast phase of CPR oxidation process could not be separated in this sample owing to its strong overlap with the Soret region of CYP17A1 spectrum.

When CYP17A1 was in complex with cyt b_5, after the formation of oxy-complex was completed at a rate of 24 s^{-1}, an intermediate kinetic phase was observed between 0.5 to 5 s. This was fit to an exponential decay constant of 0.9 s^{-1}, followed by a slower phase with a decay constant of 0.044 s^{-1}

(Figure 5.3). About 20% of the mixture decayed in the intermediate phase, which constitutes disappearance of the oxy-complex and formation of its ferric form and the simultaneous transition of cyt b_5 from reduced to oxidized form. The spectral signal observed for this process could be well represented as 1:1 combination of difference spectra corresponding to autoxidation of oxy-complex in CYP17A1 and oxidation of cyt b_5. Both the spectral signal and the stark difference between the decay rate of oxy-complex by autoxidation at 0.02 s^{-1}, and the decay to ferric form after reduction by cyt b_5 at a 45-fold faster rate, indicate the direct electron transfer from ferrous b_5 to the oxy-complex.

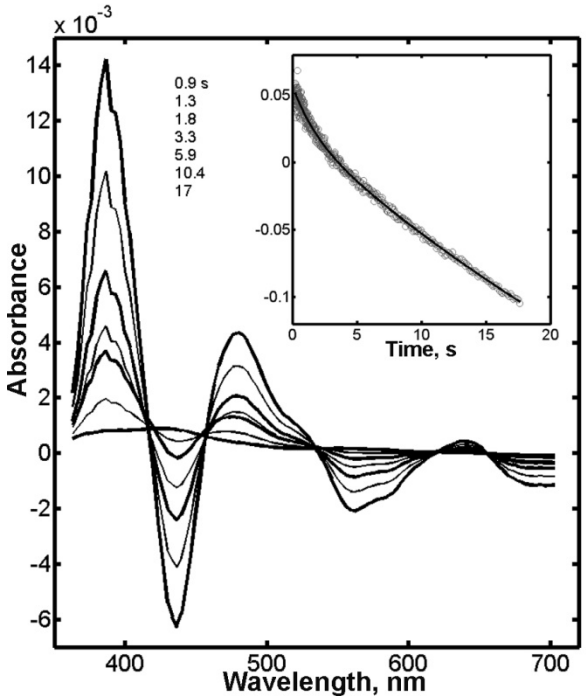

Figure 5.2: Difference spectra obtained when anaerobically reduced complex of OH-PREG bound CYP17A1 and CPR was rapidly mixed with oxygen saturated buffer containing saturating amounts of OH-PREG. Inset: exponential fit for the decay of oxy-complex and the reduced CPR component.

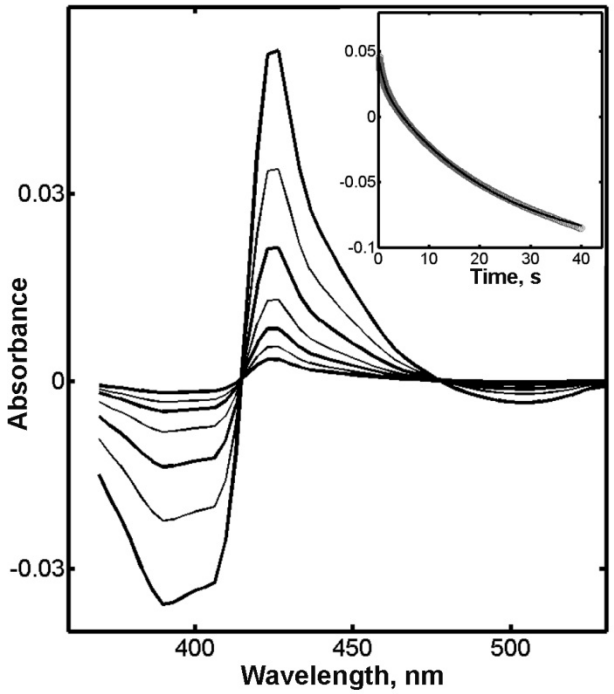

Figure 5.3: Difference spectra obtained when anaerobically reduced complex of OH-PREG bound CYP17A1 and cyt b_5 was rapidly mixed with oxygen saturated buffer containing saturating amounts of OH-PREG. Inset: exponential fit for the decay of oxy-complex and the reduced cyt b_5 component.

Scott and colleagues have used solution NMR to map to the binding sites for CPR and cyt b_5, and determined that both the redox partners occupy partially overlapping binding sites on CYP17A1 surface (Estrada et al., 2013). In light of this information, we wanted to determine how the reduction rates are affected in a situation where CYP17A1 has access to both the redox partners. In the sample with ternary complex of CYP17A1 with CPR and cyt b_5 in a nanodisc, both the redox partners are available for carrying out reduction of the oxy-ferrous enzyme. In this case, four kinetic processes were identified. Formation of oxy-complex was completed in the first 500 ms. From 500 ms to 5 s, two intermediate phases were observed: first with a decay constant of 1.3 s^{-1} and a second intermediate

phase occurring at a rate of 0.2 s^{-1}. A final slow phase with a decay constant of 0.025 s^{-1} was seen from 5 s to 200 s **(Figure 5.4)**. Comparing the kinetics observed in the binary and ternary complexes, the rates of disappearance of CYP17A1 oxy-complex in a ternary complex are more comparable to that in CYP17A1-cyt b_5 complex (1.3 and 0.9 s^{-1}). On the other hand, the decay rate in CYP17A1-CPR complex was determined to be at least 10-fold slower than that in the CYP17A1-cyt b_5 complex. All the determined values of rate constants for their respective kinetic processes for each sample are summarized in **Table 5.1**.

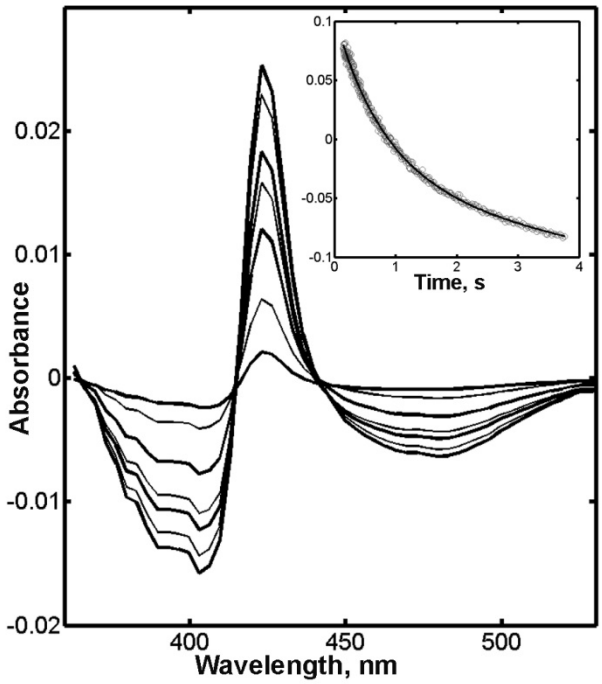

Figure 5.4: Difference spectra obtained when anaerobically reduced complex of OH-PREG bound CYP17A1 with cyt b_5 and CPR was rapidly mixed with oxygen saturated buffer containing saturating amounts of OH-PREG. Inset: exponential fit for the decay of oxy-complex and the reduced cyt b_5 and CPR component.

		O_2 Binding	Oxidation	
S. No.	**Reduced sample**	**0 – 500 ms**	**500 ms – 10 s**	**10 – 200 s**
1.	CYP17A1	20 s^{-1}		0.02 s^{-1}
2.	Cyt b_5			0.01 s^{-1}
3.	CPR	6 s^{-1} (oxidation)	1.4 s^{-1}	0.08 s^{-1}, 0.0006 s^{-1}
4.	CYP17A1 + CPR	18 s^{-1}	0.09 s^{-1} (~15%)	0.01 s^{-1} (~85%)
5.	CYP17A1 + cyt b_5	24 s^{-1}	0.9 s^{-1} (~20%)	0.044 s^{-1} (~80%)
6.	CYP17A1 + cyt b_5 + CPR	21 s^{-1}	1.3 s^{-1} (~5%) and 0.2 s^{-1} (~15%)	0.025 s^{-1} (~80%)

Table 5.1: Rate constants of all the isolated kinetic processes obtained when anaerobically reduced samples were rapidly mixed with oxygen saturated buffer in a stopped flow setup.

5.4 Conclusions

We observed that oxygen binding to ferrous CYP17A1 saturated with OH-PREG is fast, occurring within the first 500 ms and remained unaffected by the presence of CPR or cyt b_5. When the decay of the oxy-complex was compared, an intermediate phase appeared when cyt b_5 was reconstituted with CYP17A1 in nanodiscs. This kinetic process with the rate 0.9 s^{-1} at 298 K is assigned to the electron transfer from reduced cyt b_5 to the oxy-complex in CYP17A1, resulting in formation of oxidized cyt b_5 and rapid formation of ferric form of CYP17A1. This assignment is based on the clear spectral signal corresponding to the linear combination of two processes. It should be noted that this process is significantly faster than the second electron transfer from CPR to the oxy-complex in CYP17A1, which occured at a rate of 0.09 s^{-1}. Clearly, the rate of reduction of oxy-ferrous CYP17A1 by cyt b_5 is 10 times faster than that by CPR.

A significant observation was made when both redox partners were present with CYP17A1 in nanodiscs. The faster kinetic process with cyt b_5 spectral contribution was clearly observed, indicating

more favorable interaction of cyt b_5 with CYP17A1, even in the presence of CPR. This preference of cyt b_5 as a redox partner at the second electron transfer step suggests the similar mechanism of the NADPH supported catalytic cycling in CYP17A1, where CPR displaces itself from the P450 after carrying out the first electron transfer, and gets replaced by reduced cyt b_5, which serves as a faster second electron donor. In this bound state, cyt b_5 may also play the role of an allosteric effector, modulating subsequent catalytically important events, such as altering the active site orientation of the bound substrate to a more productive conformation as evidenced by our rR experiments with OH-PROG (section 4.4), or modulating the decay of hemiketal intermediate towards faster release of product.

In conclusion, we measured oxygen binding and oxidation rates of OH-PREG bound, reduced CYP17A1, cyt b_5 and CPR in nanodiscs by oxygen using stopped flow spectroscopy. Cyt b_5 was observed to reduce oxy-ferrous CYP17A1 much faster than CPR, and indicated to be the predominant redox partner in a ternary complex, where both cyt b_5 and CPR were reconstituted with CYP17A1. The finding that cyt b_5 is the predominant second electron donor in CYP17A1 lyase catalysis accounts for our and others' previous observation that presence of cyt b_5 improves coupling efficiency. This also agrees with the potential role of cyt b_5 as an allosteric modulator for steps of catalysis subsequent to the second reduction. These steps are expected to be very fast, and may be occurring before cyt b_5 gets dissociated from CYP17A1 after performing the reduction of oxy-complex.

Chapter 6

Investigation of Proton Dependence in CYP19A1 Mediated Estrogen Synthesis

6.1 Introduction

Considering the unusual solvent isotope effects and reaction chemistry in the lyase reactions leading to androgen synthesis, we set out to determine whether the similar lyase step in estrogen synthesis follows an identical mechanistic path. As explained in chapter 2, in order to distinguish compound I mediated mechanism from a peroxo-anion mediated mechanism, the proton dependence of the former can be utilized. We compared kinetic solvent isotope effects (KSIEs) on the steady-state turnover of the hydroxylation reactions (steps I and II) and lyase (step III) reaction by human CYP19A1. The involvement of Cpd I, which depends on two protons to generate the oxo-ferryl intermediates, or nucleophilic reactivity of a ferric peroxoanion intermediate before involvement of the proton in O–O bond cleavage could be probed by this technique.

Although several steady-state parameters for the conversion of AD to estrone have been measured earlier either in human placental aromatase (Hagerman, 1987; Kellis and Vickery, 1987; Tan and Muto, 1986; Thompson Jr. and Siiteri, 1974), recombinant human CYP19A1 expressed in insects (Amarneh

Reproduced in part with permission from

Khatri, Y., Luthra, A., Duggal, R., and Sligar, S.G. Kinetic solvent isotope effect in steady-state turnover by CYP19A1 suggests involvement of Compound 1 for both hydroxylation and aromatization steps. FEBS Letters (2014) 588, 3117–3122. Copyright 2014 John Wiley and Sons. The published version may be found online at https://dx.doi.org/10.1016/j.febslet.2014.06.050.

and Simpson, 1995; Gartner et al., 2001) or bacteria (Kagawa et al., 2003, 2004; Sohl and Guengerich, 2010), the transient-state kinetic studies during the conversion of AD to estrone have not been studied except by the Guengerich group (Sohl and Guengerich, 2010). However, all previous kinetic studies were performed in detergent solubilized form and reconstituted with different stoichiometries of CPR, and the detailed mechanism of the lyase reaction was not addressed. In this study, we employed recombinant human CYP19A1 incorporated in nanodiscs, which provides a soluble, homogenous, monodispersed protein with well controlled stoichiometry during reconstitution with its redox partner CPR and hence mimics the biological integrity in the membrane (Denisov and Sligar, 2011; Luthra et al., 2013; Schuler et al., 2013).

6.2 Materials and methods

6.2.1 Expression and purification of human CYP19A1 and rat CPR:

The expression and purification of CYP19A1 was performed as described (Gantt et al., 2009). CPR expression and purification protocol has been described earlier in chapter 2.

6.2.2 Incorporation of CYP19A1-CPR functional complex in nanodiscs:

The reconstitution of purified CYP19A1 in nanodiscs was performed as described (Luthra et al., 2013). Incorporation of CPR into purified human CYP19A1 nanodiscs was done by direct addition of oligomeric CPR at 1:4 molar ratio (200 pmol CYP19A1/800 pmol CPR (Grinkova et al., 2010a).

6.2.3 Determination of steady state kinetic solvent isotope effects on CYP19A1 catalysis:

1 mL of CYP19A1 and CPR solution in 100 mM potassium phosphate buffer, pH 7.4, containing 50 mM NaCl and 50 μM substrate (AD, 19-OH-AD, or 19-oxo-AD) was brought to 37 °C in a stirred quartz cuvette, path length of 0.4 cm. The sample was incubated for 3 min and the reaction initiated with 300 μM of NADPH. The NADPH oxidation was monitored by recording the absorbance at 340 nm for 10 min. The reaction was stopped by adding 50 μl of 8.9 N sulfuric acid to bring the pH below 4.0. The sample was removed from the cuvette, flash frozen in liquid nitrogen, and stored at −80 °C until product analysis. The optical measurements were performed using Hitachi U-3300 spectrophotometer with a temperature controller and built-in magnetic stirrer. The rate of NADPH oxidation was determined from the slope of absorption at 340 nm during the first three minutes using an extinction coefficient of 6.22 $cm^{-1}mM^{-1}$.

The conversion of AD, 19-OH and 19-oxo-AD to estrone was analyzed by HPLC (Waters). Briefly, 1 μL of 18 mM progesterone solution in methanol was added to 1 mL each of the reaction sample, as an internal standard, and vortexed for 30 sec. 2 mL of chloroform was added to each aliquot and vortexed for 30 seconds. The organic phase was removed and dried under the stream of nitrogen. The dried sample was dissolved in 100 μL of methanol and 30 μL was injected onto C18 HPLC (150 x 2.1 mm) ACE-111-1502 with the mobile phase of 45% each of methanol and acetonitrile in water and a flow rate of 0.2 ml/min. The 19-hydroxylated and 19-oxo product of AD was separated in the linear gradient of methanol and acetonitrile from 20% to 80% in 30 min, and detected at 240 nm. The formation of estrogen was detected at 280 nm. Peak integration was performed with GRAM/32 software (Thermo Fisher Scientific).

6.3 Results

6.3.1 Steady-state turnover by CYP19A1 in protiated and deuterated solvent systems:

CYP19A1 and CPR self-assembled in nanodiscs was used to quantitate product formation and NADPH oxidation rates in the presence of saturating concentrations of AD and 19-OH-AD for hydroxylation and 19-oxo-AD for the lyase reaction at 37 °C and pH/pD 7.4. Deuterated samples were prepared by exhaustive exchange of the proteins in corresponding D_2O buffers. In order to determine the reaction time for the substrates AD, 19-OH-AD and 19-oxo-AD, time-dependent substrate conversion was performed and the 10 min incubation time was chosen for the catalytic activity, during which the catalytic activity was in linear phase **(Figure 6.1)**. Using AD as the starting substrate, 19-OH-AD and 19-oxo-AD were obtained in the reaction mixture under steady state conditions. Similarly, when 19-OH-AD was used as the starting substrate, 19-oxo-AD and estrone were formed. Starting with AD, 19-OH-AD and 19-oxo-AD were obtained with the individual rates of 1.63 ± 0.04 min^{-1} and 4.06 ± 0.30 min^{-1} respectively, (total rate of 5.70 ± 0.34 min^{-1}) when the reaction was carried out in a protiated buffer system. Rates of formation of both these products showed substantial slowing upon H/D substitution, yielding a KSIE for the step I hydroxylation reaction of k_H/k_D = 2.7. In both the cases, the rate of second product formation was almost 2.5 times faster, suggesting a distributive nature of the enzyme. It is noteworthy that both the rates of formation of individual products (0.62 ± 0.07 min^{-1} and 1.52 ± 0.15 min^{-1} for 19-OH-AD and 19-oxo-AD, respectively) as well as total product (2.14 ± 0.22 min^{-1}), displayed an isotope effect of 2.6 **(Figure 6.2)**.

The observed KSIE ratios are very similar to reports for hydroxylation reactions catalyzed by other P450s (Batabyal et al., 2013; Liu and Ortiz de Montellano, 2000; Vidakovic et al., 1998). This therefore confirms that the first two steps of CYP19A1 catalysis i.e. AD to 19-OH-AD and 19-OH-AD to 19-oxo-AD are classical P450 hydroxylation reactions and involve the classical Cpd I intermediate. For the lyase substrate 19-oxo-AD, the rate of estrone formation was 2.5 times slower in D_2O (i.e. 7.1 ± 0.8

min^{-1} in H_2O versus 2.8 ± 0.8 min^{-1} in D_2O) **(Figure 6.2)**. This corresponds to the KSIE of k_H/k_D = 2.53, similar to that seen when AD was used as the starting substrate. This suggests the involvement of same reactive intermediate Cpd I during lyase catalysis as well, in contrast to what we observed in the case of lyase reaction mediated by CYP17A1.

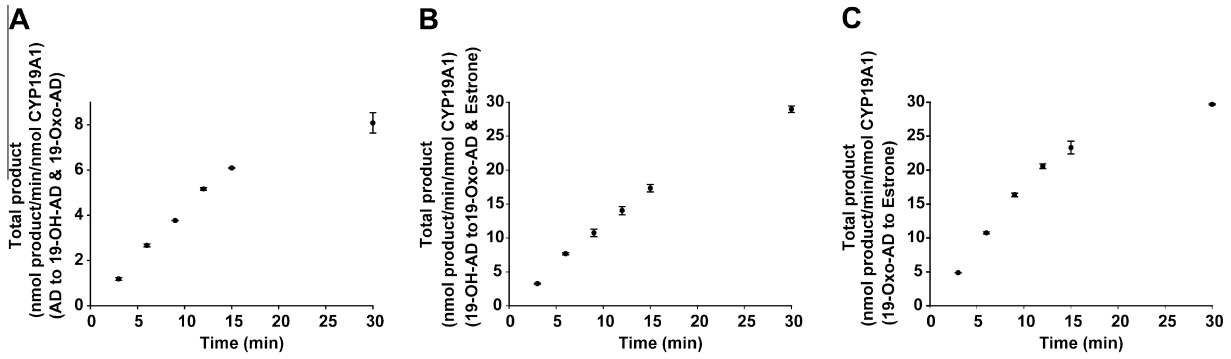

Figure 6.1: Product formation rates as a function of reaction time for AD to 19-(OH)-AD and 19-oxo-AD (A); 19-OH-AD to 19-oxo-AD and estrone (B); 19-oxo-AD to estrone (C). Based on these results, reaction time of 10 min was used for subsequent experiments.

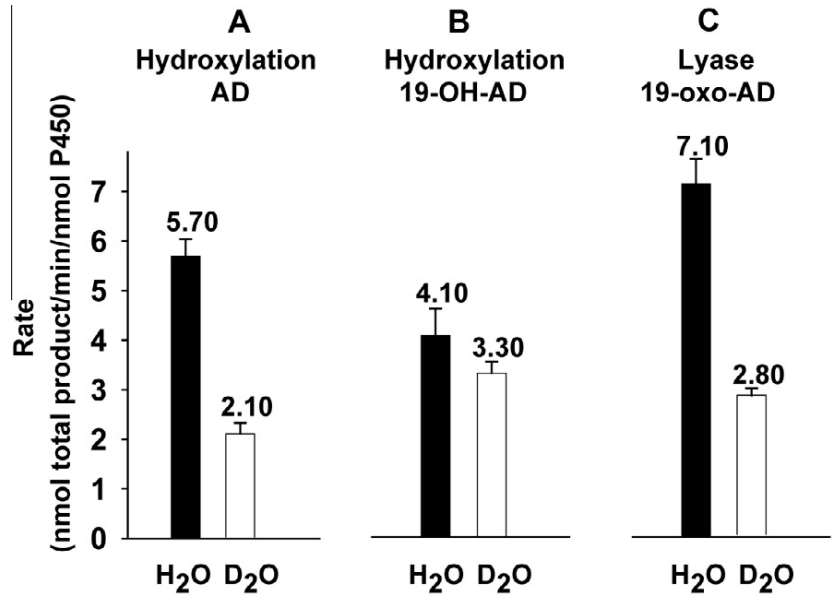

<u>Figure 6.2:</u> Product formation rates for CYP19A1 mediated catalysis highlighting kinetic solvent isotope effects on conversion of AD to 19-OH-AD and 19-oxo-AD (A); 19-OH-AD to 19-oxo-AD and estrone (B); 19-oxo-AD to estrone (C). Black bars represent turnover in protiated buffer system, white bars represent turnover in deuterated buffer system.

The conversion of 19-OH-AD to its products by CYP19A1 is unusual. In H_2O, 19-oxo-AD and estrone were obtained at a rate of 2.3 ± 0.2 min^{-1} and 1.8 ± 0.3 min^{-1} respectively with a total rate of 4.1 ± 0.5 min^{-1}. The second hydroxylation step of CYP19A1 also showed the same distributive nature of the enzyme and gave two products. However, the rate of second product formation was slower in this case. The rates of 19-oxo-AD and estrone decreased to 2.39 ± 0.14 min^{-1} and 0.91 ± 0.09 min^{-1}, respectively (the total of 3.30 ± 0.23 min^{-1}) in D_2O, which gave an overall KSIE of k_H/k_D = 1.2 **(Figure 6.2)**. Formation of estrone showed a KSIE of 2.0 (1.8 min^{-1} in H_2O versus 0.91 min^{-1} in D_2O). However, the formation of 19-oxo-AD showed virtually no solvent isotope effect bringing the net KSIE of product formation down to 1.2. Conversion of 19-OH-AD to 19-oxo-AD goes through a hydroxylation at the C19 to produce a gem-diol that then undergoes dehydration to yield the 19-oxo-AD intermediate **(Figure 6.3)**. It is plausible that the rate of dehydration of the gem-diol intermediate is partially rate

limiting resulting in a diminished KSIE for 19-oxo-AD formation and giving rise to a smaller observed KSIE with respect to total product for step II as compared to steps I and III of CYP19A1 catalysis. It is noteworthy that the formation of estrone from 19-OH-AD shows a KSIE >2, which is consistent with other data.

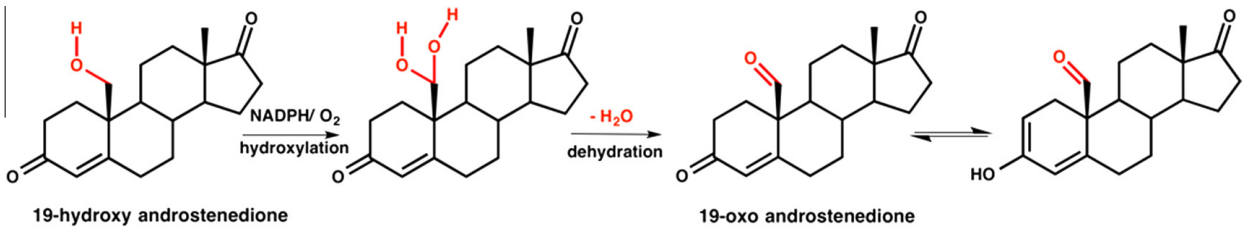

Figure 6.3: CYP19A1 mediated conversion of 19-OH-AD to 19-oxo-AD by dehydration of a geminal-diol at C-19 position formed following the hydroxylation steps I and II.

6.3.2 Effect of H_2O vs. D_2O on coupling efficiency in CYP19A1 mediated reactions:

The overall rate of NADPH oxidation in the presence of various substrates of CYP19A1 was also studied. The total rates of conversion of AD and 19-OH in H_2O are 37±4.5 min^{-1} and 37±4 min^{-1}, and in D_2O are 14 ± 1.5 min^{-1} and 8.00 ± 1.3 min^{-1}, respectively. These data correspond to the ‘‘normal’’ KSIE observed in the product formation rate **(Figure 6.4)**. Though both the conversions were highly uncoupled, the coupling efficiency was higher in D_2O (16% and 41%) compared to 15% and 11% in H_2O for the substrates AD and 19-OH-AD, respectively. Likewise, when the lyase substrate 19-oxo-AD was used, the rate of NADPH oxidation in D_2O was also decreased by 83%, from 35 ± 1 min^{-1} to 6 ± 1.2 min^{-1} **(Figure 6.4)**. A higher level of coupling in deuterated solvents is due to slowing of the proton dependent uncoupling pathways, predominantly the peroxide and oxidase shunt pathways. The higher coupling efficiency observed in the presence of 19-OH-AD and 19-oxo-AD may be attributed to

the polar nature of these substrates thereby making possible presence of additional water molecules and/or enhanced stabilization of the existing hydrogen-bonding network at the active site of the enzyme.

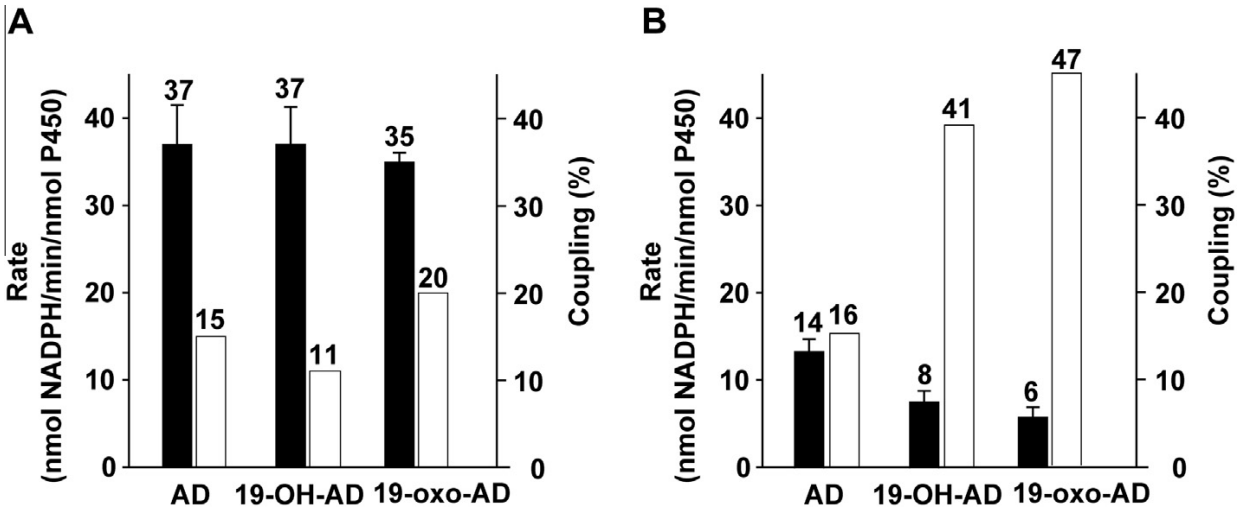

<u>Figure 6.4:</u> Rates of NADPH consumption (black bars) and coupling efficiency (white bars) during CYP19A1 mediated catalysis of AD, 19-OH-AD and 19-oxo-AD in protiated buffer system (A); Rates of NADPH consumption (black bars) and coupling efficiency (white bars) during CYP19A1 mediated catalysis of AD, 19-OH-AD and 19-oxo-AD in deuterated buffer system (B).

6.4 <u>Conclusions</u>

The hydroxylation reactions (steps I and II) in CYP19A1 catalysis were observed to be slower in D_2O, (k_H/k_D of 2.7 and 1.2) consistent with the need for two protonation steps in the formation of the hydroperoxo- ferric complex and Cpd I. These observations are also consistent with the previous reports of solvent isotope effects in CYP101A1 and other P450s (Batabyal et al., 2013; Raag et al.,

1991; Shimada et al., 1997). The presence of kinetic solvent isotope effect of a similar magnitude when 19-oxo-AD, the substrate for lyase step of CYP19A1, suggests the involvement of the Cpd I intermediate for this reaction as well. In addition, CYP19A1 also showed the highest coupling for the lyase substrate, 19-oxo-AD, compared with the hydroxylase substrates, AD and 19-OH-AD, in both protiated and deuterated solvent system.

Taken together, our results suggest that the involvement of the same high-valent iron-oxo species, Cpd I, as the reactive intermediate during the conversion of AD, 19-OH-AD and 19-oxo-AD. This is based on the significant KSIE observed during the first two steps of hydroxylation as well as the last step of lyase reaction. Our conclusions are also in line with the suggestion, albeit indirect, of Cpd I mediated C–C scission by CYP19A1 provided by the rR characterization of the oxy-complexes of AD and 19-oxo-AD bound CYP19A1 in Nanodiscs. This is in stark contrast to our results with human CYP17A1 mediated lyase reaction.

Chapter 7

Summary

CYP17A1 and CYP19A1 are the key cytochrome P450 enzymes involved in hormone biosynthesis in humans. While CYP17A1 is responsible for synthesizing androgens from the precursors progesterone and pregnenolone, CYP19A1 acts on the androgens to produce estrogens. Both these enzymes attract special interest because in addition to catalyzing conventional hydroxylation reactions, they also mediate scission of carbon-carbon bonds. The mechanism and modulation of these lyase reactions is of significant interest in efforts for drug development to target hyper-activation of both these P450s, but has remained elusive so far.

During my thesis research, I have tried to answer some of these important mechanistic questions. By determining kinetic solvent isotope effects on the product formation rates for CYP17A1 mediated formation of AD from OH-PROG, I was able to show that this reaction follows a proton independent mechanism. Using cryo-radiolytic reduction and thermal annealing to follow reaction intermediates, I observed that unlike the hydroxylation reactions, during CYP17A1 catalyzed AD formation, a new intermediate appeared following the peroxo-anion species. By employing resonance Raman spectroscopy on thermally annealed samples, we were able to deduce that the new intermediate is a peroxo-hemiketal, similar to the intermediate previously discovered in OH-PREG catalysis by (Mak et al., 2015).

A very important aspect of CYP17A1 mediated androgen synthesis is the selective modulation of the lyase reaction by cyt b_5. Whether cyt b_5 acts only as an allosteric effector, or if it acts as an electron donor has been a subject of intense debate and controversy. In order to answer this question, I

prepared redox inactive form of cyt b_5 in which the heme iron was substituted with manganese (Mn b_5). I observed that unlike cyt b_5, Mn b_5 was unable to stimulate product formation with either of the lyase substrates. This clearly suggests that for cyt b_5 mediated stimulation of CYP17A1 mediated androgen synthesis, the electron transfer ability of the former is crucial.

In order to probe any allosteric effects associated with cyt b_5 binding, we used resonance Raman spectroscopy on substrate bound ferric and oxy-ferrous CYP17A1 in complex with Mn b_5, which was used to avoid spectral overlap from heme of cyt b_5. Mn b_5 binding to ferric CYP17A1 failed to induce any significant changes in the heme vibrational modes or the active site. However, the axial Fe–S bond was observed to be strengthened in ferric CYP17A1 in complex with Mn b_5. When rR measurements were done on oxy-ferrous CYP17A1 in complex with Mn b_5 and bound to OH-PREG, the spectra appeared similar to those when no Mn b_5 was present. It should be recalled that previous rR studies with OH-PREG and OH-PROG bound oxy-ferrous CYP17A1 performed by (Gregory et al., 2013) show that in the absence of any cyt b_5, there is a hydrogen bonding interactions between the substrate 17-OH group and dioxygen ligand of the heme.

In the case of OH-PREG, the 17-OH group donates a hydrogen bond to the proximal oxygen atom, whereas 17-OH group of OH-PROG is involved in a hydrogen bond with the distal oxygen of the Fe–O–O of the P450. Taken together, it follows that for OH-PREG catalysis, cyt b_5 enhances the rate of DHEA product formation solely on account of its redox donor role. On the other hand, similar rR experiments with OH-PROG bound oxy-ferrous CYP17A1 in complex with Mn b_5 showed partial conversion to a conformer in which the 17-OH group of the substrate was involved in hydrogen bond with the proximal oxygen atom. This orientation of substrate is most conducive for the distal oxygen of the peroxo-anion to initiate nucleophilic attack on the C-20, thereby giving rise to the peroxo-hemiketal intermediate. Therefore, in addition to the aforementioned redox role, cyt b_5 also exerts subtle conformational changes which are dependent on the identity of the substrate in the active site.

In order to investigate how the electron transfer role of cyt b_5 stimulates OH-PREG turnover to DHEA, we measured reduction rates of substrate bound oxy-ferrous CYP17A1 by CPR and by cyt b_5 using a stopped flow setup. We determined that cyt b_5 reduces OH-PREG bound oxy-complex 10-fold faster than CPR, and in a ternary complex, the reduction predominantly occurs by cyt b_5. The results from the CYP17A1 study can be summarized in a simplified version as **Figure 7.1.**

Upon investigation of kinetic solvent isotope effects on the product formation rates for CYP19A1 catalyzed synthesis of estrogens from androgen substrates, I observed that unlike CYP17A1, CYP19A1 lyase reaction proceeds through the proton dependent compound I pathway.

In a nutshell, while CYP17A1 follows different mechanistic pathways for carrying out different reaction chemistries in the same active site, CYP19A1 employs the same intermediate for all its reactions. Cytochrome b_5 mediated modulation of CYP17A1 lyase step requires a critical redox transfer from the former, and cyt b_5 reduces oxy-complex 10 times faster than the reduction rate by CPR. Furthermore, while we observed subtle conformational changes associated with this interaction, they are strictly dependent on the identity of the substrate in the active site.

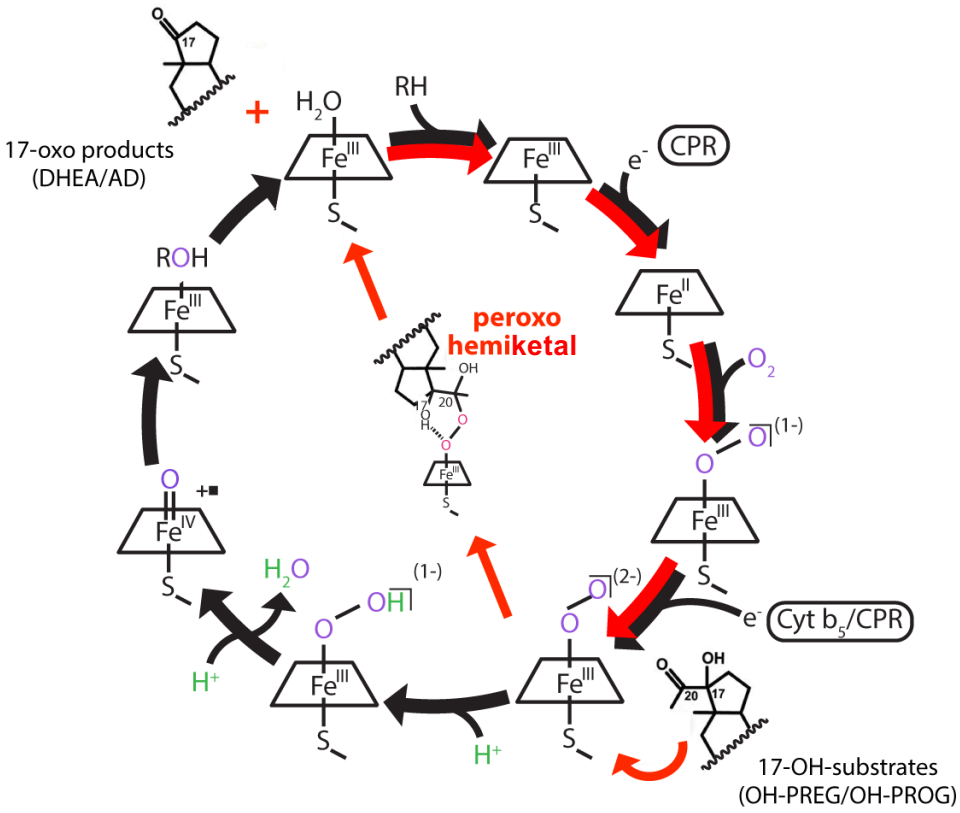

Figure 7.1: Updated P450 reaction cycle for CYP17A1 catalysis. Black arrows represent the canonical Cpd I mediated hydroxylation reaction and red arrows depict the lyase reaction mechanism involving the new peroxo-hemiketal intermediate formed as a result of the peroxo-anion mediaetd nucleophilic attack on carbonyl 20 of lyase susbtrates. Also shown is the second electron transfer, which can be performed by CPR or by cytochrome *b_5*.

Chapter 8

References

Akhtar, M., and Skinner, S.J. (1968). The intermediary role of a 19-oxoandrogen in the biosynthesis of oestrogen. Biochem. J. *109*, 318–321.

Akhtar, M., Calder, M.R., Corina, D.L., and Wright, J.N. (1982). Mechanistic studies on C-19 demethylation in estrogen biosynthesis. Biochem. J. *201*, 569–580.

Akhtar, M., Njar, V.C.O., and Neville Wright, J. (1993). Mechanistic studies on aromatase and related C-C bond cleaving P-450 enzymes. J. Steroid Biochem. Mol. Biol. *44*, 375–387.

Akhtar, M., Corina, D., Miller, S., Shyadehi, A.Z., and Wright, J.N. (1994). Mechanism of the acyl-carbon cleavage and related reactions catalyzed by multifunctional P-450s: studies on cytochrome P-450(17)alpha. Biochemistry *33*, 4410–4418.

Amarneh, B., and Simpson, E.R. (1995). Expression of a recombinant derivative of human aromatase P450 in insect cells utilizing the baculovirus vector system. Mol. Cell. Endocrinol. *109*, R1–R5.

Annalora, A.J., Goodin, D.B., Hong, W.-X., Zhang, Q., Johnson, E.F., and Stout, C.D. (2010). Crystal structure of CYP24A1, a mitochondrial cytochrome P450 involved in Vitamin D metabolism. J. Mol. Biol. *396*, 441–451.

Auchus, R.J. (2001). The genetics, pathophysiology, and management of human deficiencies of P450c17. Endocrinol. Metab. Clin. *30*, 101–119.

Auchus, R.J., and Rainey, W.E. (2004). Adrenarche - physiology, biochemistry and human disease.

Clin. Endocrinol. (Oxf). *60*, 288–296.

Auchus, R.J., Lee, T.C., and Miller, W.L. (1998). Cytochrome b5 augments the 17,20-lyase activity of human P450c17 without direct electron transfer. J. Biol. Chem. *273*, 3158–3165.

Baas, B.J., Denisov, I.G., and Sligar, S.G. (2004). Homotropic cooperativity of monomeric cytochrome P450 3A4 in a nanoscale native bilayer environment. Arch. Biochem. Biophys. *430*, 218–228.

Batabyal, D., Li, H., and Poulos, T.L. (2013). Synergistic effects of mutations in cytochrome P450cam designed to mimic CYP101D1. Biochemistry *52*, 5396–5402.

Bayburt, T.H., Carlson, J.W., and Sligar, S.G. (1998). Reconstitution and imaging of a membrane protein in a nanometer-size phospholipid bilayer. J. Struct. Biol. *123*, 37–44.

Bayburt, T.H., Grinkova, Y. V, and Sligar, S.G. (2002). Self-assembly of discoidal phospholipid bilayer nanoparticles with membrane scaffold proteins. Nano Lett. *2*, 853–856.

Benson, D.E., Suslick, K.S., and Sligar, S.G. (1997). Reduced oxy intermediate observed in D251N cytochrome P450 cam. Biochemistry *2960*, 5104–5107.

Bhattacharya, P., Grimme, S., Ganesh, B., Gopisetty, A., Sheng, J.R., Martinez, O., Jayarama, S., Artinger, M., Meriggioli, M., and Prabhakar, B.S. (2010). Nanodisc-incorporated hemagglutinin provides protective immunity against influenza virus infection. J. Virol. *84*, 361–371.

Bonfils, C., Balny, C., and Maurel, P. (1981). Direct evidence for electron transfer from ferrous cytochrome b5 to the oxyferrous intermediate of liver microsomal cytochrome P-450 LM2. J. Biol. Chem. *256*, 9457–9465.

Bonomo, S., Jørgensen, F.S., and Olsen, L. (2017). Mechanism of cytochrome P450 17A1-catalyzed hydroxylase and lyase Reactions. J. Chem. Inf. Model. *57*, 1123–1133.

Braselton, W.E., Engel, L.L., and Orr, J.C. (1974). The flux of intermediates and products in aromatization of C19 steroids by human placental microsomes. Eur. J. Biochem. *48*, 35–43.

Brewer, C.B., and Peterson, J.A. (1988). Single turnover kinetics of the reaction between oxycytochrome P-450(cam) and reduced putidaredoxin. J. Biol. Chem. *263*, 791–798.

Bull, S.C., and Doig, A.J. (2015). Properties of protein drug target classes. PLoS One *10*, 1–44.

Canova-davis, E., and Waskells, L. (1984). The identification of the heat-stable microsomal protein required for methoxyflurane metabolism as cytochrome b5. J. Biol. Chem. *259*, 2541–2546.

Carney, C.E., Lenov, I.L., Baker, C.J., Macrenaris, K.W., Eckermann, A.L., Sligar, S.G., and Meade, T.J. (2015). Nanodiscs as a modular platform for multimodal MR-optical imaging. Bioconjug. Chem. *26*, 899–905.

Champion, P.M., Stallard, B.R., Wagner, G.C., and Gunsalus, I.C. (1982). Resonance Raman detection of an Fe-S bond in cytochrome P450cam. J. Am. Chem. Soc. *104*, 5469–5472.

Collman, J.P., and Sorrell, T.N. (1975). A model for the carbonyl adduct of ferrous cytochrome P-450. J. Am. Chem. Soc. *97*, 4133–4134.

Das, A., Grinkova, Y. V, and Sligar, S.G. (2007). Redox potential control by drug binding to cytochrome P450 3A4. J. Am. Chem. Soc. *129*, 13778–13779.

Davydov, R.M. (1980). Optical and ESR-spectroscopic study of electronic adducts of oxymyoglobin and oxyhemoglobin. Biofizika *25*, 203–207.

Denisov, I.G., and Sligar, S.G. (2011). Cytochromes P450 in nanodiscs. Biochim. Biophys. Acta *1814*, 223–229.

Denisov, I.G., Makris, T.M., and Sligar, S.G. (2001). Cryotrapped reaction intermediates of cytochrome

p450 studied by radiolytic reduction with phosphorus-32. J. Biol. Chem. *276*, 11648–11652.

Denisov, I.G., Makris, T.M., and Sligar, S.G. (2002). Cryoradiolysis for the study of P450 reaction intermediates. Methods Enzym. *357*, 103–115.

Denisov, I.G., Grinkova, Y. V, Lazarides, A.A., and Sligar, S.G. (2004). Directed self-assembly of monodisperse phospholipid bilayer nanodiscs with controlled size. J. Am. Chem. Soc. 3477–3487.

Denisov, I.G., Makris, T.M., Sligar, S.G., and Schlichting, I. (2005a). Structure and chemistry of cytochrome P450. Chem. Rev. *105*, 2253–2277.

Denisov, I.G., McLean, M.A., Shaw, A.W., Grinkova, Y. V., and Sligar, S.G. (2005b). Thermotropic phase transition in soluble nanoscale lipid bilayers. J. Phys. Chem. B *109*, 15580–15588.

Denisov, I.G., Grinkova, Y. V, Baas, B.J., and Sligar, S.G. (2006). The ferrous-dioxygen intermediate in human cytochrome P450 3A4. Substrate dependence of formation and decay kinetics. J. Biol. Chem. *281*, 23313–23318.

Denisov, I.G., Victoria, D.C., and Sligar, S.G. (2007a). Cryoradiolytic reduction of heme proteins: Maximizing dose-dependent yield. Radiat. Phys. Chem. *76*, 714–721.

Denisov, I.G., Grinkova, Y. V, McLean, M.A., and Sligar, S.G. (2007b). The one-electron autoxidation of human cytochrome P450 3A4. J. Biol. Chem. *282*, 26865–26873.

Denisov, I.G., Mak, P.J., Makris, T.M., Sligar, S.G., and Kincaid, J.R. (2008). Resonance Raman characterization of the peroxo and hydroperoxo intermediates in cytochrome P450. J. Phys. Chem. A *112*, 13172–13179.

DeVore, N.M., and Scott, E.E. (2012). Structures of cytochrome P450 17A1 with prostate cancer drugs abiraterone and TOK-001. Nature *482*, 116–119.

Dharia, S., Slane, A., Jian, M., Conner, M., Conley, A.J., and Parker, C.R. (2004). Colocalization of P450c17 and cytochrome b5 in androgen-synthesizing tissues of the human. Biol. Reprod. *71*, 83–88.

Duivenvoorden, R., Tang, J., Cormode, D.P., Mieszawska, A.J., Izquierdo-Garcia, D., Ozcan, C., Otten, M.J., Zaidi, N., Lobatto, M.E., van Rijs, S.M., et al. (2014). A statin-loaded reconstituted high-density lipoprotein nanoparticle inhibits atherosclerotic plaque inflammation. Nat. Commun. *5*, 3065.

Efremov, R.G., Leitner, A., Aebersold, R., and Raunser, S. (2014). Architecture and conformational switch mechanism of the ryanodine receptor. Nature *517*, 39–43.

Estrada, D.F., Laurence, J.S., and Scott, E.E. (2013). Substrate-modulated cytochrome P450 17A1 and cytochrome b5 interactions revealed by NMR. J. Biol. Chem. *288*, 17008–17018.

Estrada, D.F., Skinner, A.L., Laurence, J.S., and Scott, E.E. (2014). Human cytochrome P450 17A1 conformational selection: modulation by ligand and cytochrome b5. J. Biol. Chem. *289*, 14310–14320.

Estrada, D.F., Laurence, J.S., and Scott, E.E. (2016). Cytochrome P450 17A1 interactions with the fmn domain of its reductase as characterized by NMR. J. Biol. Chem. *291*, 3990–4003.

Finn, R.D., Mclaughlin, L.A., Ronseaux, S., Rosewell, I., Houston, J.B., Henderson, C.J., and Wolf, C.R. (2008). Defining the in vivo role for cytochrome b5 in cytochrome P450 function through the conditional hepatic deletion of microsomal cytochrome b5. J. Biol. Chem. *283*, 31385–31393.

Flück, C.E., Miller, W.L., and Auchus, R.J. (2003). The 17, 20-lyase activity of cytochrome P450c17 from human fetal testis favors the delta-5 steroidogenic pathway. J. Clin. Endocrinol. Metab. *88*, 3762–3766.

Gantt, S.L., Denisov, I.G., Grinkova, Y. V, and Sligar, S.G. (2009). The critical iron-oxygen intermediate in human aromatase. Biochem Biophys Res Commun *387*, 169–173.

Gartner, C.A., Thompson, S.J., Rettie, A.E., and Nelson, S.D. (2001). Human aromatase in high yield and purity by perfusion chromatography and its characterization by difference spectroscopy and mass spectrometry. Protein Expr. Purif. *22*, 443–454.

Geller, D.H., Auchus, R.J., Mendonca, B.B., and Miller, W.L. (1997). The genetic and functional basis of isolated 17,20-lyase deficiency. Nat. Genet. *17*, 201–205.

Geller, D.H., Auchus, R.J., and Miller, W.L. (1999). P450c17 mutations R347H and R358Q selectively disrupt 17,20-lyase activity by disrupting interactions with P450 oxidoreductase and cytochrome b5. Mol. Endocrinol. *13*, 167–175.

Gerber, N.C., and Sligar, S.G. (1994). A role for Asp-251 in cytochrome P-450cam oxygen activation. J. Biol. Chem. *269*, 4260–4266.

Ghosh, D., Griswold, J., Erman, M., and Pangborn, W. (2010). X-ray structure of human aromatase reveals an androgen-specific active site. J. Steroid Biochem. Mol. Biol. *118*, 197–202.

Gingras, A.R., Ye, F., and Ginsberg, M.H. (2013). Reconstructing integrin activation in vitro. Adhesion Protein Protocols, A.S. Coutts, ed. (Totowa, NJ: Humana Press), 1–17.

Glasoe, P.K., and Long, F.A. (1960). Use of glass electrodes to measure acidities in deuterium oxide. J. Phys. Chem. *64*, 188–190.

Graham-lorence, S., Amarneh, B., White, R.E., Peterson, J.A., and Simpson, E.R. (1995). A three-dimensional model of aromatase cytochrome P450. Protein Science *4,* 1065–1080.

Gregory, M.C. (2016). Understanding the mechanism of androgen biosynthesis. University of Illinois at Urbana-Champaign.

Gregory, M., Mak, P.J., Sligar, S.G., and Kincaid, J.R. (2013a). Differential hydrogen bonding in human

cyp17 dictates hydroxylation versus lyase chemistry. Angew. Chemie *52*, 5342–5345.

Gregory, M.C., Denisov, I.G., Grinkova, Y. V, Khatri, Y., and Sligar, S.G. (2013b). Kinetic solvent isotope effect in human p450 cyp17a1-mediated androgen formation: evidence for a reactive peroxoanion intermediate. J. Am. Chem. Soc. *135*, 16245–16247.

Gregory, M.C., McLean, M.A., and Sligar, S.G. (2017). Interaction of KRas4b with anionic membranes: a special role for PIP2. Biochem. Biophys. Res. Commun. *487*, 351–355.

Grinkova, Y. V, Denisov, I.G., and Sligar, S.G. (2010a). Functional reconstitution of monomeric CYP3A4 with multiple cytochrome P450 reductase molecules in Nanodiscs. Biochem. Biophys. Res. Commun. *398*, 194–198.

Grinkova, Y. V., Denisov, I.G., and Sligar, S.G. (2010b). Engineering extended membrane scaffold proteins for self-assembly of soluble nanoscale lipid bilayers. Protein Eng. Des. Sel. *23*, 843–848.

Groves, J.T., and McClusky, G.A. (1976). Aliphatic hydroxylation via oxygen rebound. Oxygen transfer catalyzed by iron. J. Am. Chem. Soc. *98*, 859–861.

Gruenke, L.D., Sun, J., Loehr, T.M., and Waskell, L. (1997). Resonance Raman spectral properties and stability of manganese protoporphyrin IX cytochrome b5. Biochemistry *36*, 7114–7125.

Guengerich, F.P. (2001). Uncommon P450-catalyzed reactions. Curr. Drug Metab. *2*, 93–115.

Guryev, O.L., Gilep, A.A., Usanov, S.A., and Estabrook, R.W. (2001). Interaction of apo-cytochrome b5 with cytochromes P4503A4 and P45017A: relevance of heme transfer reactions. Biochemistry *40*, 5018–5031.

Hagerman, D.D. (1987). Human placenta estrogen synthetase (aromatase) purified by affinity chromatography. J. Biol. Chem. *262*, 2398–2400.

Hayaishi, O., Katagiri, M., and Rothberg, S. (1955). Mechanism of the pyrocatechase reaction, J. Am. Chem. Soc. 77 (1955) 5450– 5451. J. Am. Chem. Soc. *77*, 5450–5451.

Hayano, M., Lindberg, M.C., Dorfman, R.I., Hancock, J.E., and Von Doering, W.E. (1955). On the mechanism of the c-11 beta-hydroxylation of steroids: a study with H2O18 and O218. Arch. Biochem. Biophys. *59*, 529–532.

Holmans, P.L., Shet, M.S., Martin-Wixtrom, C.A., Fisher, C.W., and Estabrook, R.W. (1994). The high-level expression in escherichia coli of the membrane-bound form of human and rat cytochrome b5 and studies on their mechanism of function. Arch. Biochem. Biophys. *312*, 554–565.

Im, S.-C., and Waskell, L. (2011). The interaction of microsomal cytochrome P450 2B4 with its redox partners, cytochrome P450 reductase and cytochrome b5. Arch. Biochem. Biophys. *507*, 144–153.

Imai, Y., and Sato, R. (1977). The roles of cytochrome b5 in a reconstituted N-demethylase system containing cytochrome P-450. Biochem. Biophys. Res. Commun. *75*, 420–426.

Jones, M.E.E., Boon, W.C., Mcinnes, K., Maffei, L., Carani, C., Simpson, E.R., and Gene, C. (2007). Recognizing rare disorders : aromatase deficiency. Nat. Clin. Prac. *3*, 414–421.

Kagawa, N., Cao, Q., and Kusano, K. (2003). Expression of human aromatase (CYP19) in Escherichia coli by N-terminal replacement and induction of cold stress response. Steroids *68*, 205–209.

Kagawa, N., Hori, H., Waterman, M.R., and Yoshioka, S. (2004). Characterization of stable human aromatase expressed in E. coli. Steroids *69*, 235–243.

Kappl, R., Hohn-Berlage, M., Hutterman, J., Bartlett, N., and Symons, M.C.R. (1985). Electron spin and electron nuclear double resonance of the [FeO2] - centre from irradiated oxyhemo- and oxymyoglobin. Biochim. Biophys. Acta *827*, 327–343.

Kawai, Y., Yoneyama, Y., and Yoshikawa, H. (1963). The oxidation-reduction potential of cytochrome b5 in soluble and particulate form with reference to the role of lipid. Biochim. Biophys. Acta *67*, 522–524.

Kellis, J.T., and Vickery, L.E. (1987). The active site of aromatase cytochrome P-450. Differential effects of cyanide provide evidence for proximity of heme-iron and carbon-19 in the enzyme-substrate complex. J. Biol. Chem. *262*, 8840–8844.

Khatri, Y., Luthra, A., Duggal, R., and Sligar, S.G. (2014a). Kinetic solvent isotope effect in steady-state turnover by CYP19A1 suggests involvement of Compound 1 for both hydroxylation and aromatization steps. FEBS Lett. *588*, 3117–3122.

Khatri, Y., Gregory, M.C., Grinkova, Y. V, Denisov, I.G., and Sligar, S.G. (2014b). Active site proton delivery and the lyase activity of human CYP17A1. Biochem. Biophys. Res. Commun. *443*, 179–184.

Kuai, R., Ochyl, L.J., Bahjat, K.S., Schwendeman, A., and Moon, J.J. (2016). Designer vaccine nanodiscs for personalized cancer immunotherapy. Nat. Mater. *1*, 1–18.

Kusumi, A., Fujiwara, T.K., Chadda, R., Xie, M., Tsunoyama, T. a., Kalay, Z., Kasai, R.S., and Suzuki, K.G.N. (2012). Dynamic Organizing Principles of the Plasma Membrane that Regulate Signal Transduction: Commemorating the Fortieth Anniversary of Singer and Nicolson's Fluid-Mosaic Model. Annu. Rev. Cell Dev. Biol. *28*, 215–250.

Lamichhane, R., Liu, J.J., Pljevaljcic, G., White, K.L., van der Schans, E., Katritch, V., Stevens, R.C., Wüthrich, K., and Millar, D.P. (2015). Single-molecule view of basal activity and activation mechanisms of the G protein-coupled receptor β_2 AR. Proc. Natl. Acad. Sci. *112*, 14254–14259.

Laursen, T., Singha, A., Rantzau, N., Tutkus, M., Borch, J., Hedegård, P., Stamou, D., Møller, B.L., and Hatzakis, N.S. (2014). Single molecule activity measurements of cytochrome P450

oxidoreductase reveal the existence of two discrete functional states. ACS Chem. Biol. *9*, 630–634.

Lee-Robichaud, P., Akhtar, M.E., and Akhtar, M. (1998). Control of androgen biosynthesis in the human through the interaction of Arg347 and Arg358 of CYP17 with cytochrome b5. Biochem. J. *332*, 293–296.

Lee-Robichaud, P., Akhtar, M.E., Wright, J.N., Sheikh, Q.I., and Akhtar, M. (2004). The cationic charges on Arg 347, Arg 358 and Arg 449 of human cytochrome P450c17 (CYP17) are essential for the enzyme's cytochrome b 5-dependent acyl-carbon cleavage activities. J. Steroid Biochem. Mol. Biol. *92*, 119–130.

Li, D., Kabir, M., Stuehr, D.J., Rousseau, D.L., and Yeh, S.R. (2007). Substrate- and Isoform-Specific Dioxygen Complexes of Nitric Oxide Synthase. J. Am. Chem. Soc. *129,* 6943-6951.

Lipscomb, J.D., Sligar, S.G., Namtvedt, M.J., and Gunsalus, I.C. (1976). Autooxidation and hydroxylation reactions of oxygenated cytochrome P-450cam. J. Biol. Chem. *251,* 1116–1124.

Liu, Y., and Ortiz de Montellano, P. (2000). Reaction intermediates and single turnover rate constants for the oxidation of heme by human heme oxygenase-1. J. Biol. Chem. *275*, 5297–5307.

Lo, J., Di Nardo, G., Griswold, J., Egbuta, C., Jiang, W., Gilardi, G., and Ghosh, D. (2013). Structural basis for the functional roles of critical residues in human cytochrome P450 aromatase. Biochemistry *52*, 5821–5829.

Luthra, A. (2015). Spectroscopic characterization of iron-oxygen intermediates in human aromatase (CYP19A1). ProQuest Diss. Theses 123.

Luthra, A., Gregory, M., Grinkova, Y. V, Denisov, I.G., and Sligar, S.G. (2013). Nanodiscs in the studies of membrane-bound cytochrome P450 enzymes. Methods Mol. Biol. *987*, 115–127.

Mak, P.J. (2016). Resonance Raman spectroscopy as a structural probe of the cytochrome p450 enzymatic cycle. Handb. Porhyrin Sci. 1–120.

Mak, P.J., and Denisov, I.G. (2017). Spectroscopic studies of the cytochrome P450 reaction mechanisms. Biochim. Biophys. Acta - Proteins Proteomics [Epub ahead of print].

Mak, P.J., Im, S.-C.C., Zhang, H., Waskell, L.A., and Kincaid, J.R. (2008). Resonance Raman studies of cytochrome P450 2B4 in its interactions with substrates and redox partners. Biochemistry *47*, 3950–3963.

Mak, P.J., Denisov, I.G., Grinkova, Y. V, Sligar, S.G., and Kincaid, J.R. (2011). Defining CYP3A4 structural responses to substrate binding. Raman spectroscopic studies of a nanodisc-incorporated mammalian cytochrome P450. J Am Chem Soc *133*, 1357–1366.

Mak, P.J., Yang, Y., Im, S., Waskell, L.A., and Kincaid, J.R. (2012). Experimental documentation of the structural consequences of hydrogen-bonding interactions to the proximal cysteine of a cytochrome P450. Angew. Chemie - Int. Ed. *51*, 10403–10407.

Mak, P.J., Zhu, Q., and Kincaid, J.R. (2013). Using resonance Raman cross-section data to estimate the spin state populations of Cytochromes P450. J. Raman Spectrosc. *44*, 1792–1794.

Mak, P.J., Luthra, A., Sligar, S.G., and Kincaid, J.R. (2014a). Resonance raman spectroscopy of the oxygenated intermediates of human CYP19A1 implicates a compound i intermediate in the final lyase step. J. Am. Chem. Soc. *136*, 4825–4828.

Mak, P.J., Gregory, M.C., Sligar, S.G., and Kincaid, J.R. (2014b). Resonance raman spectroscopy reveals that substrate structure selectively impacts the heme-bound diatomic Ligands of CYP17. Biochemistry *53*, 90–100.

Mak, P.J., Gregory, M.C., Denisov, I.G., Sligar, S.G., and Kincaid, J.R. (2015). Unveiling the crucial

intermediates in androgen production. Proc. Natl. Acad. Sci. *112*, 15856–15861.

Makris, T.M., Davydov, R., Denisov, I.G., Hoffman, B.M., and Sligar, S.G. (2002). Mechanistic enzymology of oxygen activation by the cytochromes P450. Drug Metab. Rev. *34*, 691–708.

McLaughlin, L.A., Ronseaux, S., Finn, R.D., Henderson, C.J., and Roland Wolf, C. (2010). Deletion of microsomal cytochrome b5 profoundly affects hepatic and extrahepatic drug metabolism. Mol. Pharmacol. *78*, 269–278.

Mokashi, V., Li, L., and Porter, T.D. (2003). Cytochrome b5 reductase and cytochrome b5 support the CYP2E1-mediated activation of nitrosamines in a recombinant Ames test. Arch. Biochem. Biophys. *412*, 147–152.

De Montellano, P.R.O. (2015). Cytochrome P450 Structure, Mechanism, and Biochemistry.

Morgan, E.T., and Coon, M.J. (1984). Effects of cytochrome b5 on cytochrome P-450-catalyzed reactions. Studies with manganese-substituted cytochrome b5. Drug Metab. Dispos. *12*, 358–364.

Morrissey, J.H., Pureza, V., Davis-Harrison, R.L., Sligar, S.G., Rienstra, C.M., Kijac, A.Z., Ohkubo, Y.Z., and Tajkhorshid, E. (2009). Protein-membrane interactions: Blood clotting on nanoscale bilayers. J. Thromb. Haemost. *7*, 169–172.

Mulrooney, S.B., and Waskell, L. (2000). High-level expression in Escherichia coli and purification of the membrane-bound form of cytochrome b(5). Protein Expr. Purif. *19*, 173–178.

Naffin-olivos, J.L., and Auchus, R.J. (2006). Human cytochrome b 5 requires residues E48 and E49 to stimulate the 17,20-lyase activity of cytochrome P450c17. Biochemistry *45*, 755–762.

Nathanson, I.T., Jones, J., and Towne, L.E. (1939). The urinary excretion of estrogens, androgens and fsh following the administration of testosterone to human female castrates. Endocrinology *25*,

754.

Nelson, D.R. (2017). Cytochrome P450 diversity in the tree of life. Biochim. Biophys. Acta - Proteins Proteomics [Epub ahead of print].

Nguyen, A.D., Corbin, C.J., Pattison, J.C., Bird, I.M., and Conley, A.J. (2009). The developmental increase in adrenocortical 17, 20-lyase activity (biochemical adrenarche) is driven primarily by increasing cytochrome b5 in neonatal rhesus macaques. Endocrinology *150*, 1748–1756.

Oloo, W.N., Meier, K.K., Wang, Y., Shaik, S., Munck, E., and Que, L. (2014). Identification of a low-spin acylperoxoiron(III) intermediate in bio-inspired non-heme iron-catalysed oxidations. Nat. Commun. *5*, 3046.

Onoda, M., and Hall, F. (1982). Cytochrome b5 stimulates purified testicular microsomal cytochrome P-450 (C21 side-chain cleavage). Biochem. Biophys. Res. Comm.*108*, 454–460.

Oprian, D.D., and Coon, M.J. (1982). Oxidation-reduction states of FMN and FAD in NADPH-cytochrome P-450 reductase during reduction by NADPH. J. Biol. Chem. *257*, 8935–8944.

Oshino, N., Imai, Y., and Sato, R. (1971). A function of cytochrome b5 in fatty acid desaturation by rat liver microsomes. J. Biochem. *69*, 155–167.

Peng, H.M., Im, S.C., Pearl, N.M., Turcu, A.F., Rege, J., Waskell, L., and Auchus, R.J. (2016). Cytochrome b5 activates the 17,20-lyase activity of human cytochrome p450 17a1 by increasing the coupling of NADPH consumption to androgen production. Biochemistry *55*, 4356–4365.

Petrunak, E.M., DeVore, N.M., Porubsky, P.R., and Scott, E.E. (2014). Structures of human steroidogenic cytochrome P450 17A1 with substrates. J. Biol. Chem. *289*, 32952–32964.

Podstawka, E., Rajani, C., Kincaid, J.R., and Proniewicz, L.M. (2000). Resonance Raman studies of

heme structural differences in subunits of deoxy hemoglobin. Biopolym. - Biospectroscopy Sect. *57*, 201–207.

Pompon, D., and Coon, M.J. (1984). On the mechanism of action of cytochrome P-450. Oxidation and reduction of the ferrous dioxygen complex of liver microsomal cytochrome P-450 by cytochrome b5. J. Biol. Chem. *259*, 15377–15385.

Porter, T.D., Wilson, T.E., and Kasper, C.B. (1987). Expression of a functional 78,000 dalton mammalian flavoprotein, NADPH-cytochrome P-450 oxidoreductase, in Escherichia coli. Arch. Biochem. Biophys. *254*, 353–367.

Poulos, T.L., Finzel, B.C., and Howard, A.J. (1987). High-resolution crystal structure of cytochrome P450cam. J Mol Biol *195*, 687–700.

Raag, R., Martinis, S. a, Sligar, S.G., and Poulos, T.L. (1991). Crystal structure of the cytochrome P-450CAM active site mutant Thr252Ala. Biochemistry *30*, 11420–11429.

Rodgers, K.K., and Sligar, S.G. (1991). Surface Electrostatics, Reduction Potentials, and the Internal Dielectric Constant of Proteins. J. Am. Chem. Soc. *113*, 9419–9421.

Rues, R.B., Orbán, E., Dötsch, V., and Bernhard, F. (2014). Cell-free expression of G-protein coupled receptors: New pipelines for challenging targets. Biol. Chem. *395*, 1425–1434.

Sakai, Y., Yanase, T., Hara, T., Takayanagi, R., Haji, M., and Nawata, H. (1994). In-vitro evidence for the regulation of 17,20-lyase activity by cytochrome b5 in adrenocortical adenomas from patients with Cushing's syndrome. Clin. Endocrinol. (Oxf). *40*, 205–209.

Schuler, M.A., Denisov, I.G., and Sligar, S.G. (2013). Nanodiscs as a new tool to examine lipid--protein interactions. in lipid-protein interactions: methods and protocols, J.H. Kleinschmidt, ed. (Totowa, NJ: Humana Press), pp. 415–433.

Sergeev, G. V., Gilep, A.A., and Usanov, S.A. (2014). The role of cytochrome b5 structural domains in interaction with cytochromes P450. Biochemistry (Mosc). *79*, 406–416.

Shah, M.B., Jang, H.H., Wilderman, P.R., Lee, D., Li, S., Zhang, Q., Stout, C.D., and Halpert, J.R. (2016). Effect of detergent binding on cytochrome P450 2B4 structure as analyzed by X-ray crystallography and deuterium-exchange mass spectrometry. Biophys. Chem. *216*, 1–8.

Shaw, A.W., Pureza, V.S., Sligar, S.G., and Morrissey, J.H. (2007). The local phospholipid environment modulates the activation of blood clotting. J. Biol. Chem. *282*, 6556–6563.

Shen, A.L., Porter, T.D., Wilson, T.E., and Kasper, C.B. (1989). Structural analysis of the FMN binding domain of NADPH-cytochrome P-450 oxidoreductase by site-directed mutagenesis. J. Biol. Chem. *264*, 7584–7589.

Shimada, H., Sligar, S.G., Yeom, H., and Ishimura, Y. (1997). Heme monooxygenases in: oxygenases and model systems. in oxygenases and model systems, T. Funabiki, ed. (Dordrecht: Springer Netherlands), pp. 195–221.

Shozu, M., Sebastian, S., Takayama, K., Hsu, W.-T., Schultz, R.A., Neely, K., Bryant, M., and Bulun, S.E. (2003). Estrogen excess associated with novel gain-of-function mutations affecting the aromatase gene. N. Engl. J. Med. *348,* 1855–1865.

Shriver, D., and Dunn, J. (1974). Backscattering geometry for Raman-spectroscopy of colored materials. Appl. Spectrosc. *28*, 319–323.

Sligar, S.G., Denisov, I.G., Baas, B.J., Grinkova, Y. V, and Sligar, S.G. (2007). Cooperativity in cytochrome P450 3A4 - Linkages in substrate binding, spin state, uncoupling, and product formation. J. Biol. Chem. *282*, 7066–7076.

Sohl, C.D., and Guengerich, F.P. (2010). Kinetic analysis of the three-step steroid aromatase reaction

of human cytochrome P450 19A1. J. Biol. Chem. *285*, 17734–17743.

Sondhi, V., Owen, B.M., Liu, J., Chomic, R., Kliewer, S.A., Hughes, B.A., Arlt, W., Mangelsdorf, D.J., and Auchus, R.J. (2016). Impaired 17,20-lyase activity in male mice lacking cytochrome b_5 in leydig cells. Mol. Endocrinol. *30*, 469–478.

Stein, M.N., Goodin, S., and DiPaola, R.S. (2012). Abiraterone in prostate cancer: a new angle to an old problem. Clin. Cancer Res. *18*, 1848–1854.

Suzuki, T., Sasano, H., Sawai, T., Mason, J.I., and Nagura, H. (1992). Immunohistochemistry and in situ hybridization of P45017a. J. Histochem. Cytochem. *40*, 903–908.

Symons, M.C., and Petersen, R.L. (1978). Electron capture by oxyhaemoglobin: an e.s.r. study. Proc. R. Soc. London. Ser. B, Biol. Sci. *201*, 285–300.

Tan, L., and Muto, N. (1986). Purification and reconstitution properties of human placental aromatase: A cytochrome P-450-type monooxygenase. Eur. J. Biochem. *156*, 243–250.

Tavoosi, N., and Morrissey, J.H. (2014). Influence of membrane composition on the enhancement of factor VIIa/tissue factor activity by magnesium ions. Thromb. Haemost. *111*, 770–772.

Thompson Jr., E.A., and Siiteri, P.K. (1974). The involvement of human placental microsomal cytochrome P-450 in aromatization. J. Biol. Chem. *249*, 5373–5378.

Vermilion, J.L., and Coon, M.J. (1978). Identification of the high and low potential flavins of liver microsomal NADPH-cytochrome P-450 reductase. J. Biol. Chem. *253*, 8812–8819.

Vidakovic, M., Sligar, S.G., Li, H., and Poulos, T.L. (1998). Understanding the role of the essential Asp251 in cytochrome P450cam using site-directed mutagenesis, crystallography, and kinetic solvent isotope effect. Biochemistry *37*, 9211–9219.

Williams, P.A., Cosme, J., Sridhar, V., Johnson, E.F., and McRee, D.E. (2000). Mammalian microsomal cytochrome P450 monooxygenase. Mol. Cell *5*, 121–131.

Willis, K.J., London, D.R., Ward, H.W., Butt, W.R., Lynch, S.S., and Rudd, B.T. (1977). Recurrent breast cancer treated with the antioestrogen tamoxifen: correlation between hormonal changes and clinical course. Br. Med. J. *1*, 425–428.

Yamaori, S., Yamazaki, H., Suzuki, A., Yamada, A., Tani, H., Kamidate, T., Fujita, K.I., and Kamataki, T. (2003). Effects of cytochrome b5 on drug oxidation activities of human cytochrome P450 (CYP) 3As: Similarity of CYP3A5 with CYP3A4 but not CYP3A7. Biochem. Pharmacol. *66*, 2333–2340.

Yamazaki, H., Gillam, E.M.J., Dong, M.-S., Johnson, W.W., Guengerich, F.P., and Shimada, T. (1997). Reconstitution of recombinant cytochrome P450 2C10(2C9) and comparison with cytochrome P450 3A4 and other forms: effects of cytochrome P450–P450 and cytochrome P450–b5 interactions. Arch. Biochem. Biophys. *342*, 329–337.

Yamazaki, H., Nakamura, M., Komatsu, T., Ohyama, K., Hatanaka, N., Asahi, S., Shimada, N., Guengerich, F.P., Shimada, T., Nakajima, M., et al. (2002). Roles of NADPH-P450 reductase and apo- and holo-cytochrome b5 on xenobiotic oxidations catalyzed by 12 recombinant human cytochrome P450s expressed in membranes of escherichia coli. Protein Expr. Purif. *24*, 329–337.

Ye, X., McLean, M.A., and Sligar, S.G. (2016a). Conformational equilibrium of talin is regulated by anionic lipids. Biochim. Biophys. Acta - Biomembr. *1858*, 1833–1840.

Ye, X., McLean, M.A., and Sligar, S.G. (2016b). Phosphatidylinositol 4,5-bisphosphate modulates the affinity of talin-1 for phospholipid bilayers and activates its autoinhibited form. Biochemistry *55*, 5038–5048.

Zhang, H., Im, S.C., and Waskell, L. (2007). Cytochrome b5 increases the rate of product formation

by cytochrome P450 2B4 and competes with cytochrome P450 reductase for a binding site on cytochrome P450 2B4. J. Biol. Chem. *282*, 29766–29776.

Zhang, M., Huang, R., Im, S.C., Waskell, L., and Ramamoorthy, A. (2015). Effects of membrane mimetics on cytochrome P450-cytochrome b5 interactions characterized by NMR spectroscopy. J. Biol. Chem. *290*, 12705–12718.